

博士論文

Evaluation on RCIC turbine behavior during Fukushima -Daiichi NPP Accident

(福島第一原子力発電所事故時の RCIC タービン挙動に関する研究)

ロペズ デ アバジョ ヘクタ

EVALUATION ON RCIC TURBINE BEHAVIOR DURING FUKUSHIMA-DAIICHI NPP ACCIDENT.

A dissertation submitted to
The University of Tokyo
In partial fulfillment of the requirements
For the degree of

Doctor of Philosophy

In

NUCLEAR ENGINEERING AND MANAGEMENT

By

Hector Lopez de Abajo

June 2015

Table of contents

List of figures.....	I
List of tables.....	VI
Abstract.....	1
Chapter 1 Introduction.....	4
1.1- Boiler Water Reactor history.....	4
1.2- Containment.....	7
1.3- Safety Relief Valves (SRV).....	8
1.4- Reactor Core Isolation Cooling system (RCIC system).....	9
1.5- Fukushima accident outline.....	14
1.6- Simulation codes.....	17
1.6.1- MAAP.....	18
1.6.2- RELAP/ScdapSIM.....	19
1.6.3- MELCOR.....	21
1.7- Severe accident management.....	25
1.8- Objectives.....	27
Chapter 2 Steam turbine design.....	29
2.1- RCIC steam turbine.....	30
2.1.1- Nozzle design.....	36

2.1.2- Blade design.....	39
2.2- RCIC steam turbine degradation coefficient calculation.....	42
2.2.1- Critical flow model description.....	44
2.2.2- Homogeneous Equilibrium Model.....	44
2.2.3- Non-Homogeneous Equilibrium Model.....	48
2.2.4- Degradation coefficient formation and discussion.....	53
2.3- Summary.....	58
Chapter 3 Application of the turbine design into F1D2 RCIC system numerical analysis.....	59
3.1- Fukushima Daiichi Unit 2 plant description.....	59
3.2- Accident progression.....	62
3.2.1- Measured data.....	65
3.3- RCIC system numerical analysis.....	67
3.3.1- RCIC system description.....	67
3.3.2- Accident analysis.....	70
3.3.3- Analysis results and discussion.....	72
3.4- Summary.....	80
Chapter 4 RELAP/ScdapSIM.....	81
4.1- Code architecture.....	82
4.1.1- Transient/steady-state (TRNCTL) block.....	83
4.1.2- Heat structure model.....	84

4.1.3- Hydrodynamic model.....	85
4.1.3.1- Mass continuity.....	86
4.1.3.2- Momentum conservation.....	87
4.1.3.3- Energy conservation.....	94
4.2- RELAP RCIC system nodalization.....	95
4.3- RELAP code modifications.....	101
4.3.1- Turbine degradation coefficient.....	101
4.2.2- Steam Flashing.....	105
4.4- RCIC Pump.....	107
4.4.1- Description.....	108
4.4.2- Performance curves.....	112
4.4.3- Pump homologous curves generation.....	119
4.5- Summary.....	124
Chapter 5 Simulation results and discussion.....	125
5.1- Single phase flow analysis.....	125
5.2- Two-phase flow analysis – Accident progression.....	129
5.2.1- Open loop simulations.....	129
5.2.1.1- Torus room flooding.....	136
5.2.2- Close loop simulations.....	140
5.2.2.1- Steam flashing phenomenon.....	144

5.3- Comparison of F1D2 accident results obtained by different codes.....	148
5.4- Summary.....	152
Chapter 6 Conclusions.....	154
References.....	156

List of figures

Figure 1-1 BWR development [1].....	5
Figure 1-2 BWR core structure [2].....	6
Figure 1-3 BWR Mark 1 containment [2].....	8
Figure 1-4 SRV [5].....	9
Figure 1-5 RCIC system diagram [2].....	11
Figure 1-6 Suppression chamber thermal stratification.....	13
Figure 1-7 Suppression chamber geometry	13
Figure 1-8 RHR suppression chamber cooling function layout [9].....	14
Figure 1-9 Fukushima Daiichi site map [10].....	16
Figure 2-1 RCIC Terry turbine schematics 1 [7].....	33
Figure 2-2 RCIC Terry turbine schematics 2 [7].....	34
Figure 2-3 Principle of fluid expansion in nozzle [20].....	37
Figure 2-4 Convergent nozzle schematic	38
Figure 2-5 Principle of blade design [20].....	40
Figure 2-6 Generic velocity triangle diagram.....	41
Figure 2-7 Turbine thermal hydraulic concept.....	45
Figure 2-8 HEM mass flux calculation.....	47
Figure 2-9 HEM pseudo-fluid velocity calculation [29].....	48
Figure 2-10 Critical mass flux value applying different slip ratios [26].....	50
Figure 2-11 Relationship between the stagnation pressure and the critical mass flux using different models [26].....	51

Figure 2-12 NHEM mass flux calculation.....	52
Figure 2-13 HEM/NHEM model flow chart.....	53
Figure 2-14 Turbine momentum and energy conservation concepts [30].....	54
Figure 2-15 HEM degradation coefficient.....	56
Figure 2-16 NHEM degradation coefficient.....	56
Figure 2-17 HEM/NHEM degradation coefficient comparison.....	57
Figure 3-1 RPV pressure [11].....	65
Figure 3-2 Drywell/Wetwell pressure [11].....	66
Figure 3-3 Decay heat [11].....	66
Figure 3-4 RPV water level [11].....	67
Figure 3-5 RCIC system thermal hydraulic diagram.....	68
Figure 3-6 RCIC system numerical analysis flow chart.....	72
Figure 3-7 MSL quality without turbine degradation.....	73
Figure 3-8 RCIC mass flow rates applying HEM coefficient.....	74
Figure 3-9 RCIC mass flow rates applying NHEM coefficient.....	74
Figure 3-10 RCIC mass flow rates applying by IAE [24].....	76
Figure 3-11 RCIC turbine steam mass flow rates comparison.....	76
Figure 3-12 RCIC turbine power comparison.....	77
Figure 3-13 IAE-NHEM comparison.....	78
Figure 3-14 RCIC pump-turbine mass balance.....	79
Figure 4-1 RELAP/ScadpSIM main blocks [36].....	82
Figure 4-2 Transient block main subroutines [36].....	83
Figure 4-3 Horizontal pipe flow regimes [14].....	90

Figure 4-1 $\theta - \alpha_g$ relationship [14].....	91
Figure 4-5 Laguna Verde nodalization [37].....	96
Figure 4-6 Laguna Verde RCIC system nodalization [37].....	97
Figure 4-7 Iteration of RCIC system nodalization.....	98
Figure 4-8 Final version of the RCIC nodalization.....	99
Figure 4-9 Heat structure volume and area conservation.....	100
Figure 4-10 Turbine stages diagram [14].....	102
Figure 4-11 Flow path [40].....	108
Figure 4-12 Centrifugal pump cutaway view [41].....	110
Figure 4-13 Primary and secondary flows at the impeller [39].....	110
Figure 4-14 Impeller classification [39].....	112
Figure 4-15 Affinity parabola.....	116
Figure 4-16 F1D2 RCIC pump QH curves.....	117
Figure 4-17 F1D2 RCIC pump NPSH curve.....	118
Figure 4-18 Pump head first quadrant map.....	120
Figure 4-19 Pump torque first quadrant map.....	120
Figure 4-20 Pump head homologous curves.....	122
Figure 4-21 Pump torque homologous curves.....	123
Figure 5-1 RCIC turbine power.....	127
Figure 5-2 RCIC turbine-pump rotational speed.....	127
Figure 5-3 Pump head.....	128
Figure 5-4 High pressure limit mass flow rates.....	128
Figure 5-5 Low pressure limit mass flow rates.....	129

Figure 5-6 Mass flow rates.....	130
Figure 5-7 S/C water level.....	131
Figure 5-8 Steam mass flow rate through vacuum breakers.....	132
Figure 5-9 S/C pressure.....	132
Figure 5-10 S/C temperatures at different heights.....	133
Figure 5-11 Turbine power.....	134
Figure 5-12 Pumped mass flow rate comparison.....	135
Figure 5-13 CST mass flow rate.....	136
Figure 5-14 Flooding level.....	137
Figure 5-15 Flooding effect on S/C pressure.....	138
Figure 5-16 Flooding effect on S/C temperature.....	138
Figure 5-17 Flooding effect on turbine power.....	139
Figure 5-18 RPV nodalization.....	141
Figure 5-19 Open/close loop RVP water level comparison.....	141
Figure 5-20 RPV pressure.....	142
Figure 5-21 Turbine power.....	143
Figure 5-22 Coolant temperatures.....	144
Figure 5-23 Cladding temperatures.....	144
Figure 5-24 Steam flashing effect on turbine fluid quality.....	146
Figure 5-25 Steam generated by flashing.....	146
Figure 5-26 Steam flashing effect on turbine power.....	147
Figure 5-27 Steam flashing effect on RPV water level.....	147
Figure 5-28 Steam flashing effect on RPV pressure.....	148

Figure 5-29 RELAP-SAMPSON-MAAP RPV pressure comparison.....	149
Figure 5-30 RELAP-SAMPSON-MAAP RPV water level comparison.....	150
Figure 5-31 RELAP-SAMPSON steam generated by flashing.....	150

List of tables

Table 1-1 RCIC specification data [6].....	10
Table 1-2 Fukushima Daiichi reactor specifications [11].....	15
Table 1-3 Severe accident codes characteristics [17].....	23
Table 2-1 RCIC Terry turbine schematics item list [7].....	35
Table 3-1 F1D2 plant specifications [11].....	59
Table 3-2 F1D2 water injection to the core [11].....	62
Table 3-3 Accident major event log [11].....	64
Table 4-1 RCIC specification data [6].....	113
Figure 4-2 Homologous curves configurations [34].....	123
Table 5-1 RCIC specification sheet [6].....	126

Abstract

Due to the Great East Japan Earthquake centered off the coast of Sanriku, which occurred on March 11, 2011, Units 1 to 3 of Fukushima Daiichi Nuclear Power Station (NPS) experienced severe accidents that not only went significantly beyond design basis, but also exceeded the extent of multiple breakdowns assumed in the preparation for accident management measures. The accident has been a wakeup call for nuclear safety and all the data recorded during the accident have been analyzed in depth in several investigation reports gathered in the Information Portal for the Fukushima Daiichi Accident Analysis and Decommissioning Activities.

Regarding Unit 2, investigation reports agreed that the accident progression was majorly conditioned by the RCIC (Reactor Core Isolation Coolant) system performance; The RCIC is initially designed to ensure that sufficient reactor water inventory is maintained in the vessel to permit adequate core cooling by providing a water makeup from either the CST (Condensate Storage Tank) or the suppression pool. This prevents the reactor fuel from overheating in the event that the reactor is isolated from the secondary plant. Usually, a RCIC trips at the reactor water level of L-8 (TAF + 5.65m) to prevent steam containing water droplets from flowing into the turbine. Therefore, the reactor water level never rises to the water surface of the reference leg. However, in case of Fukushima accident, due to the loss of DC power and the 70 hour operation time recorded by TEPCO, it is assumed that the stop order never arrived creating a two-phase flow situation in the turbine.

Another assumption made based on TEPCOs data is the flooding of the room surrounding the suppression chamber; the pressure increment in the drywell might be caused by an enhancement of the heat transfer caused by the presence of sea water outside the suppression chamber when the tsunami flood the room.

Steam turbines like RCIC one are designed to work under a single phase steam flow. In case of wet steam (steam + water) the phenomenology is more complicated, thus there are additional effects that should be taken into consideration; for example, the effect of the differing velocities between both phases.

Due to the lack of data caused by the Station Blackout (SBO) severe codes have been used to predict accurately the accident progression; the RELAP/ScdapSIM is one of the severe accident codes developed by the U.S. Nuclear Regulatory Commission (NRC) to describe the overall reactor coolant system (RCS), fission product generation and transport, core damage evolution and thermal-hydraulic response in severe accident scenarios.

The objective of this paper is focused on Fukushima Unit 2 analysis uncertainties originated from the RCIC operation which directly related with the RCIC turbine behavior. The most important analysis is based on the assumption that the turbine is underperformance due to the presence of water in the flow. A new model is developed with the consideration of two phase flow degradation. To quantify the moisture energy loss due to water Homogeneous Equilibrium Model (HEM) and Non-Homogeneous Equilibrium Model (NHEM) will be used, to set up a degradation coefficient (η_{HEM}) (η_{NHEM}) by calculating the output power using the velocity triangles at critical flow condition and at different upstream flow qualities and comparing them with the single phase flow.

The degradation coefficient has been applied to RELAP/ScdapSIM severe accident code in order to evaluate its effects on the turbine performance and resolve the problems to RCIC modeling which affect the Unit 2 accident analysis. Other phenomena are analyzed with RELAP/ScdapSIM these are the steam flashing phenomena; the sudden vaporization of the liquid into vapor due to quick expansion that drastically changes the flow quality and the flooding of the torus room.

The simulations reproducing the F1D2 accident were performed by using a complete new-brand RCIC nodalization being divided into open and close-loop configurations. For both configurations, the results show and verify the initial assumptions of constant RPV water level around the MSL height during the RCIC operation time. The main difference in the results during the first hours is due to the lack of pressure measurements which causes the open-loop configuration to lose some accuracy.

The results also show the turbine power reduction suffered by the RCIC turbine due to the water presence in the flow, this causes a reduction in the water pumped back to the RPV leading to the constant RPV water level previously mentioned and causing that the only

reduction suffered in the S/C water level is due to the steam flow to the Drywell through the vacuum breakers.

Regarding the flooding, the torus room flood greatly affected the S/C conditions but despite the relative large effect on the suppression chamber, the overall effect in the turbine, and consequently in the RCIC system, can be neglected.

On the other hand, the steam flashing indeed caused an effect on the computed results in the turbine and eventually increasing the RPV water level and reducing the RPV pressure. Despite the differences, though, no major behavior discrepancies are appreciated in the RPV water level or pressure behaviors.

Keywords: *Fukushima accident, RCIC system, steam turbines, two-phase flow, Homogeneous Equilibrium Model, Non-Homogeneous Equilibrium Model, RELAP/ScdapSIM, homologous curves*

Chapter 1 Introduction

1.1- Boiler Water Reactor history

The Boiler Water Reactor (BWR) is one of the most widely used reactors around the world. Classified as a light water reactor like the Pressurized Water Reactor (PWR) was initially developed by the Idaho National Laboratory (INL) and General Electric (GE) in the mid-1950s. The reactor, as a difference to PWR, is designed to heat the water until boiling conditions generating steam inside the pressured vessel; the steam is then driven to a turbine in order to generate electricity.

The initial concept of the BWR was developed in the decade of 50, slightly later than the PWR development, as collaboration between General Electric and several US national laboratories. The main impellers of the nuclear research in US were the 3 military services. The Navy seeing the opportunity to apply the results into military improvements for their vessels enhancing their operation time without refueling ordered Captain Hyman Rickover to lead their nuclear research program. Rickover chose the option of the PWR route for the Navy due to the advantages of the pressurized water in front of the boiler; some expert thought that the boiling water reactor might be unstable due to the direct steam generator meanwhile the pressurized water would perfectly match the military specifications of efficiency and space.

On the other hand, some researchers wanted to investigate deeper the truly effects of the steam generation instability will cause in the reactor performance and layout. During the early stages of investigation, a group of researchers prove the effect of steam generation inside the vessel by accidentally increase the power on an experimental reactor and observing their behavior. After this event Samuel Untermyer II from the Argonne National Laboratory proposed a set of experiments, the BORAX, to test the possibility to use the boiling water reactor to energy generating purposes stablishing the basis of the BWR.

After the success of those tests, GE got involved and collaborated with INL to develop this technology and bring it to market. During the decades of 50's and 60's larger test were

carried out using early designs were only a fraction of the generated steam was driven directly to feed the turbine and including heat exchangers for the generation of secondary steam to drive separate parts of the turbines. Those early designs were eliminated during the BWR production.

The current BWR characteristic features were set up during the development of the first generation of BWR; the torus room (used to heat down the reactor by extracting hot steam and injecting cold water), the drywell, the elimination of the initial heat exchangers, the addition of the steam dryer, the distinctive layout of the reactor and the standardization of the control and safety systems. Regarding the BWR, 6 major iterations were design by GE, BWR/1 through BWR/6, and the vast majority of reactors currently in use belong to one of these design phases.

- 1st generation: Includes mainly the BWR/1 with Mark I containment
- 2nd generation: BWR/2 to BWR/5 with either Mark I/II containment.
- 3rd generation: BWR/6 with Mark III containment.

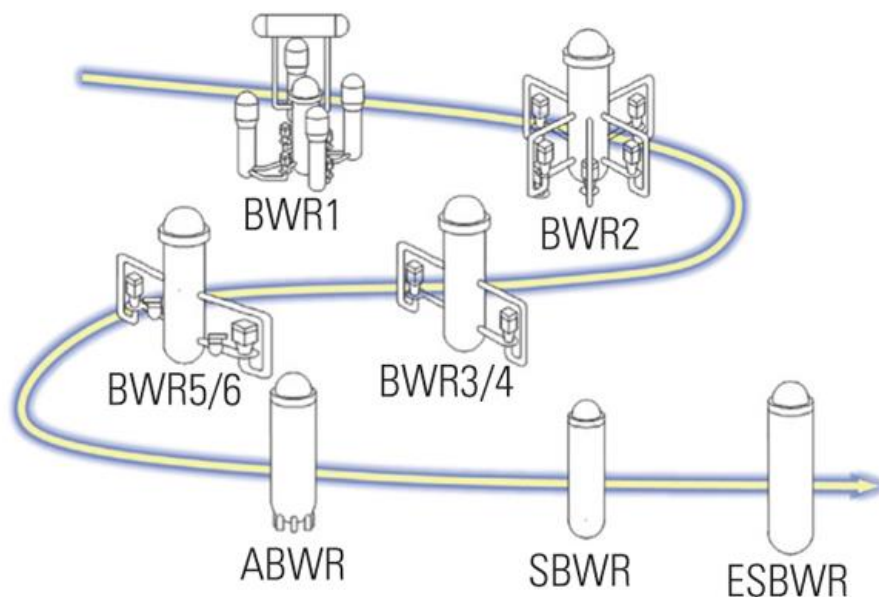


Figure 1-1 BWR development [1]

Figure 1-1 shows the evolution of the GE BWR reactors from BWR/1 to BWR/6. The new generation reactors include the Advances BWR, Simplified BWR and the Economic Simplified BWR.

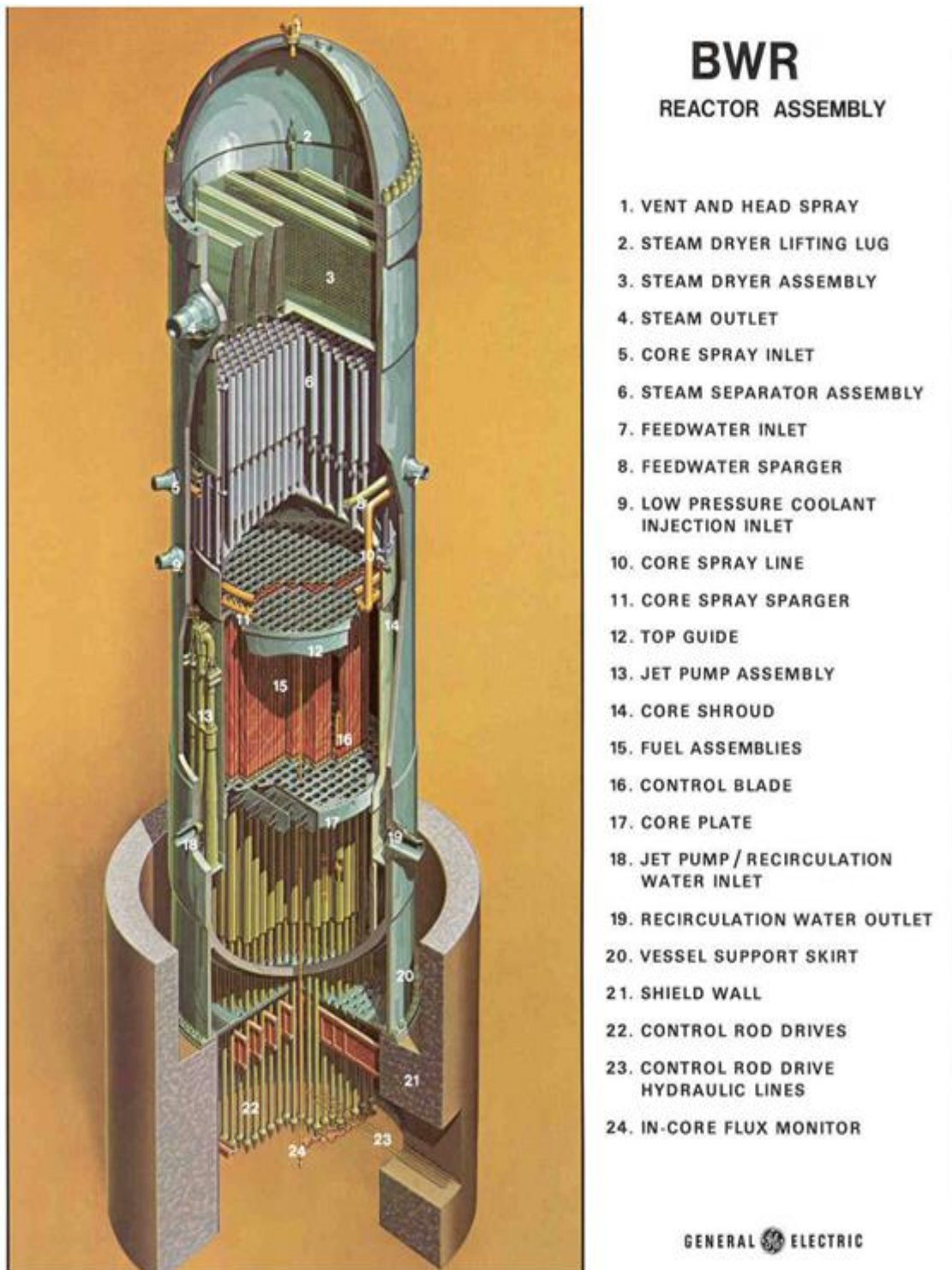


Figure 1-2 BWR core structure [2]

Figure 1-2 shows a cutaway view of the BWR core structure similar to the ones corresponding to Fukushima Units 1-6 reactors

1.2- Containment

Along with the evolution of the reactor design, the containment also suffered modifications. The nuclear power plant containment is mainly classified in one of the major containment designs; Mark I-II and III. Mark I is the specific containment of Fukushima Daiichi Unit 2 (F1D2) and it consists in a primary containment which its main elements are: [2]

- The Drywell: it is the area surrounding the Reactor Pressure Vessel (RPV) and the main recirculation loops. It is mainly a steel vessel reinforced with concrete
- The Wetwell: A huge steel made toroidal-shaped chamber located below the RPV and filled to about half of its height with water. It is also called the Suppression Chamber due to its function; cool down the hot steam from the RPV during some transients
- Venting system: A network system of venting path connecting both Drywell and Wetwell.

Figure 1-3 shows the Mark I containment cutaway view where the several elements can be clearly observed.

Mark I containments also include a secondary containment which surrounds the primary containment (Drywell+Wetwell) and also houses the spent fuel pool and the Emergency Core Cooling System (ECCS).

The containment is one of the safety layers of the Defense-in-depth, in conjunction with the cladding and the vessel/piping system, and its mainly functions are; condensate hot steam, hold the energy released during the postulated design-basis loss-of-coolant accident of any size so that offsite radiation doses specified in 10 CFR 100 are not exceeded, to provide a heat sink and water source for certain safety related equipment and protect the reactor from external hazards. It has to be able to maintain its integrity under the different loads caused by pressure, temperature and earthquakes

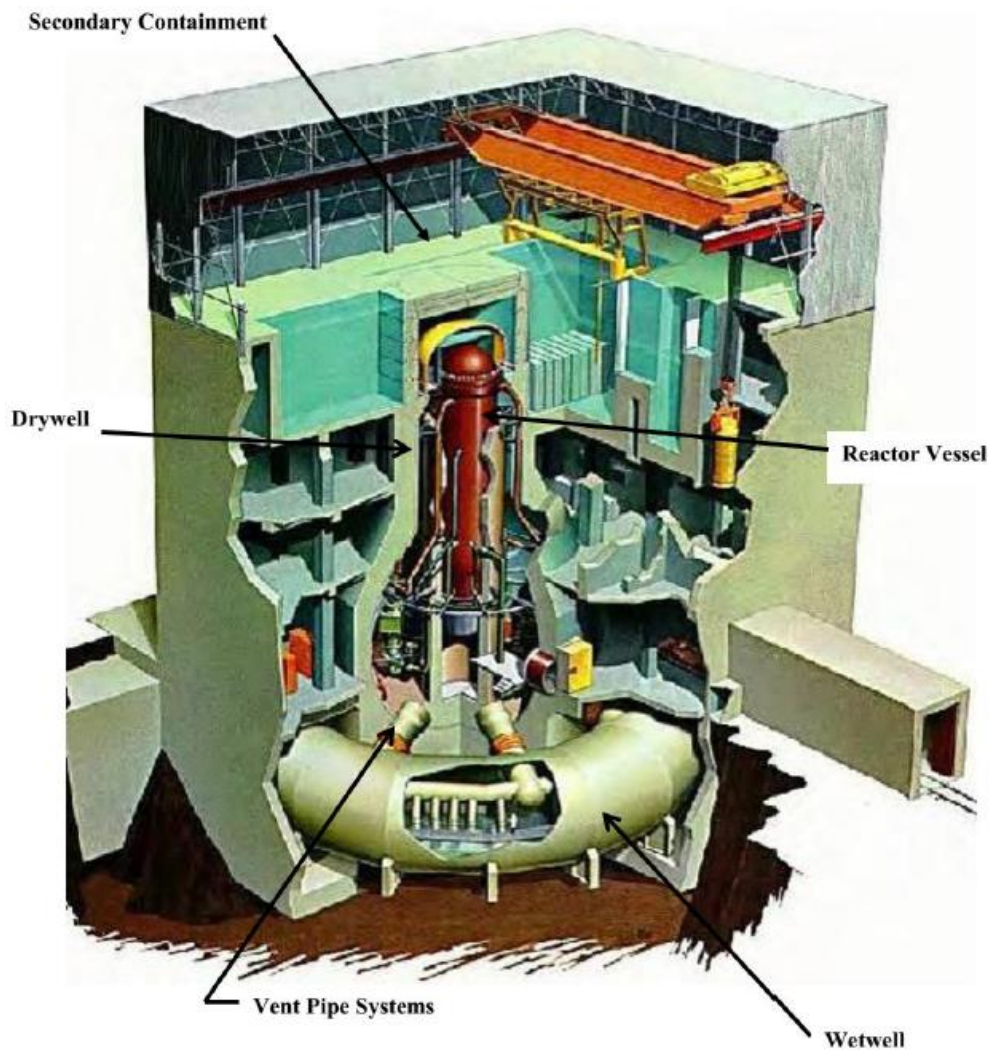


Figure 1-3 BWR Mark 1 containment [2]

1.3- Safety Relief Valves (SRV)

BWRs include several Safety Relief Valves (SRVs) in order to protect the primary system from over-pressurization (**Figure 1-4**). Each one with its own automatic opening and closing pressure setpoints being the closing pressure setpoint typically 50-100 psi (0.34 MPa to 0.69 MPa) lower than the opening setpoint. The SRV are valves which high flow capacities and through each of them can pass up to 6.5% of the full power steam flow. They can be operated remote-manually by use of control air. At low reactor vessel pressure, the flow through the valves can become unchoked. The depressurization transients that each valve produces before dosing causes the two-phase region to swell considerably. This increase in the level swell provides much better cooling to the

previously uncovered regions of the core and also provides considerable steam flow, an important parameter influencing the zirconium/steam reaction. As a result it is undesirable, in a best estimate sense, to model SRVs as devices which only limit the upper pressure at which the primary system can exist. The core thermal-hydraulics is heavily influenced by the SRV cyclical nature of operation. [3]

The open-close cycles at high temperatures may induce a failure of SRVs where the valve may seize in an open position resulting in the depressurization of the RPV, only in this case the blow down is directed to the suppression pool. According to the previous research, there is a possibility that the SRVs may lose its function and remain stuck open after 10 cycles of valve opening and closing above 1000 K [4].

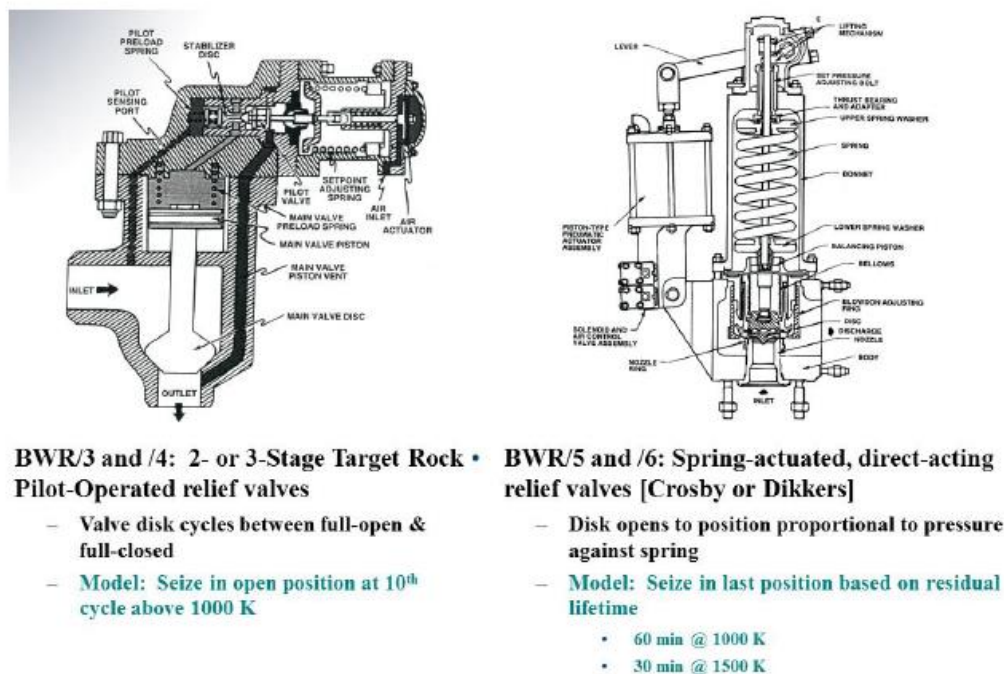


Figure 1-4 SRV [5]

1.4- Reactor Core Isolation Cooling system (RCIC system)

The Reactor Core Isolation Cooling system is an auxiliary system used for safe shut down of the plan. The system main objective is to supply enough water inventory into the reactor in order to keep the water level inside the vessel constant and to permit an adequate

cooling of the core. It is not part of the ECCS neither has a LOCA function. The RCIC operation prevents the fuel from overheating causing the core melting.

Figure 1-5 shows a simplified diagram of the RCIC. Once the main steam lines are isolated and the normal supply of water to the reactor vessel is lost a fraction of the generated steam created by the fission products (decay heat) is redirected in order to run the RCIC turbine. Then, the steam is driven into the suppression chamber (S/C) where is cooled down by the water mass. At the same time cold water is being pumped back by the RCIC pump into the reactor using the work generated by the RCIC steam turbine. The two sources of water are the Condensate Storage Tank (CST) and the S/C itself.

The normal operation behavior of the RCIC system is a cyclic based operation; the system is usually activated either due to RPV lower water level or manually, then the action of the RCIC causes an increment in the RPV water level (increment caused by the steam/water mass flow rate unbalance observed in **Table 1-1**). The RCIC is usually stopped due to RPV high water level signal once the water level reaches L-8 (TAF + 5.65m) height to prevent steam containing water droplets from flowing into the turbine. As it would be described later, in F1D2 accident the trip off signal never arrived due to the station blackout and the RCIC worked unstopped for almost 70 hours.

Table 1-1 RCIC specification data [6]

	RCIC design specifications	
	Upper pressure limit	Lower pressure limit
Pressure [MPa][abs]	7.83	1.14
Power [kW]	373.0	60.0
Speed [RPM]	4500	2000
Pump Head [m]	850.0	160.0
Water mass flow rate injected to RPV [kg/s]	26.0	26.0
Steam mass flow rate extracted from RPV [kg/s]	2.51	2.51

This operation continues until the vessel pressure and temperature is reduced to the point that the residual heat removal (RHR) system can be placed into operation.

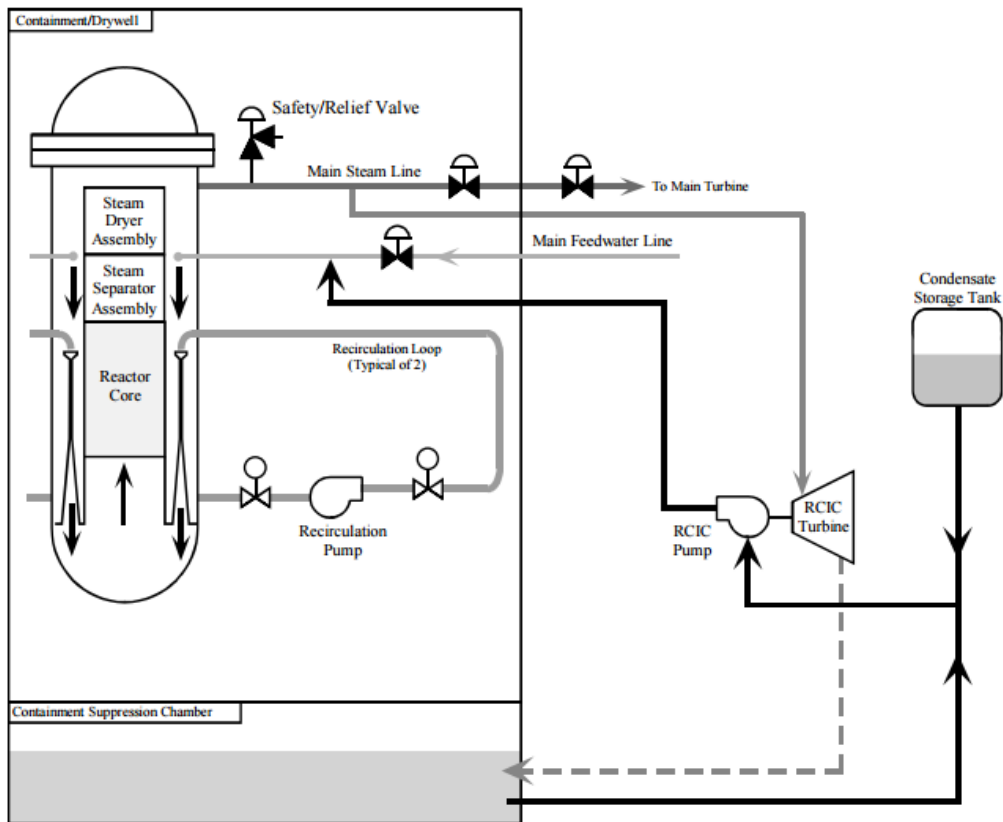


Figure 1-5 RCIC system diagram [2]

The main elements of the RCIC system are:

- Steam turbine: The RCIC system steam turbines are Dresser-Rand Terry-Turbodyne (Terry) helical impulse turbines designed for constant capacity over varying ranges of inlet steam pressure, typically 110 psi (75 bar) to 85 psi (5.85 bar) at a wide range of velocities (4700rpm to 2000rpm). RCIC systems are standby systems being off in normal plant operation and only running during accident conditions or during routine testing causing the turbine to be able to quick-start from cold without pre-warming or other operator option. [7]

The RCIC turbine will be deeper described in Chapter 2

- Suppression Chamber (S/C): Already described in the containment section (1.2), the S/C or Wetwell is a torus-shaped room of 30m of large diameter and 8m of small diameter. It has a major role in the RCIC acting as a heat sink for the hot steam coming from the RPV as well as a water source for the coolant make up. An important phenomenon that takes place inside the S/C is the thermal stratification.

The thermal stratification is the phenomenon caused by the injection of hot steam inside the cold water mass of the S/C; once the steam is injected it is driven upwards due to the density difference and being cooled down in the process. That creates a high temperature region at the upper section of the water pool meanwhile the lower section remains cold. **Figure 1-6** shows the temperature profile at different heights meanwhile **Figure 1-7** shows the S/C geometry.

- Pump: The RCIC pump is a horizontal, single stage turbine driven pump capable to move around 93m³/h with a pump head of 850m [6]. Being a turbine driven pump makes its water pumping capability dependent on the turbine generated power.

The RCIC pump will be deeper described in Chapter 4

- Residual Heat Removal: The RHR is an auxiliary system which one of its functions is the suppression pool cooling. The RHR ensures that the temperature inside the S/C just at critical scenarios (blowdown or high reactor vessel gauge pressure) never exceeds the predetermined limit (generally 77°C). The water from the suppression chamber is pumped into a recirculation loop which includes a heat exchanger where it is cooled down and returned to the S/C directly or via spray. The heat removed by the heat exchanger is transferred to the residual heat removal system service water. The S/C cooling function has to be activated manually. During the F1D2 accident, TEPCO reported the RHR was lost due to the station blackout. **Figure 1-8** shows the layout of the S/C cooling function of the RHR. [8][9]
- Vacuum breakers: The vacuum breakers are a set of valves located between the S/C and the Drywell have the function of equalize the pressure between them in case the steam generation in the S/C is higher than expected increasing the pressure out of control. They are triggered on once the pressure difference is higher than 25psi. [8][9]

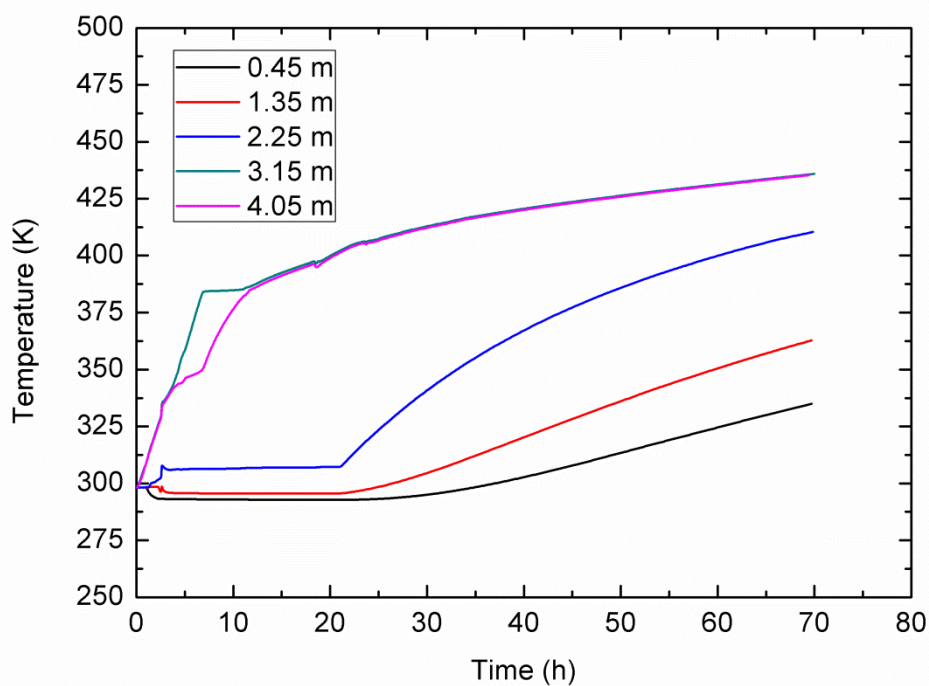


Figure 1-6 Suppression chamber thermal stratification

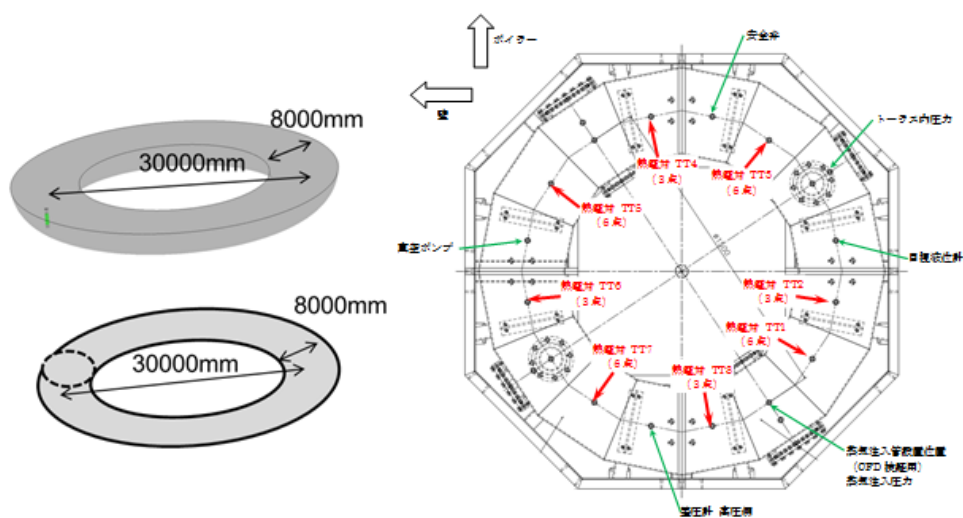


Figure 1-7 Suppression chamber geometry

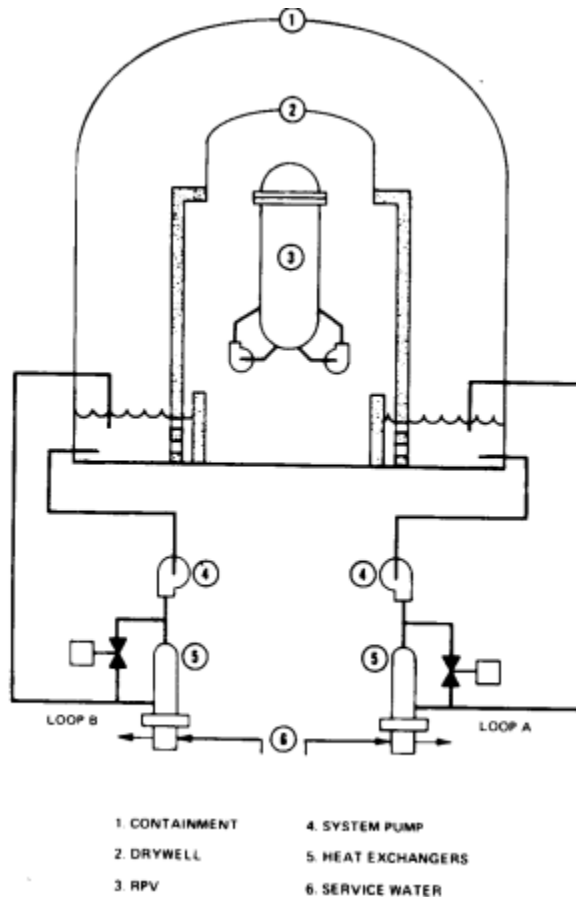


Figure 1-8 RHR suppression chamber cooling function layout [9]

1.5- Fukushima accident outline

On March 11, 2011, the Great East Japan Earthquake and the consequent tsunami affect several nuclear power plants around the country and triggered an extremely severe nuclear accident at the Fukushima Daiichi Nuclear Power Plant, which site map is displayed in **Figure 1-9**, owned and operated by the Tokyo Electric Power Company (TEPCO). Due to the final consequences this devastating accident was ultimately declared a Level 7 ("Severe Accident") by the International Nuclear Event Scale (INES). When the earthquake occurred three of the six reactors were operating meanwhile the rest were under stabilish periodical inspections; that is, Unit 1, 2 and 3 of the Fukushima Daiichi plant was in normal operation at the rated electricity output according to its specifications and Units 4 to 6 were undergoing periodical inspections. [10] **Table 1-2** describes the unit main specifications overview. [11]

Table 1-2 Fukushima Daiichi reactor specifications [11]

Unit	Unit 1	Unit 2	Unit 3	Unit 4	Unit 5	Unit 6
Reactor type	BWR/3	BWR/4	BWR/4	BWR/4	BWR/4	BWR/5
Containment	Mark-1	Mark-1	Mark-1	Mark-1	Mark-1	Mark-2
Electric power	460 MWe	784 MWe	784 MWe	784 MWe	784 MWe	1100 MWe
Commissioned date	26 March 1971	18 July 1974	27 March 1976	12 Oct. 1978	18 April 1978	24 Oct. 1979
Decommissioned date	19 April 2012	19 April 2012	19 April 2012	19 April 2012	31 Jan. 2014	31 Jan. 2014
Status March 11	Operating	Operating	Operating	Revision	Revision	Revision

The emergency shut-down feature, or SCRAM, went into operation at Units 1, 2 and 3 immediately after the commencement of the seismic activity. The seismic tremors damaged electricity transmission facilities between the TEPCO Shinfukushima Transformer Substations and the Fukushima Daiichi Nuclear Power Plant, resulting in a total loss of off-site electricity. There was a back-up 66kV transmission line from the transmission network of Tohoku Electric Power Company, but the back-up line failed to feed Unit 1 via a metal-clad type circuit (M/C) of Unit 1 due to mismatched sockets.

When the tsunami caused by the earthquake arrived one hour later it was higher than expected, overwhelming the sea level barriers and flooding and totally destroying the emergency diesel generators, the seawater cooling pumps, the electric wiring system and the DC power supply for Units 1, 2 and 4, resulting in loss of all power—except for an external supply to Unit 6 from an air-cooled emergency diesel generator. In other words, Units 1, 2 and 4 lost all power; Unit 3 lost all AC power, and later lost DC before dawn of March 13, 2012. Unit 5 lost all AC power. The tsunami did not damage only the power supply but also destroyed or washed away vehicles, heavy machinery, oil tanks, and gravel along with destroyed buildings, equipment installations and other machinery. Seawater from the tsunami inundated the entire building area and even reached the extremely high pressure operating sections of Units 3 and 4, and a supplemental operation common facility (Common Pool Building). After the water retreated, debris from the flooding was scattered all over the plant site, hindering movement and delaying the power backup and water injection operations. Manhole and ditch covers had disappeared, leaving gaping holes in the ground. In addition, the earthquake lifted, sank, and collapsed building interiors and pathways, and access to and within the plant site became extremely difficult.

Recovery tasks were further interrupted as workers reacted to the intermittent and significant aftershocks and tsunami.

The station blackout led to the sudden loss any control equipment such as scales, meters and the control functions in the central control room. Lighting and communications were also affected making the communication between the personnel extremely difficult. All this events force the personnel to make critical decisions on spot without any kind of references or manuals making it very difficult to effectively cool down the reactors in a timely manner. Generally, cooling the reactors and observing the results were heavily dependent on electricity due to the auxiliary systems used for high-pressure water injection, depressurizing the reactor, low pressure water injection, the cooling and depressurizing of the reactor containers and removal of decay heat at the final heat-sink. During the accident, however, the staff had almost no way to check the effect of their decisions into the reactor behavior. The lack of access, as previously mentioned, obstructed the delivery of necessities such as alternative water injection using fire trucks, the recovery of electricity supply, the line configuration of the vent and its intermittent operation.

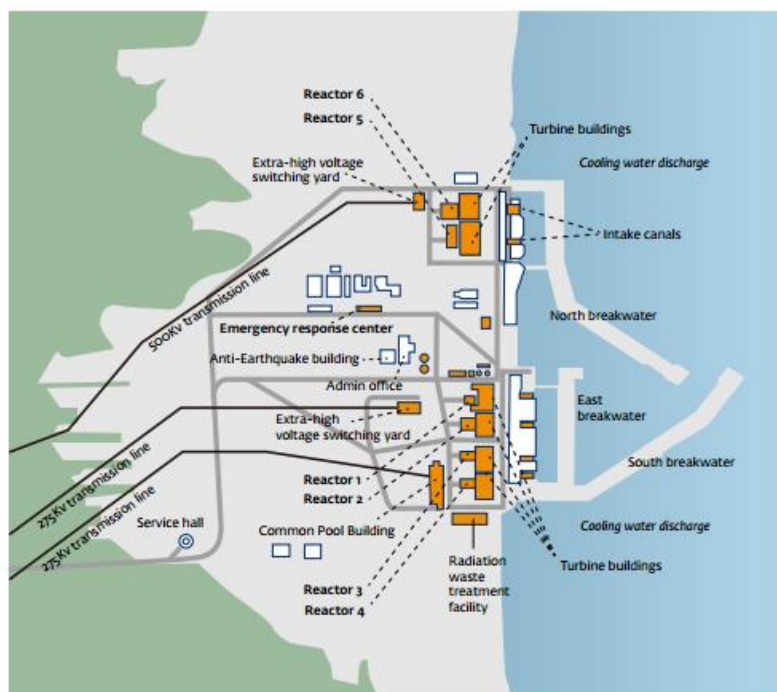


Figure 1-9 Fukushima Daiichi site map [10]

1.6- Simulation codes

After the TMI2 accident in 1979 the development of computer codes for simulation of severe accidents (SA) scenarios suffered a huge acceleration, starting in the United States and then spread progressively in the 1980s in Europe and Japan. The SA codes can be divided into three major categories, depending on their scope of application: integral codes, detailed codes, and dedicated codes [12].

- Integral codes (also called engineering-level codes): These codes have the larger scope of application, and they are used to simulate the overall nuclear power plant response, that is, the response of the reactor coolant system, the containment, and, most important, the source term to the environment, using —integrated models for a self-consistent analysis of the accident [12]. They include a combination of phenomenological and parametric models for the simulation of the relevant phenomena. The principal internationally used codes today are MAAP, MELCOR, and ASTEC.
- Detailed codes (also called mechanistic codes): They are characterized by best-estimate phenomenological models, consistent with the state of the art, to enable, as far as possible, an accurate simulation of the behavior of an NPP in the event of SA. In order to better illustrate the differences with the approach of integral codes, in most cases, a numerical solution is found for integral-differential equations, while in integral codes some correlations may be used [12].
- Dedicated codes: The scope of these codes is centered on the simulation of a single phenomenon. They have become important in the context of the requirements that regulatory authorities take into account SAs in the design of new NPPs and that the uncertainties of risk-relevant phenomena be reduced [12].

MELCOR, RELAP/Scdap, MAAP are three of the most used computer codes developed in the U.S. that are being widely used for the integral analysis of core melt accident progression and the resultant lower head response expected at the reactor lower plenum: MELCOR and RELAP/Scdap were initially developed by NRC meanwhile MAAP is an industrial code [13]. The main difference between them is that RELAP5/ScdapSIM can only model the in-vessel phase of the SA, while MAAP4 is capable to calculate processes in the

containment following the release of water, non-condensable gases, and corium from the primary circuit [12].

Table 1-3 displays a summary of the three codes with their main features and differences

1.6.1- MAAP

The Modular Accident Analysis Program (MAAP) is an integral severe accident code initially developed by Fauske and Associates (FAI) in the early 80s as a part of the Industry Degraded Code Rulemaking (IDCOR) project, which was funded by EPRI. The programs principal goal was to satisfy the needs of a reliable tool for use in developing physical studies and providing the severe accident consequences for conducting Probabilistic Risk Assessment/Probabilistic Safety Assessment (PRA/PSA) studies. [13]

MAAP code has been evolving since its early versions and now, the current version of the code, MAAP4, can simulate the response of light water reactor NPP, even if it is based on advanced light water reactor designs (ALWR), in a wide range of accident sequences, independent of the initial conditions of the installation; full power or shutdown conditions. There are two different versions of the code, one used for BWR and another used for PWR (also exists other versions for less used reactors such as CANDU or VVER)

MAAP4 functional modeling is particularly adapted to investigate the impact of operator actions taken as part of accident management on the progression of sequences. MAAP4 can be used for the PSA level 2 studies supporting the elaboration of SAM procedures and for the design of mitigation systems.

The last version of the code released by FAI (MAAP4.0.7) was released in January 2008. It includes several major models developed to support EPR design. The models are listed below.

- Modeling of boron carbide thermal-chemistry (degradation, oxidation, and melting of B₄C).
- Modeling of core heavy reflector, including thermal attack, penetration by molten material, and corium draining down the side of the core barrel.

- Modeling of core heavy reflector, including thermal attack, penetration by molten material, and corium draining down the side of the core barrel.
- Improvement of energy transfer from core debris to vessel and concrete during accumulation of corium in the reactor pit.
- Discharge of corium in the spreading compartment after breach of the melt plug.
- Diversity of floor and wall configurations in the reactor pit and spreading area, including concrete composition and heat removal from the bottom of the structural heat sinks.
- Modeling of AREVA NP PARs.
- Improvement of the pressurizer relief tank rupture and pressurizer breaks.

1.6.2- RELAP/ScdapSIM

The RELAP/ScdapSIM is one of the severe accident codes developed by the U.S. Nuclear Regulatory Commission (NRC) to describe the overall reactor coolant system (RCS), fission product generation and transport, core damage evolution and thermal-hydraulic response in severe accident scenarios.[14]

The code was initially developed at the Idaho National Laboratory (INL) under the sponsorship of the Office of Nuclear Regulatory Research of the NRC as a part of the international Scdap development and training program (SDTP).

The two primary modules of RELAP/Sdap severe accident code are the RELAP5 module, acronym for Reactor Excursion and Leak Analysis Program, and the Scdap module, acronym for Severe Core Damage Analysis Package. The RELAP5 part takes care of the overall RCS thermal-hydraulics, reactor kinetics, non-condensable gases transport and the control system interactions calculations. It is based on a two-fluid model solved either by a semi-implicit or nearly-implicit numerical processes to allow economical calculations of system transients with unequal temperatures and velocities of the different phases.

On the other hand, the Scdap module is related to the core behavior during a severe accident. The module includes calculations for the fuel rod heat-up, deformation and rupture, oxidation, fission product generation and transport, Zirconium-Uranium

interactions, flow and freezing of molten fuel and cladding, and debris formation processes.

The followings are some of the modeling strengths of the code:

- An integral diffusion method to calculate oxygen and hydrogen uptake accounting in mechanistic manner for steam starvation and rapid changes in temperature.
- Calculation of the relocation in the circumferential direction of melted metallic cladding retained by the oxide portion of cladding.
- Calculation of the re-slumping of cladding that previously slumped and froze.
- Calculation of heat transfer in porous debris using correlations specific to porous debris.
- Calculation of flow losses in porous debris locations based on Darcy's Law and applying relative permeabilities and possibilities based on local debris conditions and volume fractions of the liquid and vapor phases of the coolant.
- Calculation of oxidation of both intact and slumped cladding under reflood conditions.
- Calculation of the heat up of the lower core structures and its interaction with slumping core material
- Calculation of the behavior of jets of core material penetrating into a pool of water.
- Calculation of the permeation of melted core plate material into porous debris in the lower head of reactor vessel and effect of this permeation on lower head heat up, and melting pools.
- Calculation of the permeation of melted core plate material into porous debris in the lower head of reactor vessel and effect of this permeation on lower head heat up, and melting pools.
- Calculation of heat up of lower head containing melted core material and accounting for whether the melted material is well-mixed or stratified into oxidic and metallic pools.
- A semi-mechanistic stress-based model instead of a wholly empirical model for failure of the oxide portion of cladding retaining melted metallic cladding, and more simplistic but accurate models for calculating position, configuration, and oxidation of melted fuel rod cladding that slumped to a lower location and froze.

The INEEL version is currently a frozen version and it would not receive any further update by the NRC, currently is only used at PSI for various analyses. The ScdapSIM version however, which initially is based on the NRC version is being maintained and in constant development. SCDAPSIM in parallel to the NRC version is in use.

1.6.3- MELCOR

MELCOR is a severe accident code developed by Sandia National Laboratory (SNL) in 1982 at it has been updated to several versions since then. It is a state-of-the-art computer code, which enables to simulate the severe accident progression postulated for light water reactors. The development has been almost entirely funded by the USNRC and its development has been strongly influenced by the participation of several international NRC partners through the USNRC's Severe Accident Cooperative Research Program (CSARP).

MELCOR is used in institutes around the world for analyses mainly focused on the BWR and PWR, despite its capability to be applied to other reactors and non-reactor facilities or scenarios (spent fuel pools, active handling areas and so on).

MELCOR validation has been the hot topic of numerous studies at all levels; process, component, subsystem and whole-plant due to the wide range of phenomena covered. Those studies made MELCOR better, making it the capability to reproduce with accuracy the evolution of bundle temperatures (with the use of four thermocouples). The discrepancies on the maximum rod temperatures are about 100 to 200K; underestimation on the first peak after the oxidation runaway, and overestimation in the next phase of bundle degradation.

MELCOR latest version, 1.8.6, includes models for silver release and in-vessel melt pool evolution [15]. The latter capability makes it possible to perform realistic estimates of lower head failure and to solve issues such as the focusing effect of metallic layers on heat transfer from corium in the lower head to the vessel walls and in-vessel retention by external cooling of the vessel.

In order to achieve a more complete and consistent account of the in-vessel behavior, the treatment of the vessel structures should be extended. A further generalization of the core

material models may be necessary to simulate the inter-component interactions, as concluded in the Phebus experiments FPT4, which showed the strong effect that the B_4C control rod has on the degradation in the surrounding fuel rods. The treatment of the B_4C oxidation of gas-phase chemistry can furnish the conditions of organic iodine formation in the circuit. To solve that, an improved model is under development for Zircaloy cladding oxidation in air or steam-air mixtures, which is essential for its effect on the certain fission product volatility. Regarding the error of MELCOR prediction, despite it is challenging to assess the prediction error of the calculation results, the code includes a bunch of correlations and empirical models to simulate the severe accident. [16]

The initial applications were centered on broad source term evaluation and PSA support, but, with the time, they have been extended to new areas such as accident management, mitigation, spent fuel issues, and operation training. The original simple treatments that were adequate for scoping and bounding calculations are being substituted by more physically based models. Among the questions being addressed now are whether to use igniters or passive autocatalytic recombiners for hydrogen control, and whether to inject available water within the vessel or flood the cavity.

The code has been improved to be able to simulate new scenarios

- Accidents in glove box facilities
- Accidents in reactor auxiliary buildings
- Accidents in nuclear warhead disassembly facilities
- Assessments of fire in nonnuclear buildings

This wider range of applications forces an improvement in the detail level and fidelity in representing physical processes. Models with more detailed nodalizations are now used to resolve certain issues such as the effect of natural circulation in the vessel on core damage progression, the effect of countercurrent flow in hot legs and steam generator pipe rupture. These extensions are consequently with the model developments previously mentioned.

Table 1-3 Severe accident codes characteristics [17]

Code	MAAP	MELCOR	RELAP/SCDAP	SAMPSON	THALES2
Developer	US EPRI	US NRC	US INEL→ Society	NUPEC(IAE)	JAEA
Objective	In + Ex-Vessel		In-Vessel	In + Ex-Vessel	In + Ex-Vessel
Functions	No models on hydrogen explosion and steam explosion			Various areas in a hypothesized core melt event	No models on hydrogen explosion and steam explosion
Number of choosing parameter	A lot	A lot	Few	Few	A lot
Simulation time	Short	Several times faster than the real time	1/2~1/4 of real time	20~30 times slower than the real time	Several times of real time.

Table 1-3 Severe accident codes characteristics (cont.) [17]

Characteristics	(1) Users can adjust the calculation results by adjusting the choosing parameters (2) Simulation results might different from users to users	In-Vessel models are similar to SAMPSON code Simplified models for core relocation are used comparing to SAMPSON	Based upon computer simulation with using fundamental physics principles and sophisticated modeling technologies	Thermal-hydraulics and FPs transport analysis for LWRs under severe accident. PSA analysis
V&V of the code modeling	Continuous improvements	Continuous improvements	OECD/NEA International benchmark problem (ISP: International Standard Problem) Continuous improvements	OECD/NEA International benchmark problem (ISP: International Standard Problem) Continuous improvements
				Continuous improvements made by JAEA

1.7- Severe accident management

The Severe Accident Management (SAM) birth was after the Chernobyl and TMI accidents when the community realized the effect of the dynamic losses in the containment that can caused its failure, SAM can be defined as the use of existing and alternative resources, systems and actions to arrest and terminate accidents that exceed the design basis of a nuclear power plant. [12]

In addition, a severe accident is defined as a Beyond Design Basis Accident (BDBA), an accident that excess the design basis concerning initiating events or number of failures [], with significant coder degradation.[18]

Under these conditions, the principal objectives of severe accident management are as follows:

- Terminate core degradation
- Ensure containment integrity
- Mitigate radiological releases

And generally, accident management actions should include [19]

- Establish and maintain reactivity control
- Ensure availability of a heat sink for the heat generated in the core
- Depressurize the primary heat transport system
- Maintain coolant inventory in the primary heat transport system
- Control pressure and water inventory in steam generators (for PWR)
- Ensure containment isolation
- Control the containment pressure and temperature
- Control the concentration of flammable gases
- Control radioactive releases

The Severe Accident Management Guidance (SAMG) are a written decision guidance documents designed to support the Emergency Response Organization (ERO), and specially the decision-making part of the ERO, the emergency Response Team (ERT), during severe accidents in order to achieve the objectives listed above.

SAMGs are not only a written decision-making guidance; they also include other helpful tools, such as calculational guidance and computer simulation models to support that decision-making. In many EROs, a SAMG Group reporting to the ERT typically uses these tools. Finally, the SAMG includes procedures for implementing the SAM measures.

SAMG provides a structured guidance to identify the appropriate strategy and subsequent actions needed to stabilize and return the plant to a controlled stable condition against a severe accident condition. In the standpoint of successful severe accident mitigation strategies, they necessitate effective operator actions established through validated analysis and practice. In particular, successful operator actions may delay or prevent RPV and containment building failures [12].

1.8- Objectives

The study is principally focused on the two-phase flow RCIC turbine behavior and how it affected to the overall RCIC system performance during the F1D2 accident. Both, numerical and simulation analyses are done to explain how the RCIC turbine was capable to work during 70h beyond its basis design parameters allowing the RCIC system to delay the core degradation

The objectives are summarized below:

- Analyze the Fukushima Daiichi Unit 2 accident progression focused on the RCIC system performance
- Analyze the RCIC turbine behavior under two-phase flow
 - Numerical analysis based on the data recorded by TEPCO
 - Computational analysis using RELAP/ScdapSIM

Chapter 2 Steam turbine design

Steam turbines are an indispensable element in the energy generation facilities such as the nuclear power plants. A steam turbine might be described as a kind of heat engine in which the energy of the fluid is first converted into kinetic energy by means of expansion through the nozzles, and then transformed into force doing work when the fluid impacts the rotating blades of each stage. [20] [21]

The usual steam turbines consists of four principal elements: the rotor which carries the blades or buckets; the stator consisting basically in the cylinder and casing, which are usually combined and within the rotor is placed; the nozzles or flow passages which are usually fixed inside the cylinder; and the frame or base used to support both, the stator and rotor.

The previous elements are generally supported by accessories necessary for the successful commercial operation such as the governing system for adjusting the energy supply to the turbine to suit the load and for maintaining constant speed, the lubricating system, piping for steam supply and exhaust and a condensing system.

The steam turbines can be classified based in several criterions depending on their features [20]

- Form of blade passages
- General arrangement of the flow
- Steam flow direction relative to plane of rotation
- Repetition of steam flow through blades
- Rotational speed
- Relative motion of rotor
- Steam and exhaust conditions

2.1- RCIC steam turbine

The RCIC system is an auxiliary system which only enters into operation during accident transients or routine testing. Under these conditions, the RCIC turbines require to be able to quick-start from cold conditions with no pre-warming or other operator action.

The RCIC turbine is a Terry turbine model, which schematics are shown in **Figure 2-1** and **Figure 2-2**. Following the previous classifications for steam turbine, the RCIC turbine can be classified as an impulse, single-flow, axial, with reentry, single-motion and back pressure turbine presenting some advantages due its features. [7]

- Rugged one-piece wheel construction
- Good resistance to degraded steam conditions
- Minimal axial thrust steam loads under all operation conditions
- Suitability for required cold, quick-start transients

Steam enters the RCIC turbines through a single governor valve. Steam is then directed into an individual high-pressure steam ring, which is an integral part of the turbine casing. Expanding nozzles then direct the steam tangential into the turbine's solid-wheel buckets where its direction is reversed 180°. Reversing chambers, located at each nozzle, cause the steam to re-enter the turbine wheel several times, thereby utilizing most of the steam's available energy.

All Terry RCIC applications use a solid wheel design of 610mm in a G turbine frame size. The frame can be divided in GS-1 or GS-2 models indicating lower-half steam admission only (GS-1) or both upper- and lower-half admission (GS-2) depending on the output requirements of the application; power, rotating speed and the specific operating steam conditions. [7]

The turbine is designed based on the pressure conditions in the RPV; mainly three pressures are associated with RCIC systems

- The maximum pressure which is the required design pressure of the inlet components of the turbines and is only reached under severe accident transients. Its values is around 8.6MPa

- The normal pressure is the steam pressure available at the turbine under normal operating conditions with a range from 6.2 to 8.1MPa
- The low pressure is used for the thermodynamic design of the turbine. Corresponds to the lowest pressure and is typically around 0.58 to 1MPa

As mentioned, the low pressure is used for thermodynamic design. Typically, the power at that inlet conditions determines the necessary steam flow capability and, consequently, the governor valve size, the number and size of the nozzles and the frame size. [7]

The low-pressure design criterion yields a design with a considerable excess steam flow capability, an consequently a excess of power, at high pressure conditions causing an extreme acceleration during startup and resulting in the RCIC turbine governor valve to operate nearly closed (20% of the full area or less).

These turbines also operate a wide range of rotational speed. Their design bases for low-speed operation is usually fixed around 2000-2500rpm while the values for high-speed are around 4000-4700rpm. These requirements are coupled with the additional request of, cold, quick-start capability with the rated flow within 30 to 90 seconds. [7]

For the required quick-start control, a Woodward EG-type control system configuration is used. This configuration, when properly installed, calibrated and maintained, allows controlling the required quick-start transients on the turbine, as well as the steady-state. It is important that the control system would be able to sense turbine speed below 1000rpm and to limit its maximum speed to avoid overspeed transients. In the case of control system failure, the turbine is usually provided with an overspeed trip protection set up at velocity around 10% to 25% above the normal maximum velocity.

The most common issues related the steam supply are related with the presence of water in the flow. Due its characteristics, the Terry turbine can generally handle of receiving water carryover from the RPV without sustaining damage. However, experience has demonstrated that transients under two-phase flow can result in loss of system operability due to control system problems and turbine overspeed trips.

The most common scenario is when the water starts to move through the turbine decreasing the output power, and then the control system opens further the governor valve. This procedure causes an overspeed once the water has passes and pure steam

passes again through the turbine. An alternative scenario is caused by the steam flashing of the water due to the pressure drop causing an increment of speed. [7]

The RCIC system suppose a containment penetration which connects the RPV and the S/C so several valves have to be added in the RCIC supply and exhaust lines. Two isolation valves are added to the supply line, one inboard and one outboard the primary containment, with appropriate automatic closing signals. Analogously, isolation valves are also added to the exhaust line.

As noted in the RCIC diagrams, the exhaust line of the RCIC turbine discharge under water. During turbine operation, the temperature in the discharge area is increased due to the steam injection. This causes, during the turbine shutdown and consequent coldown, vacuum formation drawing water into the exhaust line. This condition has the potential for a water hammer cycle against the valves which is increased as the height between the injection point and the S/C water level is decreases. To avoid that, vacuum breakers are added to protect the valves. In addition to the vacuum breakers, most BWR RCIC turbine exhaust lines have been provided with underwater condensing spargers, to further stabilize the turbine exhaust pressure during system operation.

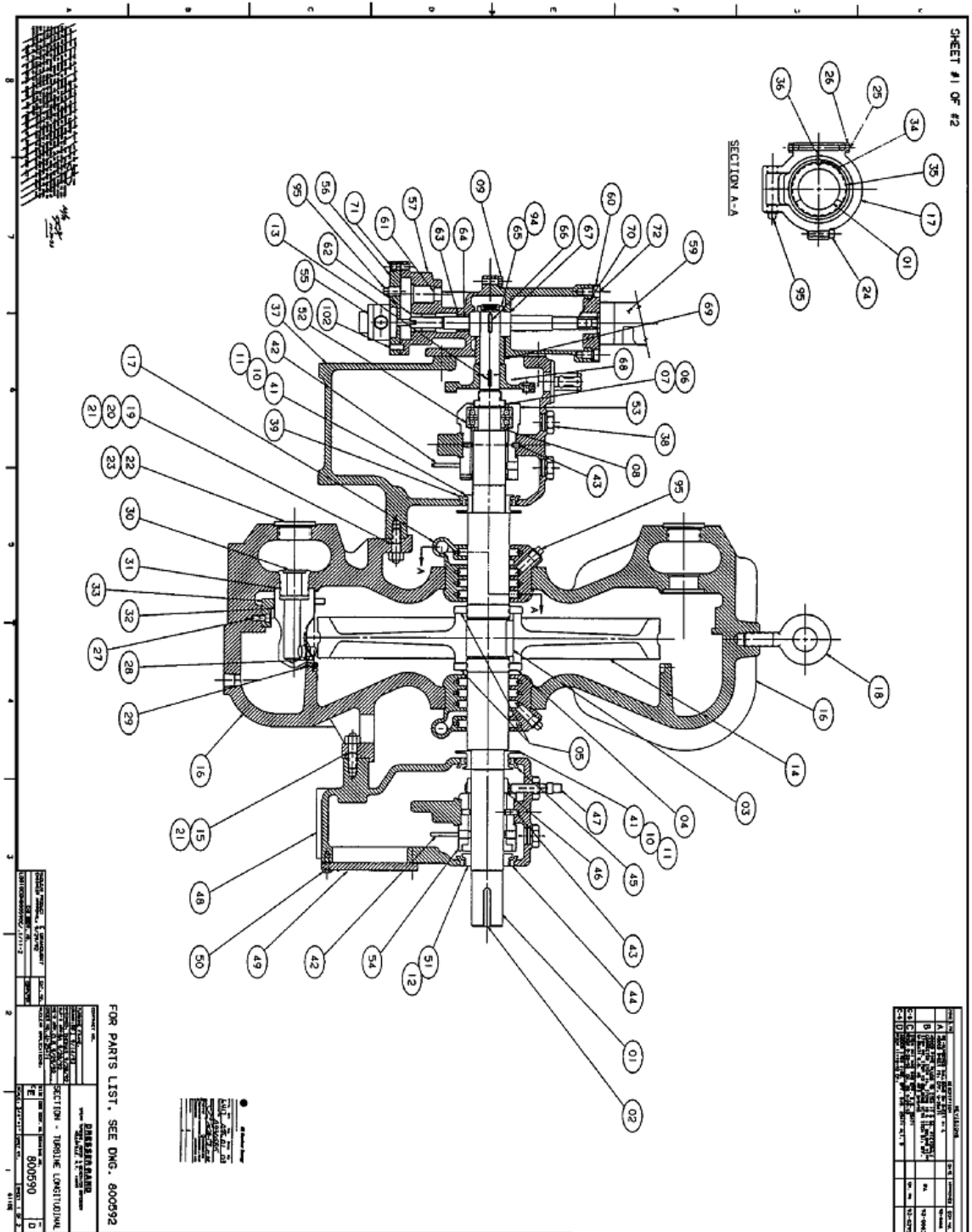
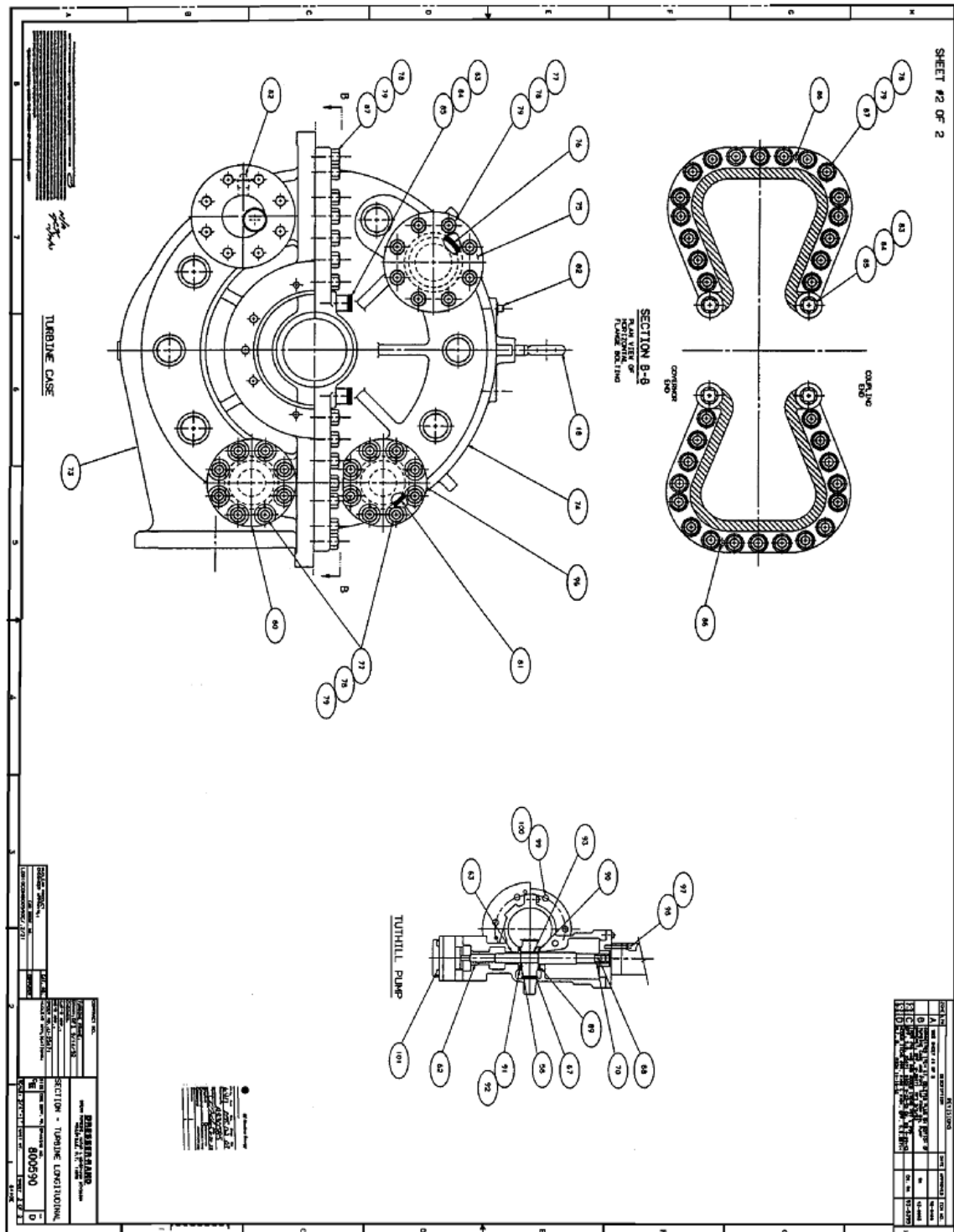


Figure 2-1 RCIC Terry turbine schematics 1 [7]



The elements of the turbine described in **Figure 2-1** and **2-2** are listed below [7]

Table 2-1 RCIC Terry turbine schematics item list [7]

Item No.	Description	Item No.	Description
001	Turbine Shaft	041	Thrust Collar
002	Coupling Key	042	Oil Ring
003	Wheel Key	043	Journal Bearing Alignment Pin
004	Wheel Nut	044	Oil Seal
005	Locking Setscrew	045	Oil Seal
006	Thrust Bearing Locknut	046	Speed-Sensing Spur Gear
007	Thrust Bearing Lockwasher	047	Magnetic Speed Pickup
008	Thrust Bearing Spacer	048	Coupling End Pedestal
009	Pump Bracket Joint Screws	049	Coupling End Pedestal Flange
010	Thrust Collar Pin	050	Pedestal Flange Hex Head Screw
011	Thrust Collar Setscrew	051	Oil Deflector
012	Oil Deflector Setscrew	052	Ball Thrust Bearing
013	Overspeed Trip Disc Key	053	Governor End Journal Bearing
014	Turbine Wheel	054	Coupling End Journal Bearing
015	Coupling End Pedestal Stud	055	Shaft-Driven Oil Pump
016	Turbine Case Assembly	056	Pump Case Cover
017	Gland Case Assembly	057	Pump Bracket and Cap
018	Lifting Eye Bolt	058	Truarc Retaining Ring
019	Governor End Pedestal Stud	059	Electric Governor Remote – (EG-R) Hydraulic Actuator
020	Governor End Pedestal Stud	060	EG-R Hydraulic Actuator Adapter
021	Pedestal Stud Nut	061	1 in. NPT Pipe Plug
022	Steam Jet Plug	062	Drive Shaft Lower Bushing
023	Steam Jet Plug Gasket	063	Drive Shaft Upper Bushing
024	Gland Case Socket Head Screw	064	Drive Shaft
025	Gland Case Fitted Stud	065	Spiral Drive Gear Locknut
026	Gland Case Fitted Stud Nut	066	Spiral Drive Gear Key
027	Chamber Support Ring Screw	067	Spiral Gear Assembly
028	Reversing Chamber	068	Overspeed Trip Disc Assembly
029	Reversing Chamber Screw	069	Spiral Gear Spacer
030	Jet Body Holder	070	EG-R Hydraulic Actuator Coupling
031	Jet Body Flexitallic Gasket, R4-9F	071	Pump Case Cover Screw
032	Jet Body Assembly	072	Actuator Adapter Plate Screw
033	Reversing Chamber Support Ring	073	Lower-Half Turbine Casing
034	Carbon Ring Spring	074	Upper-Half Turbine Casing
035	Carbon Ring	075	Steam Ring Blank Flange
036	Carbon Ring Stop	076	Steam Ring Blank Flange Gasket
037	Governor End Pedestal	077	Steam Ring Blank Flange Stud
038	Inspection Plug	078	Steam Ring Blank Flange Nut
039	Oil Seal	079	Steam Ring Blank Flange Washer
040		080	Steam Ring Blank Flange

Item No.	Description
081	Steam Ring Blank Flange Gasket
082	Steam Ring Plug
083	Turbine Casing Joint Allen Nut
084	Turbine Casing Joint Washer
085	Turbine Casing Joint Stud
086	Turbine Casing Joint Dowel Pin
087	Turbine Casing Joint Stud
088	Actuator Coupling Roll Pin
089	Upper Thrust Washer Screw
090	Upper Thrust Washer
091	Lower Thrust Washer
092	Lower Thrust Washer Screw
093	Spiral-Driven Gear Key
094	Spiral Drive Gear Locknut Setscrew
095	Pipe Plug
096	Steam Ring Blank Flange
097	EG-R Hydraulic Actuator Stud
098	EG-R Hydraulic Actuator Stud Nut
099	Pump Bracket Hex Head Cap Screw
100	
101	Oil Pump Socket-Head Cap Screw
102	Oil Pump Dowel Pin

In order to be able to analyze the turbine response under two-phase flow and develop a turbine degradation coefficient it is mandatory to know some of the geometric parameters of the RCIC turbine. These parameters, the nozzle area (A_{cr}) and the inlet/outlet angles (α, δ) of the blade, are estimated (since the real values are not available) based on the nozzle and blade design equations assuming the same single phase conditions described in **Table 1-1**.

2.1.1- Nozzle design

As explained early in this chapter, the turbine first uses the nozzles to extract the largest amount of steam energy into kinetic energy evidenced by the high velocity of the issuing jet. By steam available energy is meant the maximum work which a perfect steam engine could produce when receiving steam at nozzle inlet conditions; pressure, velocity an temperature and discharging it at nozzle outlet pressure.

In order to describe the fundamental equation of the energy transformation suffered in the nozzle relating the change of state of the steam passing through the nozzle to the

kinetic energy at the exit, assume that frictionless adiabatic flow is moving from and infinite reservoir R through a large cylindrical pipe A into a smaller pipe B as shown in **Figure 2-3**.

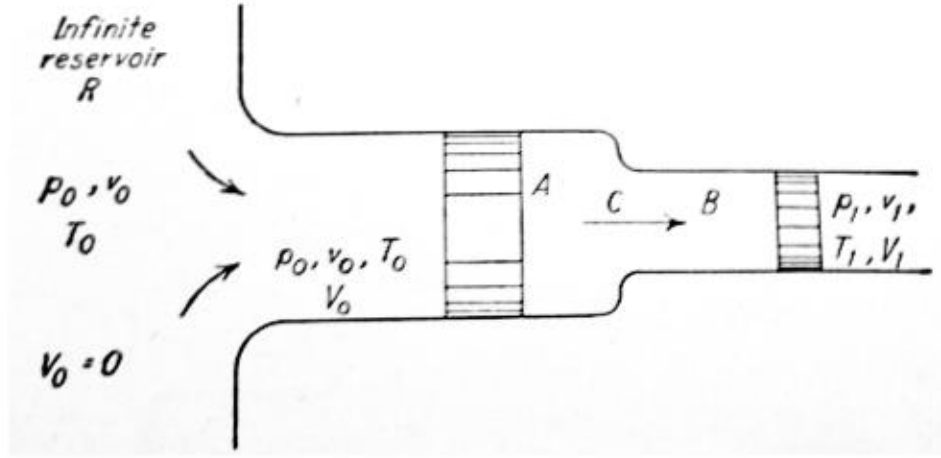


Figure 2-3 Principle of fluid expansion in nozzle [20]

The reservoir conditions are designated by the subscript 0, the pipe A by 0 and the pipe B by 1. If frictionless pistons are imagined in each cylinder such as described in **Figure 2-3**, it is logic that the piston in A will exert a specific pressure p_0 on the steam in front of it generating a work for each kg of steam as described in equation 2.1

$$E_o = p_o v_o \text{ [J/kg]} \quad (2.1)$$

Where

E_o : Is the external work generated by the pressure. [J/kg]

p_o : Is the pressure. [Pa]

v_o : Is the specific volume of the steam. [m^3/kg]

Analogously, the piston in B will exert a similar work. If the steam internal and kinetic energies are also considered, the energy conservation equation in the expansion suffered by the steam from pipe A to pipe B is for a steady flow

$$\text{Internal energy}_0 + \text{external work}_o + \text{kinetic energy}_0 = \text{internal energy}_1 + \text{external work}_1 + \text{kinetic energy}_1 \quad (2.2)$$

Rearranging the equation terms and substituting, equation 2.2 becomes

$$h_o + \frac{V_o^2}{2} = h_1 + \frac{V_1^2}{2} \quad (2.3)$$

Where:

V_o : Is the steam velocity at A. [m/s]

V_1 : Is the steam velocity at B. [m/s]

$h_o - h_1 = \Delta h_s$: Is the available energy, or isentropic decrease of enthalpy. [J/kg]

Analogously, the equation between reservoir (point 0) and A (point o) will be the same as equation 2.3, with the difference than the velocity in the reservoir is zero ($V_o = 0$) since the fluid is at rest.

Now imagine the real nozzle in the RCIC turbine. It causes an expansion of the steam flow (m_1) between an upstream pressure (0) and downstream pressure (1) as described in **Figure 2-4**. The convergent nozzles such as the ones used in the RCIC turbine are usually design to achieve critical conditions on the exit creating a chocking plane.

The chocking effect on a system is generally defined as the maximum mass flow rate as a function of downstream pressure and it has been widely studied. [20][22]

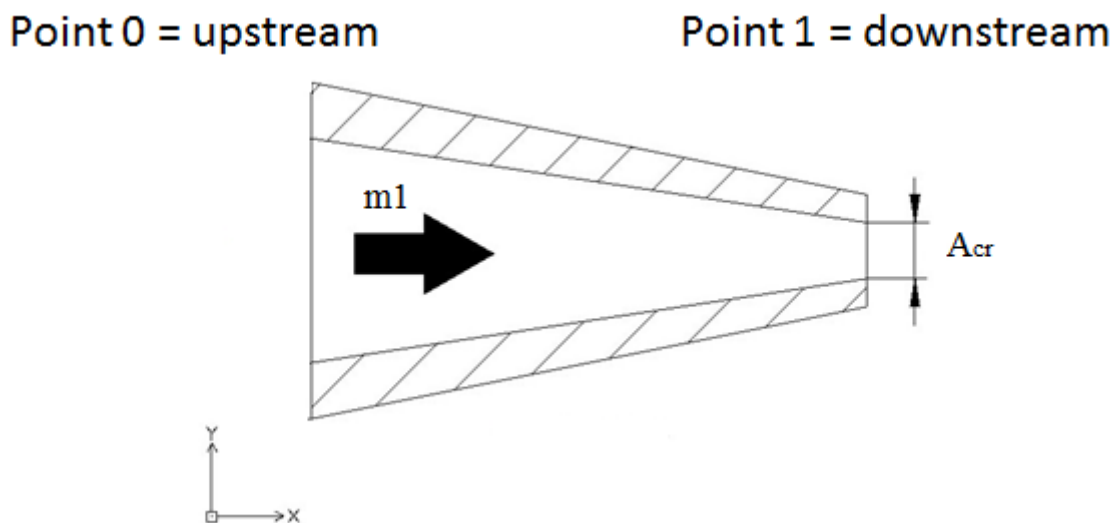


Figure 2-4 Convergent nozzle schematic

Reducing the downstream pressure (p_1) promotes the flow of fluid through the nozzle at a rate which increases with pressure drop until the velocity at some point in the connector achieves the local sonic velocity forming a choked plane at that location. The pressure at that plane is known as critical pressure p_c and corresponds where the area is minimum (A_{cr}). The ratio between the critical pressure p_c and the upstream pressure p_0 for single phase flow, called the critical pressure ratio (p_c/p_0), can be deduced from the ideal gas equation and it is different for each gas. For saturated steam, the critical pressure is usually given by equation 2.4

$$p_1 = p_{cr} = 0.577p_0 [Pa] \quad (2.4)$$

At critical point, the critical mass flow rate (\dot{m}_{cr}) and the critical area (A_{cr}) are related by the ideal gas equation rearranged into equation 2.5. [20][22]

$$\dot{m}_{cr} = A_{cr} * \sqrt{n * p_0 * \rho_0} * \left(\frac{2}{n+1} \right)^{\frac{n+1}{2*(n-1)}} [kg/s] \quad (2.5)$$

Where

p_0 : Is the pressure upstream. [Pa]

ρ_0 : Is the steam density upstream. [kg/m^3]

n : Is the specific heat. For saturated steam = 1.135

Applying the mass conservation, $\dot{m}_{cr} = \dot{m}_1$ and it is equal to the steam mass flow rate that appears in the RCIC specific sheet summarized in **Table 1-1**

Using equations 2.4 and 2.5, the nozzle area and the fluid velocity at the nozzle exit can be calculated.

2.1.2- Blade design

The blades form part of the rotor and are the elements used to convert the kinetic energy generated by the nozzle into work due its interaction with the fluid. The work generated depends on the blade geometry.

Assume a frictionless blade that modifies the flow direction by 180° and left the fluid with no velocity at the exit such as the geometry described in **Figure 2-5**. This configuration represents the greatest conversion achievable of kinetic energy of the entering flow into blade work [20].

Using **Figure 2-5** a general relationship between the blade velocity and the inlet flow velocity can be developed allowing to design the blade which provide the maximum energy conversion, or, in other words, the maximum efficiency. [20]

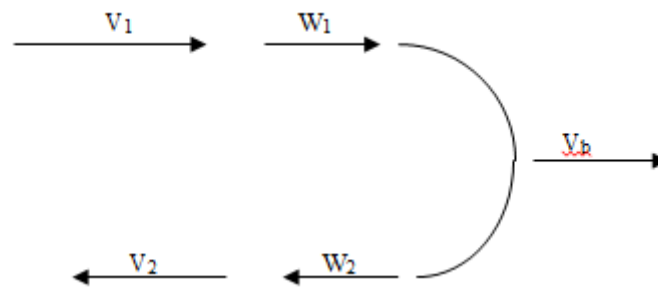


Figure 2-5 Principle of blade design [20]

Where

V_1 / V_2 : Are the inlet/outlet absolute flow velocities. [m/s]

W_1 / W_2 : Are the inlet/outlet relative flow velocities respect the blade. [m/s]

V_b : Is the velocity of the blade. [m/s]

Since the blade is frictionless $W_1 = -W_2$. In addition, the outlet absolute flow velocity is assumed to be zero ($V_2 = 0$). Then the relationship between the inlet velocity and the blade velocity is expressed by equation 2.6.

$$V_1 + V_2 = W_1 + W_2 + 2V_b \rightarrow V_1 = 2V_b \quad (2.6)$$

The angle between the inlet velocity and the blade velocity is called the nozzle angle (α), which in **Figure 2-5** is equal to zero. In a real turbine, due to physical constraints, the nozzle angle must be greater than zero but not so great as to cause an appreciable loss in efficiency. Nor should the angle be so small as to cause an excessively long nozzle that would increase friction and decrease efficiency.

Then, equation 2.6 becomes

$$V_1 \cos \alpha = 2V_b \text{ [m/s]} \quad (2.7)$$

Equation 2.7 describes the theoretical value of V_1 , the actual values is usually increased around 10% of the theoretical values due to disk friction and fanning losses [20]

Once the inlet flow velocity, the nozzle angle and the blade velocity are calculated the velocity triangles can be developed. **Figure 2-6** shows generic velocity triangles for inlet and outlet conditions. The velocity triangles are a useful tool to determine the change in absolute tangential velocity and calculate the shaft work.

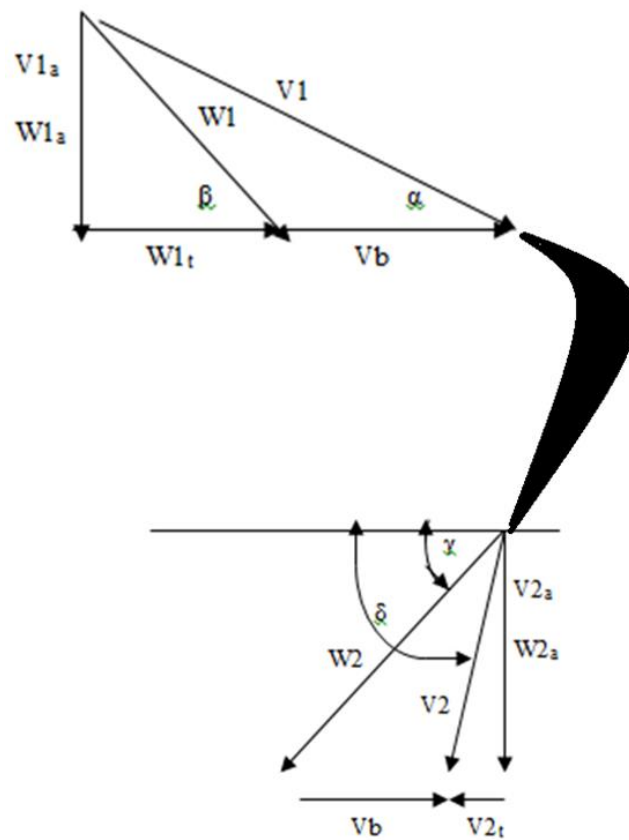


Figure 2-6 Generic velocity triangle diagram

The entrance velocity triangle consists of a horizontal line representing the tangential direction. Then we construct a vector representing V_1 at angle α , after which the entering triangle using the vector relation between the velocities. The angle between the relative velocity and the tangential direction is designated β .

The exit velocity triangle is somehow developed using the same principle, draw W_2 at angle γ to the previous tangent which values is found by multiplying W_1 by the velocity coefficient, k_b , which accounts for friction and turbulence.

The velocity coefficient is a function of the total change of direction of the steam in the blade $[180^\circ - (\beta + \gamma)]$; the blade width to radius ratio; and the relative velocity and density at blade entrance. Due to the lack of data regarding the RCIC turbine for the design, the following empirical formula described in equation 2.8 is used. [20]

$$k_b = (0.892 - 6.00 \times 10^{-5} W_1)^{1/2} \quad (2.8)$$

The following formulas are just a numerical description of the velocity triangles by using the basic trigonometrical rules.

$$\begin{aligned} V_{\theta 1} &= V_1 \cos \alpha & W_2 &= k_b W_1 \\ V_{a1} &= W_{a1} = V_1 \sin \alpha & V_{a2} &= W_2 \sin \gamma \\ W_{\theta 1} &= V_{\theta 1} - V_b & W_{\theta 2} &= W_2 \cos \gamma \\ W_1 &= \sqrt{W_{a1}^2 + W_{\theta 1}^2} & V_{\theta 2} &= V_b + W_{\theta 2} \\ \beta &= \tan^{-1} \frac{W_{a1}}{W_{\theta 1}} & V_2 &= \sqrt{V_{a2}^2 + V_{\theta 2}^2} \end{aligned} \quad (2.9)$$

With equation 2.7 and the trigonometric formulas gathered in equation 2.9, the nozzle angle (α) and the exit angle (δ) can be calculated.

2.2- RCIC steam turbine degradation coefficient calculation

As mention in Chapter 1, the RCIC system is designed to ensure that sufficient reactor water inventory is maintained in the vessel to permit adequate core cooling by providing a water makeup from either the CST or the S/C. This prevents the reactor fuel from overheating in the event that the reactor is isolated from the secondary plant. Usually, a RCIC trips at the reactor water level of L-8 (TAF + 5.65m) to prevent steam containing water droplets from flowing into the turbine. Therefore, the reactor water level never rises to the water surface of the reference leg. However, in case of Fukushima accident, due to the loss of DC power and the 70 hour operation time recorded by TEPCO [11], it is assumed that the stop order never arrived creating a two-phase flow situation in the turbine.

Steam turbines like RCIC one are designed to work under a single phase steam flow. In case of wet steam (steam + water) the phenomenology is more complicated, thus there are additional effects that should be taken into consideration; for example, the effect of the differing velocities between both phases. Soderberg (1933) analyzed the moisture losses in different turbines and proved the reduction of the velocity of the moisture compared with the single phase.

In a normal steam turbine, the blade angles have been designed to fit the steam velocity vector. Water, even assuming a correct inlet angle, due to its properties would easily adhere to the blades, moving outward toward the tips on account of centrifugal force. Since this phenomenon takes place over the entire blade it will lead to a larger moisture concentration being incremented at each successive stage.

Although some water would be trapped by the called water catchers, the rest of the water will lose almost all its kinetic energy leading to a reduced energy of the moisture. The water presence not only reduces the turbine efficiency due to the reduction in the moisture energy but also poses a danger of intense to the turbine's steam path. The water erosion in the turbine is accompanied with the corrosion process due to the impurities such as chlorides and sulfates on the working fluid. These impurities present in the water are also adhered to the blade causing zones of high concentration of corrosive elements. []

Several analysis have been done regarding the RCIC performance during Fukushima Unit 2; TEPCO [11][23] and the Institute of Applied Energy (IAE) [24] stated the incongruence between the simulation results and the onsite measured data.

In their analysis, TEPCO [23] fail to reproduce the reactor pressure vessel (RPV) pressure due to the difficult to quantitatively evaluate the water injection capability of RCIC in a two-phase flow scenario. For their results they assumed that the water injection flow was smaller than the rated flow due to a lower rotational speed and they simply fixed the flow rate of RCIC to $30 \text{ m}^3/\text{h}$, which is about one-third of the rated flow rate of $95 \text{ m}^3/\text{h}$.

IAE [24] also assumed degradation in the turbine due to water presence. They used an iteration process based on a numerical analysis of the RCIC system to fit their simulation results to the TEPCO data obtaining a reduction factor for the turbine as a function of the void fraction of the flow.

2.2.1- Critical flow model description

The idea behind the theory of the critical flow is quite simple. Assuming a system, such as a BWR RPV, containing fluid and connected to a receiver, such the suppression chamber (which is at lower pressure and temperature), via a flow path.

The pressure expansion suffered by the fluid due to upstream (RPV) and downstream (S/C) pressure conditions will increase the flow rate between them until a maximum value is achieved, at this point, a further increment of the pressure different will not affect the flow rate of the fluid which is critical. In critical conditions, the flow rate is independent of the downstream conditions and this lack of influence can be explained by mechanisms, such as the formation of perturbation in the flow. [25][26]

The critical flow of a single-phase ideal gas has already been discussed earlier in this chapter. It usually happens when the Mach number is equal to one at the smallest cross-section [22]

On the other hand, the critical flow in two-phase flow is a more complicated phenomenon. The influence of nucleation, heat, mass and momentum transfer as well as the evolution of the flow pattern are comparable with the period spent by the fluid in critical conditions. Although it can be possible to define mathematically the critical conditions at one specific location, an entire area, which can include sections of the upstream region, plays a major role determining how this condition is approached. [27]

Two-phase flow critical models are usually divided into the following three categories.

- Analytic models.
- Fitted functions.
- Numerical solution of the conservation equations.

2.2.2- Homogeneous Equilibrium Model

The HEM (Homogeneous Equilibrium Model), Henry and Fauske (1971)[28], is based on the assumption of isentropic and equilibrium flow. In this model, the two-phase flow mixture is treated as a pseudo-fluid which can be described by the same single phase equations. In this pseudo-fluid, both phases are in perfect equilibrium having the same

velocities and temperatures; properties such as enthalpy, entropy and quality can be obtained by using the general Steam tables. [25-27]

HEM has been the basis of several severe accident codes, like the early versions of RELAP/Scdap, for LOCA analysis involving two-phase flow fluids.

Despite HEM has a good average accuracy predicting the critical flux, it has some flaws that have to be considered.

- It loses accuracy in short pipes where the fluid does not have enough time to reach the equilibrium between both phases.
- It loses accuracy when the pseudo-fluid is representing a low quality mixture. One of the assumptions of the Hem is that both phases have the same velocities. Although it can be true at high quality flow rates where the small water droplets can be easily carried by the steam flow it is not true when the water phase becomes larger.

To calculate the critical mass flux at a given conditions the turbine has to be assumed as a black box with fixed upstream and downstream (throat) pressure and flow quality properties. **Figure 2-7** displays a basic diagram describing these assumptions.

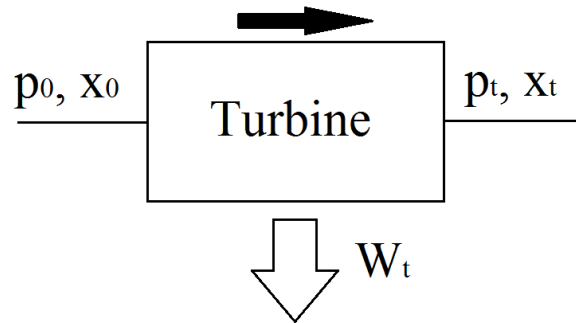


Figure 2-7 Turbine thermal hydraulic concept

In the HEM, the mass flux is calculated using equation 2.10 which depends on the upstream and downstream conditions show in **Figure 2-7**. The objective is to maximize the mass flux with respect to pressure ($\frac{dG}{dp} = 0$). The process followed to accomplish it, is to fix the desired upstream pressure p_0 and quality x_0 and swipe the parameter p_t using random values between 0 and p_0 ($0 < p_t < p_0$) and plot the resulting mass flux. [27]

$$G = \sqrt{[2 * \rho_t^2 * (h_0(p_0, x_0) - h_t(p_t))]} \quad (2.10)$$

Where:

G : Is the mass flux [$\text{kg/s}\cdot\text{m}^2$]

ρ_t : Is the density downstream (throat) [kg/m^3]

h_0 : Is the enthalpy at upstream which depends on the upstream pressure (p_0) and quality (x_0)

h_t : Is the enthalpy at downstream (throat) assuming and isentropic expansion in the turbine. It depends on the downstream pressure (p_t)

The properties at downstream are calculated using the equations 2.11 to 2.13

$$x_t = \frac{s_0 - s_l}{s_v - s_l} \quad (2.11)$$

$$h_t = h_l + x_t * h_{lv} \quad (2.12)$$

$$\rho_t = \rho_l + x_t * \rho_{lv} \quad (2.13)$$

Where:

x_t : Is the quality downstream (throat)

s_0 : Is the entropy upstream [$\text{J/kg}\cdot\text{K}$]

s_l : Is the saturated water entropy at downstream pressure (p_t) [$\text{J/kg}\cdot\text{K}$]

s_v : Is the saturated steam entropy at downstream pressure (p_t) [$\text{J/kg}\cdot\text{K}$]

h_t : Is the enthalpy downstream [J/kg]

h_l : Is the saturated water enthalpy at downstream pressure (p_t) [J/kg]

h_{lv} : Latent heat at downstream pressure (p_t) [J/kg]

ρ_t : Is the density downstream [kg/m^3]

ρ_l : Is the saturated water density at downstream pressure (p_t) [kg/m^3]

ρ_{lv} : Is the steam-water density change at downstream pressure (p_t) [kg/m^3]

Figure 2-8 shows the mass flux resulting from the application of HEM equations 2.10 to 2.13 for several flow qualities $0 < x_0 < 1$ and an upstream pressure (p_0) of 7.83 MPa.

The maximum value of mass flux for each curve, called G_c , corresponds to the mass flux under critical conditions. Using the mixture specific volume at G_c conditions, the mixture velocity of sound can be obtained for each quality. This velocity corresponds to the inlet velocity (V_1) in the turbine velocity triangle.

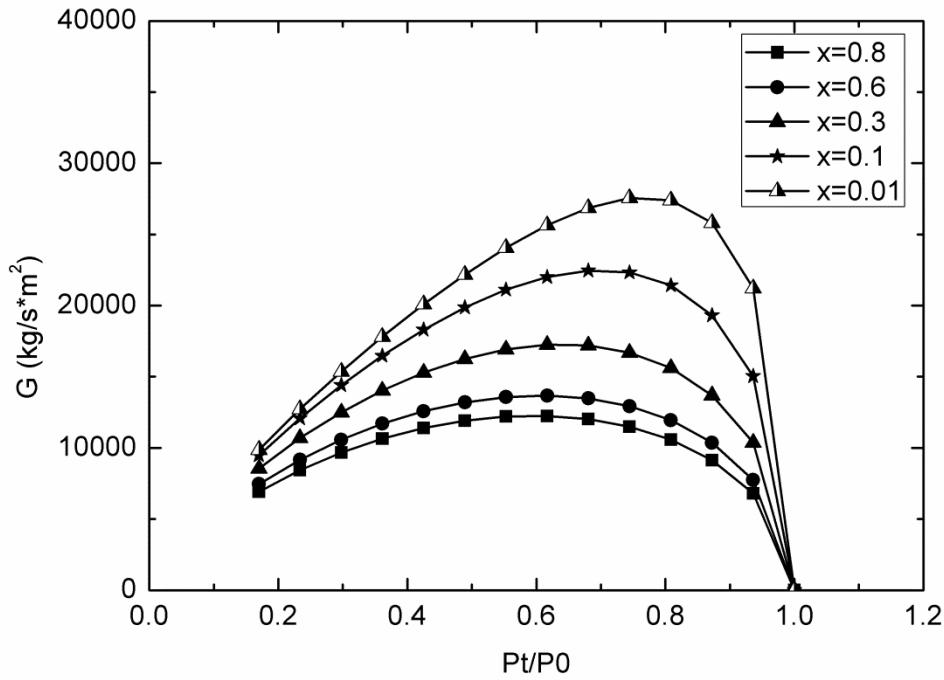


Figure 2-8 HEM mass flux calculation

For each upstream quality (x_0), the velocity is

$$V(x_0) = G_c * \frac{1}{\rho_t} \quad (2.14)$$

Where:

G_c : Is the mass flux at the maxim point of the curve. [$\text{kg/s} \cdot \text{m}^2$]

ρ_t : Is the density downstream corresponding to the pressure (p_t) related with the maximum mass flux (G_c). [kg/m^3]

Figure 2-9 shows the HEM pseudo-fluid velocity behavior as a function of the quality and the pressure at saturated conditions. [29]

Once the fluid velocity corresponding to the critical mass flux is calculated, the critical flow rate as well as rest of the velocities components of the turbine blade velocity triangles can

be obtained by applying the turbine geometry parameters found by applying the equations 2.7 to 2.9.

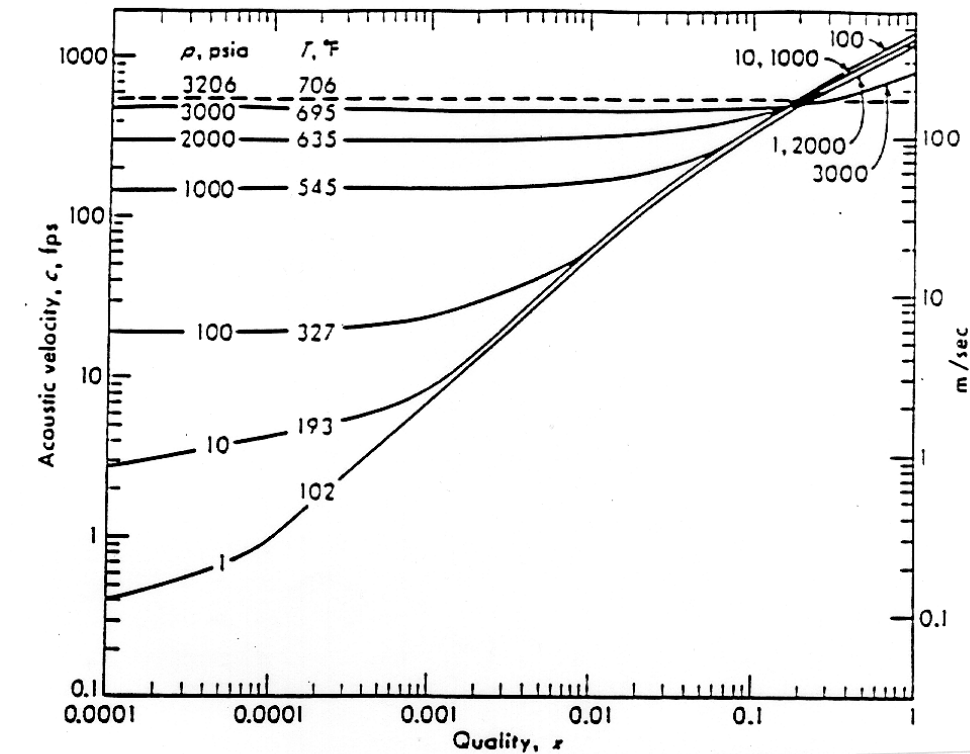


Fig. Theoretical values for the velocity of sound in equilibrium, homogeneous

Figure 2-9 HEM pseudo-fluid velocity calculation [29]

2.2.3- Non-Homogeneous Equilibrium Model

The NHEM model (Non-homogeneous equilibrium model), originally developed by Moody (1965)[27], is an derivation of the HEM (Homogeneous Equilibrium Model) created by the addition of other limiting assumptions. This avoids the necessity of taking any account of the details of the non-equilibrium phenomena.

The NHEM allows different velocities between vapor and liquid phases. The slip ratio, S , is defined as the ratio between velocities. This ratio is also considered as a variable which determines the conditions of maximum mass flux. The mass flux can be described by equation 2.15.

$$G = \sqrt{[2 * \rho_t^2 * (h_0(p_0, x_0) - h_t(p_t))]} \quad (2.15)$$

Where:

G : Is the mass flux [kg/s*m²]

ρ_t : Is the density downstream (throat) [kg/m³]

h_0 : Is the enthalpy at upstream which depends on the upstream pressure (p_0) and quality (x_0)

h_t : Is the enthalpy at downstream (throat) assuming and isentropic expansion in the turbine. It depends on the downstream pressure (p_t)

The process is analogous to the one described for the HEN; find the critical mass flux (G_c) at a given conditions fixing the upstream conditions p_0 and x_0 , and then swipe p_t using values from $0 < p_t < p_0$ and plot the corresponding G .

The downstream density is dependent on S

$$\frac{1}{\rho_t} = \left[\frac{x_t}{\rho_g} + \frac{S * (1 - x_t)}{\rho_l} \right] * \left[x_t + \frac{1 - x_t}{S^2} \right]^{\frac{1}{2}} \quad (2.16)$$

Where:

ρ_g : Is the saturated steam density at downstream [kg/m³]

ρ_l : Is the saturated water density at downstream [kg/m³]

x_t : Is the downstream quality

S : Is the slip ratio

Considering the different equations, it can be noticed that the mass flux not only depends on pressure but also on the slip ratio, S . Assuming that G should not only be maximized with respect to pressure but also with respect to the slip ratio leads to the inclusion of a new restrain $\left. \frac{dG}{dS} \right|_p = 0$ (with a negative second derivative). This leads equation 2.15 to yield at maximum flow conditions.

$$S = \left(\frac{\rho_l}{\rho_g} \right)^{1/3} \quad (2.17)$$

The slip ratio used for this research, which is described in equation 2.17 minimizes the specific kinetic energy of the two-phase mixture. There are other theoretical values, like the slip ratio formulated by Fauske (1962) which minimizes the specific two-phase flow momentum would be discussed but not applied in the calculations.

It is also possible to use a variable slip ration and solve the momentum and energy equations simultaneously. **Figure 2-10** shows the resulting curves for a particular case (Wallis 1969) where a saturated liquid obeying Bernoulli's equations is assumed in the nozzle. [26]

The energy and momentum curves explain the dependency of the mass flux with the velocity ratio resulting from the combination of the continuity equation with either, energy or momentum in the control volume. The marked points in each curve correspond to the slip ratios that minimize either, the kinetic energy or the momentum. At the intersection point, both properties are conserved. [26]

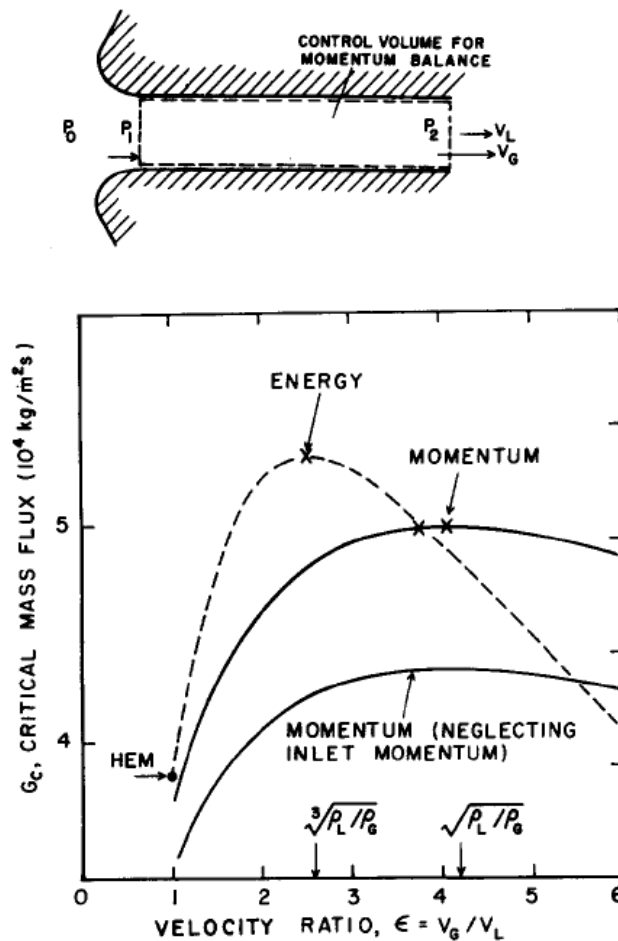


Figure 2-10 Critical mass flux value applying different slip ratios [26]

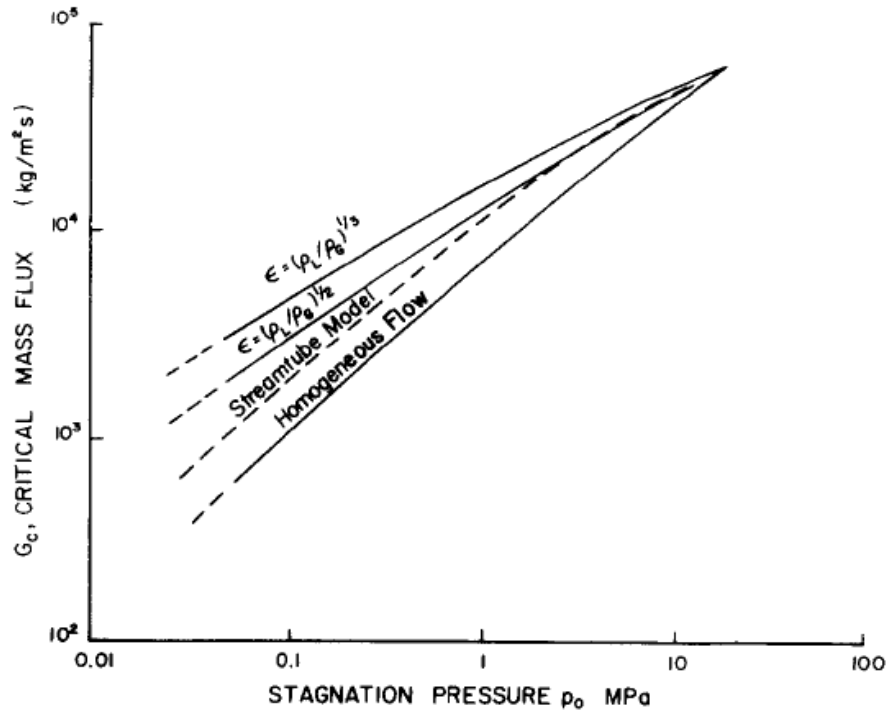


Figure 2-11 Relationship between the stagnation pressure and the critical mass flux using different models [26]

A comparison between the predictions resulting of the two different slip ratios, as well as other models, is shown in **Figure 2-11**. The figure describes the critical mass flux for water expanding from saturation pressure ($x=0$), and shows the little influence of the slip ratio choice, as long as the thermodynamic equilibrium is achieved. [26]

Applying the NHEM equation for different upstream qualities $0 < x_0 < 1$ and an upstream pressure (p_0) of 7.83 MPa allows plotting the mass flux curve as shown in **Figure 2-12**.

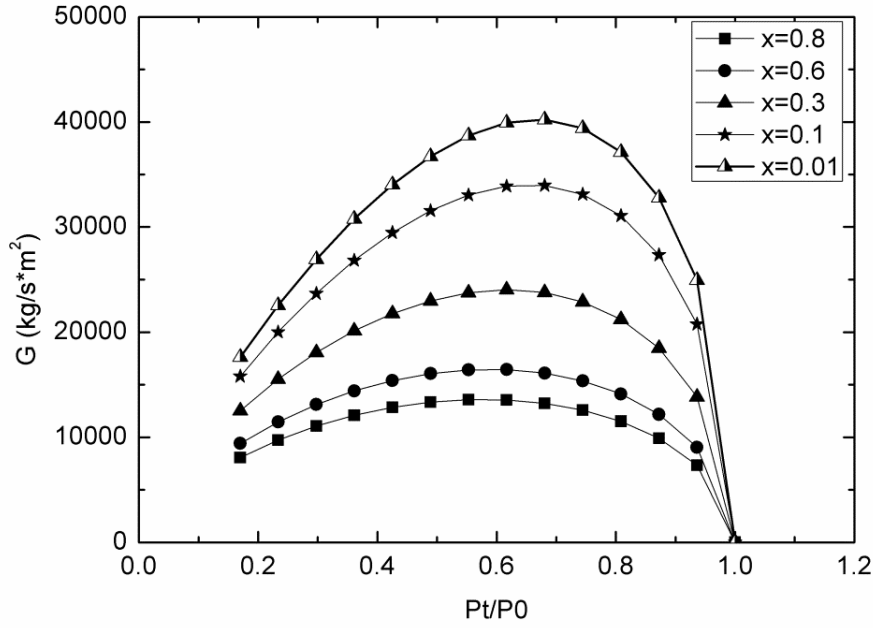


Figure 2-12 NHEM mass flux calculation

G_c , corresponds to the mass flux under critical conditions and is located at the maximum point of each curve. Using the mixture specific volume at G_c conditions both, steam and water, velocities can be found by using eq. 2.18 and 2.19. These velocities correspond to the inlet steam and water velocities ($V_{1\text{steam}}/V_{1\text{water}}$) in the turbine velocity triangle.

$$V_{\text{steam}} = \frac{G_c * x_t}{\rho_g * \alpha_t} \quad (2.18)$$

$$V_{\text{water}} = \frac{G_c * (1 - x_t)}{\rho_l * (1 - \alpha_t)} \quad (2.19)$$

Where:

α_t : Is the fluid void fraction at downstream pressure corresponding to G_c .

Analogous to the HEM case, once the fluid velocities ($V_{1\text{steam}}/V_{1\text{water}}$) corresponding to the critical mass flux are calculated, the critical flow rate as well as rest of the velocities components of the turbine blade velocity triangles can be obtained by applying the turbine geometry parameters found by applying the equations 2.7 to 2.9.

Figure 2-13 shows the flow chart followed to plot the mass flux applying the HEM and NHEM equations described in this section

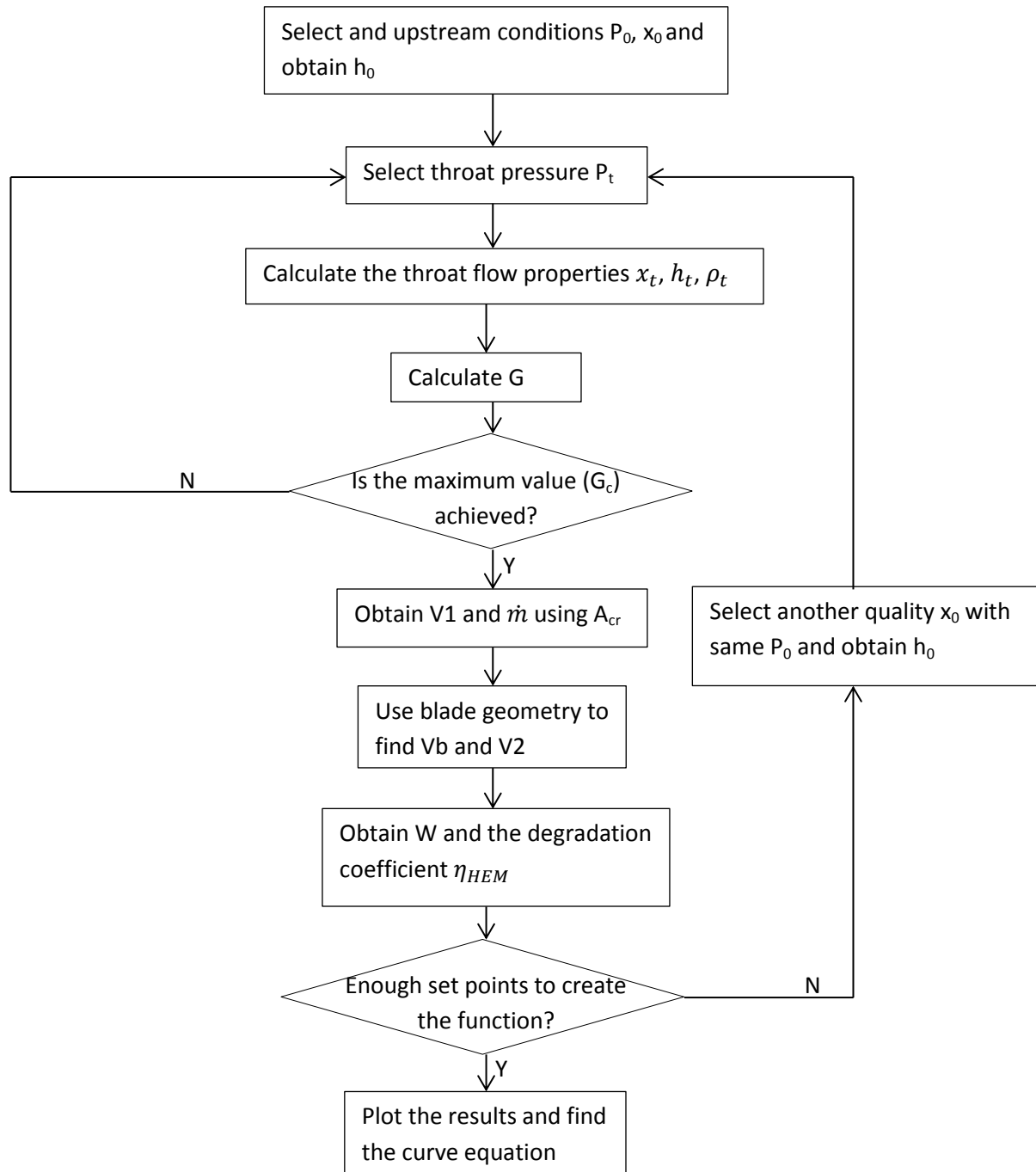


Figure 2-13 HEM/NHEM model flow chart

2.2.4- Degradation coefficient formation and discussion

Independent of which model has been used to find the velocities in the blade, the turbine work is calculated using the Euler turbine work.

Equation 2.20 describes the Euler turbine work. The Euler turbine equation relates the power added to or removed from the flow, to characteristics of a rotating blade row. The equation is based on the concepts of conservation of angular momentum and conservation of energy as is described in **Figure 2-14**. [30]

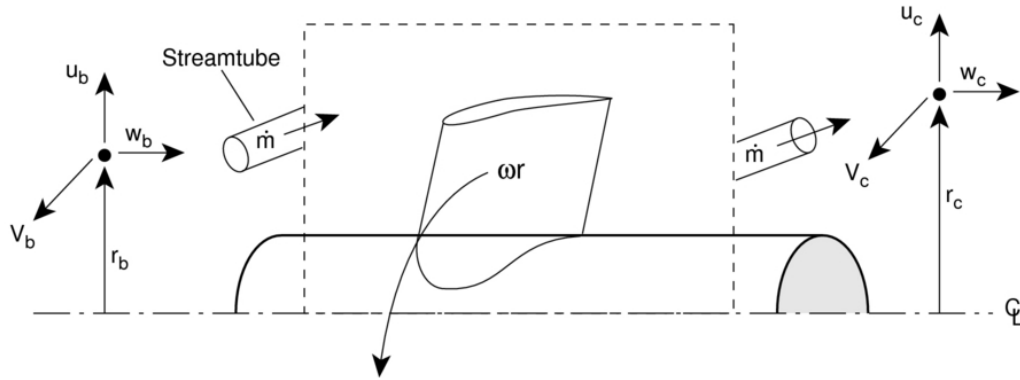


Figure 2-14 Turbine momentum and energy conservation concepts [30]

$$W_t = T * \omega \quad [W] \quad (2.20)$$

Where:

W_t : Turbine work. [W]

T: Turbine torque. [N*m]

ω : Turbine angular velocity. [rads/s]

Applying conservation of angular momentum T must be equal to the time rate of change of angular momentum in a stream tube that flows through the turbine.

$$T = \dot{m} * (V_{2t} * r_2 - V_{1t} * r_1) \quad [N * m] \quad (2.21)$$

Where:

\dot{m} : Is the mass flow rate moving through the turbine. [kg/s]

V_{1t} : Is the inlet velocity (V_1) component in the blade velocity axis. [m/s]

r_1 : Is the inlet radius. [m]

V_{2t} : Is the outlet velocity (V_2) component in the blade velocity axis. [m/s]

r_2 : Is the outlet radius. [m]

If the blade is moving then power is supplied by the fluid, and combining equations 2.20 and 2.21, the output power equation can be rewritten as:

$$W_t = \dot{m} * (V_{2t} * r_2 - V_{1t} * r_1) * \omega [W] \quad (2.22)$$

Assuming $r_2=r_1=r$ the main stage radius and knowing that the blade velocity is $V_b = \omega * r$, equation 2.22 is changed to:

$$W_t = \dot{m} * V_b * (V_{2t} - V_{1t}) [W] \quad (2.23)$$

Where:

V_b : Is the velocity of the blades. [m/s]

Once the turbine work at a given quality has been calculated using equation 2.23, the degradation coefficient curve can be found; dividing the different output powers by the pure steam power (373kW from **Table 1-1**) and plot the resulting coefficients to find the curve function.

$$\eta_{NHEM}(x_0) = \frac{W(x_0)}{W_{pure\ steam}} \quad (2.24)$$

Figure 2-15 shows the degradation coefficient curve by applying the HEM equations. Fitting the data using a second order polynomial trendline, the equation becomes

$$\eta_{NHEM} = -0.507x^2 + 1.389x + 0.11 \quad (2.25)$$

With a determination coefficient (R^2) of 0.9992 between the data and the trendline.

Analogous to HEM case, the NHEM degradation coefficient curve by applying the corresponding equations is shown in **Figure 2-16** which shows how the output power is reduced as a function of the flow quality. Fitting the data using a second order polynomial trendline, the equation becomes

$$\eta_{NHEM} = -0.623x^2 + 1.357x + 0.248 \quad (2.26)$$

With a determination coefficient (R^2) of 0.9947 between the data and the trendline.

If the flow is pure steam, the degradation factor is equal to unity representing no degradation in the turbine. Otherwise, if the flow is a mixture of steam and water, the output power should be further reduced by multiplying it by the corresponding factor.

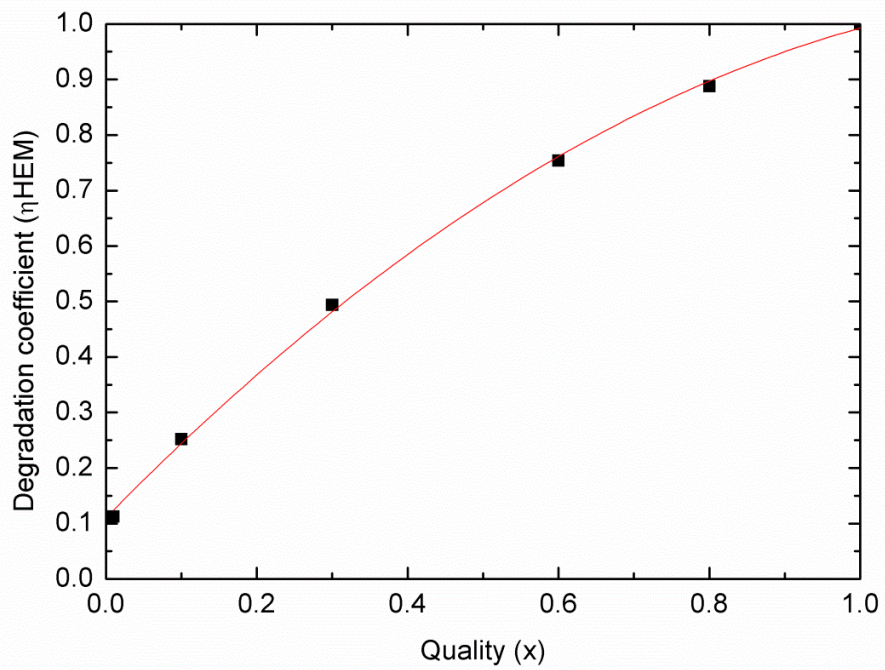


Figure 2-15 HEM degradation coefficient

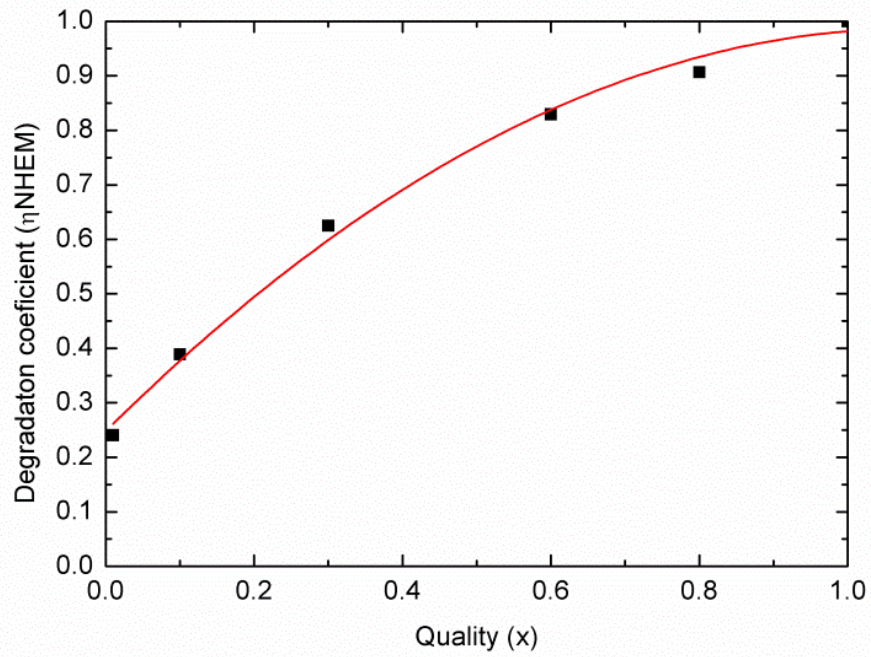


Figure 2-16 NHEM degradation coefficient

If the flow is pure steam, the degradation factor is equal to unity representing no degradation in the turbine. Otherwise, if the flow is a mixture of steam and water, the output power should be further reduced by multiplying it by the corresponding factor.

Both degradation coefficients show the same tendency to the flow quality but, as can be appreciated in **Figure 2-17**, the application of the HEM or the NHEM causes a variation of the resulting curve at low flow qualities.

The difference can be explained by the different assumptions made in both models; while the HEM assumes the mixture as a pseudo-fluid which properties are the equivalent to the initial mixture, the NHEM considers two different phases each one of them with its own different properties. These assumptions make the HEM less accurate at low qualities where the phase's differences are more relevant.

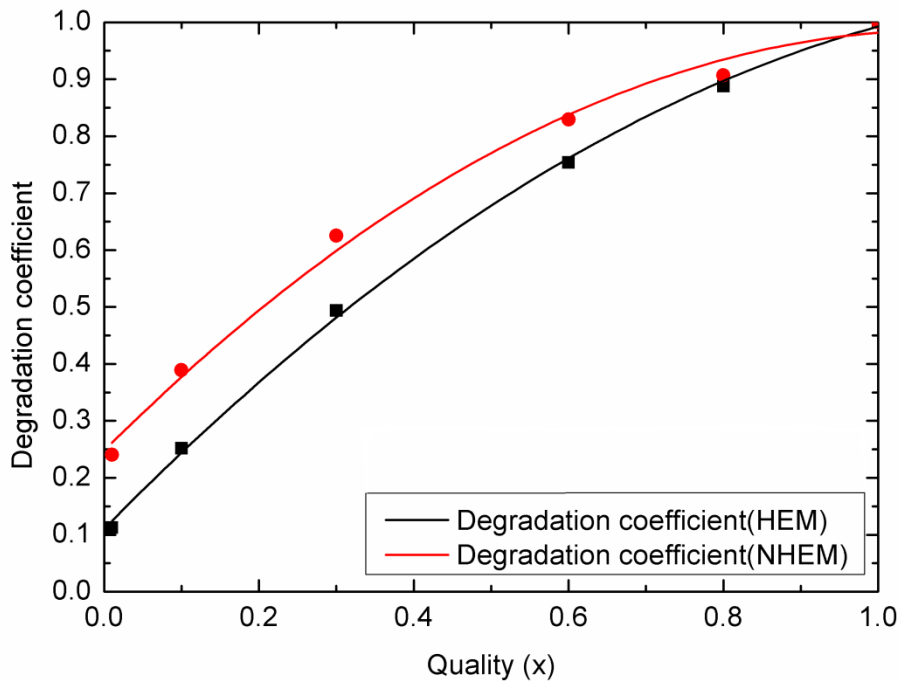


Figure 2-17 HEM/NHEM degradation coefficient comparison

2.3- Summary

The objective of this chapter is the development of a turbine degradation coefficient which tries to quantify how much the turbine output power is reduced as a function of the amount of water in the flow.

As mention earlier in this chapter, some analysis done regarding the RCIC performance of F1D2 by TEPCO[11][23] and the IAE [24] stated the incongruence of a normal turbine operation and the onsite measured data. They hypothesized that the turbine power was being overpredicted

The application of HEM and NHEM is useful to find the velocity triangles for qualities $0 < x < 1$. The velocities are then used in conjunction with the Euler turbine power equation to calculate the corresponding turbine power which is compared to the pure steam power from RCIC specification sheet which at the same time is the power corresponding to the single phase critical flow.

Both degradation coefficients show a similar tendency to the flow quality. The difference observed at low qualities is due to the assumption of two different phase velocities done in the NHEM.

Chapter 3 Application of the turbine design into F1D2 RCIC system numerical analysis

3.1- Fukushima Daiichi Unit 2 plant description

F1D2 is one of the six reactors of Fukushima Daiichi affected by the earthquake and the consequent tsunami. It is a BWR/4 reactor type originally designed by General Electrics (GE) which began its operation on 18th July 1974 and its decommission was stablish, due to the accident, on 19th April 2012. Despite BWR/4 reactors are capable to use either Mark I or Mark II containments, F1D2 uses a Mark I configuration. With a thermal power of 2384MWt it is capable to produce around 784MWe. The global plant specifications are resumed in **Table 3-1**.

Mark I primary containment configuration includes a free-standing bulb-shaped drywell backed with reinforced concrete and connected to the torus-shaped suppression pool by a venting system. The S/C acts as a heat sink which absorbs the heat in case of accident. The venting system is based on 96 downcomer vent pipes with the function to equalize the pressure between the drywell and the wetwell. The design pressure value for the S/C is around 392kPa being the rupture pressure 2.0 times this value. [11]

Table 3-1 F1D2 plant specifications [11]

Items		Value	Units
Thermal output		2381	MWt
Total flow rate of coolant		$3.33 \cdot 10^3$	t/h
Operation pressure in reactor pressure vessel (gauge)		6.93	MPa
Reactor core	Length of active fuel	3710	mm
	Hydraulic equivalent diameter	4.03	m
	Total amount of uranium	94	t

	Steam flow rate		4440	t/h
	Core temperature		286	°C
	Average uranium enrichment		3.8	wt%
	Burnup	Average	45.0	GWD/t
		Maximum	55.0	GWD/t
Fuel (9x9(B))	Diameter of the pellet		9.4	mm
	Outer diameter of the cladding tube		11	mm
	Thickness of the cladding		0.7	mm
	Fuel assembly	Number of FA (total)	548	--
		Number of fuel rod in one FA	9x9-9 (water channel)	--
		Material of channel box	Zircaloy-4	--
Control blade	Configuration		Cross-shape	--
	Number of control blades		137	--
	Pitch		304.8	mm
RPV	Inner diameter		5.57	m
	Height		22.0	m
	Thickness of base metal		138	mm
	Thickness of stainless liner		5	mm
	Material of base metal		SA533	--
			SA-508	--
	Weight		500	t
	Design pressure (gauge)		87.9	kg/cm ² g
	Design temperature		302	°C
Primary loop recirculation	Number of loops		2	--
	Inner diameter of pipe		627	mm

system	Number of jet pumps		20	--
	Flow rate of pumps		7800	t/h
	Pump head		152	m
	Output power of pump motor		3750	kW
	Rotation speed of pump motor		1380	rpm
Main steam system	Number of pipe		4	--
	Inner diameter of pipe		610	mm
	Number of main steam isolation valve		8	--
	Number of SRV		8	--
	Number of safety valve		3	--
Primary containment vessel	Drywell	Inner diameter of spherical portion	20	m
		Inner diameter of cylindrical portion	10.9	m
	S/C	Diameter of torus	33.5	m
		Minor inner diameter	8.9	m
		Number of vent pipe	8	--
		Inner diameter of v. pipe	2.06	m
		Inner diameter of header	1.46	m
		Number of downcomer	96	--
		Inner diameter of downcomer	592	mm
		Pool inventory	2980	m ³
	Design inner pressure (gauge)		3.92	kg/cm ² g
	Design outer pressure (gauge)		0.14	kg/cm ² g
	Design temperature		138	°C
	Material		ASME SA 516	--

		Gr.70	
--	--	-------	--

3.2- Accident progression

On March 11th 2011 the Fukushima Unit 2 was operating normally under its specification designs. Once the earthquake hit Japan, the plant personnel immediately perform the reactor scram, shutting down the plant. The major events after the scram are summarized in **Table 3-3**.

During the first hour after the scram, the major event log shows the RCIC being manually activated two times; the first one for minute before the high water level signal, TAF+5.65 trip off the system. The second activation last for more time but the procedure was exactly the same; manually activation and deactivation due to high water level. During this time, as can be seen in **Table 3-2** the residual heat removal system (RHR system) was operating cooling down the S/C with the spray function. [11]

Table 3-2 F1D2 water injection to the core [11]

Date & Time	RCIC	S/P cooling with RHR(A)	S/C spray with RHR(A)	Fire Truck
2011/3/11 12:00	0	0	0	0
2011/3/11 14:50	0	0	0	0
2011/3/11 14:50	1	0	0	0
2011/3/11 14:51	1	0	0	0
2011/3/11 14:51	0	0	0	0
2011/3/11 15:02	0	0	0	0
2011/3/11 15:02	1	0	0	0
2011/3/11 15:07	1	0	0	0
2011/3/11 15:07	1	1	0	0
2011/3/11 15:25	1	1	0	0
2011/3/11 15:25	1	0	1	0
2011/3/11 15:28	1	0	1	0
2011/3/11 15:28	0	0	1	0
2011/3/11 15:39	0	0	1	0
2011/3/11 15:39	1	0	1	0
2011/3/11 15:41	1	0	1	0
2011/3/11 15:41	1	0	0	0
2011/3/14 9:00	1	0	0	0
2011/3/14 9:00	0	0	0	0
2011/3/14 15:30	0	0	0	0
2011/3/14 15:30	0	0	0	1
2011/3/14 19:20	0	0	0	1
2011/3/14 19:20	0	0	0	0
2011/3/14 19:54	0	0	0	0
2011/3/14 19:54	0	0	0	1
2011/3/19	0	0	0	1

One hour after the scram, the tsunami arrived and flooded the diesel generators room shutting down the AC/DC current and all the safety systems depending on them, generating a Station Blackout scenario. Right before this event, the RCIC was manually activated a third time but, due to the loss of current, the trip off signal due to high water level never arrived. [23-24][31-33]

Checking out the RPV pressure shown in **Figure 3-1** which remain below the operation pressure it is clear that the RCIC kept operating removing the decay heat generated by the fuel by extracting hot steam and injecting cold water, first from the CST (during the first 13h) and after from the suppression pool.

Due to the loss of current and the large operating time of the RCIC system it is reasonable to hypothesize that the water level in the RPV rose without control until it reached the MSL height allowing the water to move through the turbine. It is complicated then, to quantify the coolant makeup capability of the RCIC system during the 70h of operation time. [23][24]

Regarding the S/C and drywell pressure described in **Figure 3-2** during the RCIC operation, there is no doubt that the pressure increment they suffered was below the expected values, especially with the consideration that the auxiliary systems such as the RHR system were offline. The main assumption behind this behavior is the flooding of the room where the torus is located. [23-24][31-33]. The flooding of the torus room would increase the heat exchange between in the inside of the S/C and the surroundings cooling down the fluid inside.

At 70h mark after the scram the RCIC failed and stopped to inject cold water to the RPV as can be seen in **Figure 3-1** by the drastic increment in the RPV pressure until the SRV start an open-close cycle around 80h mark after the scram [23-24][31-33].

After the RCIC fail, no water was injected during 11 hours until the injection of the sea water by trucks. Moreover, at about 2 hours before the sea water injection, the SRV were manually opened discharging water to the RPV. It is assumed that this period of lack of injected water caused damage in the bottom section of the RPV.

The explosions sound around the S/C region could be caused by the interaction of the melted zirconium with the sea water injected by the fire trucks. Those explosions might

cause the hypothetical leakage in the drywell which explains the depressurization suffered around the 90h mark.

Table 3-3 Accident major event log [11]

Date	Time	Elapsed time from reactor scram	Event	N.B.
11 th March	14:46	n/a	Earthquake attack	
	14:47	0 h	Reactor scram due to earthquake attack	
	14:50	3 min	Manual activation of RCIC	Rated flow rate:25.3 kg/s
	14:51	4 min	RCIC Trip due to high water level (L-8)	
	15:02	15 min	Manual activation of RCIC	
	15:04	17 min	S/C cooling by RHR(A) until 15:36	Assuming that RHR worked during 15:00 – 15:07
	15:25	38 min	Changing cooling mode of RHR(A) from S/P to S/C	
	15:28	41 min	RCIC Trip due to high water level (L-8)	
	15:39	52 min	Manual activation of RCIC	
	15:41	54 min	Loss of A/C power due to tsunami attack	
12 th March	4:20	13 h 33 min	Changing water source for RCIC from CST to S/C, completed at 5:00	
14 th March	9:05	66 h 18 min	Assuming trip of RCIC, confirmed by operators at 13:25 14 th March	Assuming functional decline of RCIC from 9:00 14 th March
	18:02	75 h 15 min	Opening SRV1, confirmation of depressurization in RPV at ~18:00	
	19:54	77 h 7 min	Activation of sea water injection	Flow rate:2.82 x 10 ⁻² m ³ /s
	21:20	78 h 33 min	Depressurization in RPV by opening SRV2, resulting in refueling of core	
	23:00	80 h 13 min	Assuming closure of SRV1 in analysis	
	23:25	80 h 38 min	Assuming opening of SRV1 in analysis	
15 th March	1:10	82 h 23 min	Opening SRV1	
	6:14	87 h 27 min	Explosion sound around S/C	Assuming no leakage from S/C to R/B
	7:20	88 h 33 min	Assuming leakage from D/W to R/B	

3.2.1- Measured data

The following figures show the main data measured onsite during the accident by the personnel. **Figure 3-1** shows the RPV pressure starting right after the earthquake until the 18th March 2011. In the figure, the evolution during the RCIC operational time can be observed, as well as, the pressure drastic reduction after the RCIC fail.

Analogously, **Figure 3-2** the drywell and wetwell pressure evolution during the same period. The pressure in both spaces is assumed to be similar due to the vacuum breaker and the venting system between them. A pressure slow increment can be observed during the RCIC operation time (lower than expected due to the hypothetical tors room flood). The pressure starts to fluctuate and decreases due to a leakage.

Figure 3-3 describes the decay heat generated by the fuel after the scram during the RCIC operation time.

Figure 3-4 shows, the RPV water level measured (green and yellow) and the water level once it was corrected by the simulation code (blue). The figure shows a constant water level around the MSL height during the RCIC operation time but it is only the measure taken by the sensor, actually there is no method to completely verify the real RPV water level.

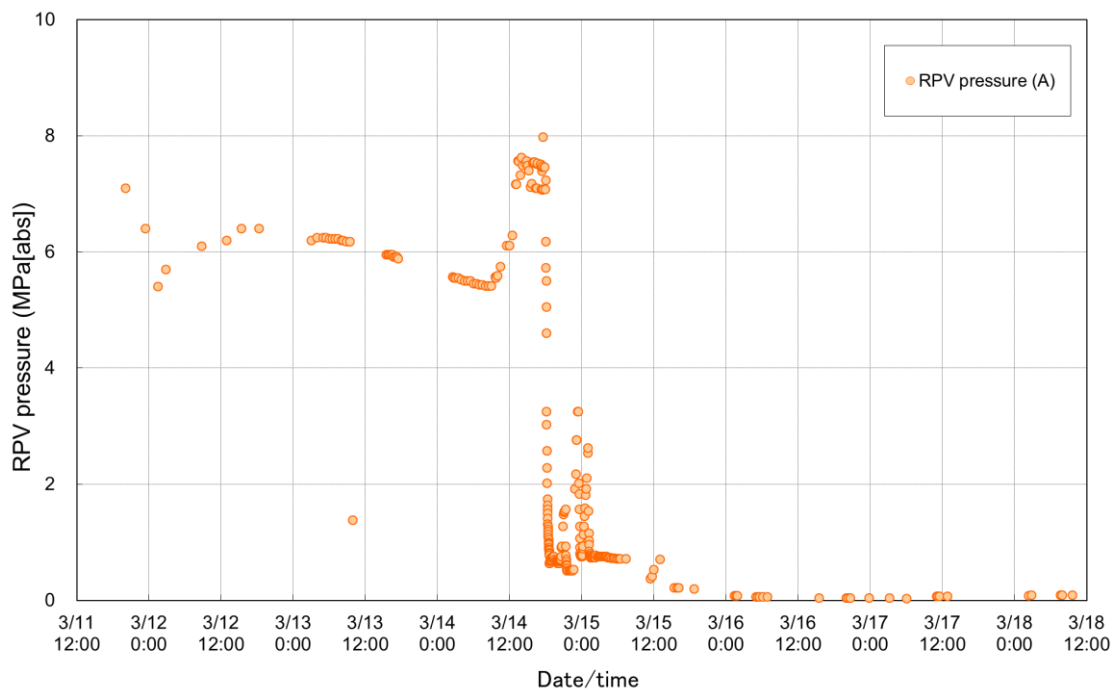


Figure 3-1 RPV pressure [11]

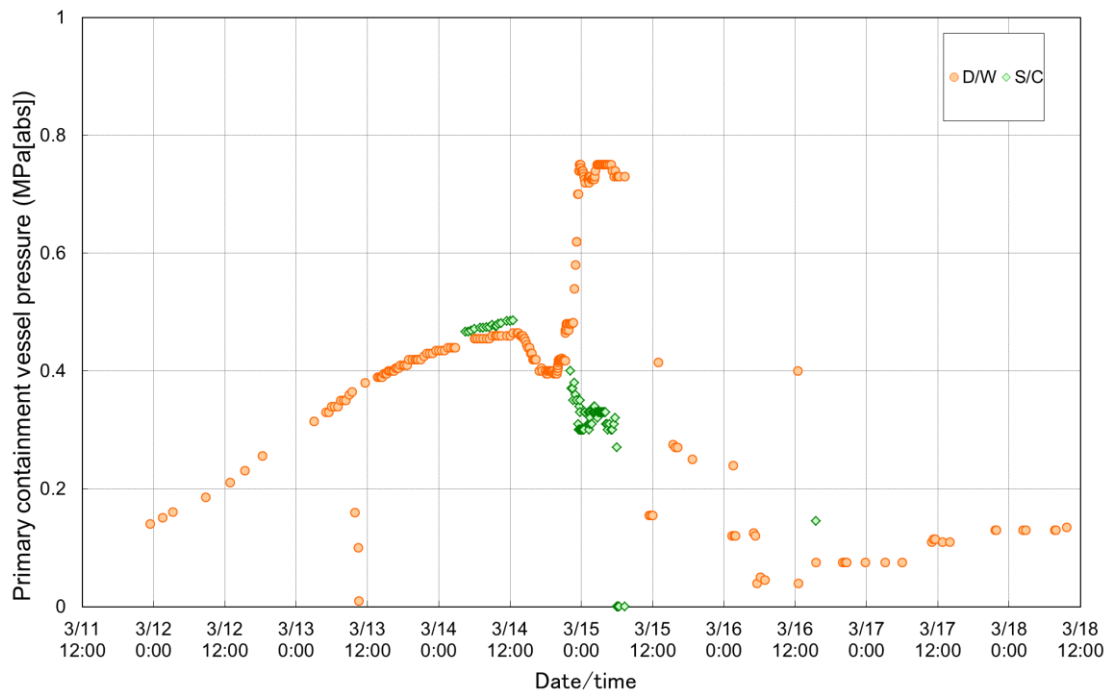


Figure 3-2 Drywell/Wetwell pressure [11]

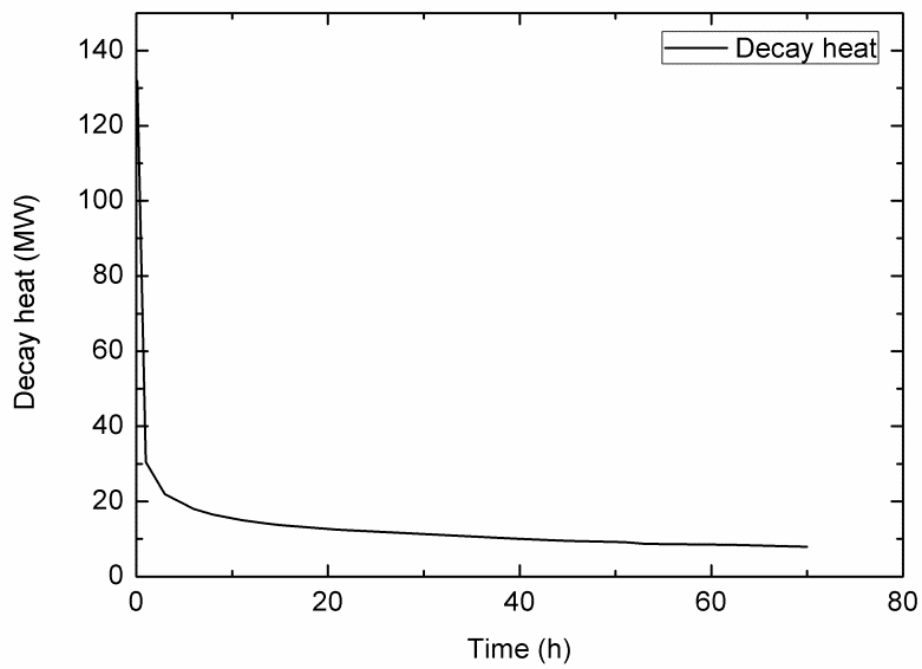


Figure 3-3 Decay heat [11]

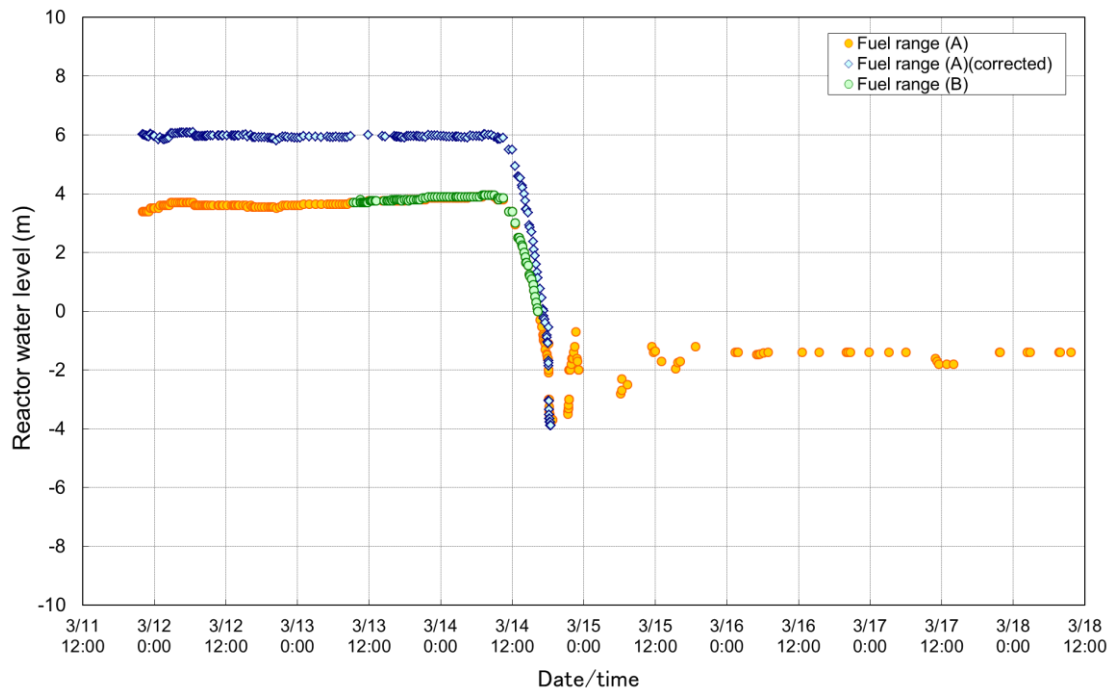


Figure 3-4 RPV water level [11]

3.3- RCIC system numerical analysis

3.3.1- RCIC system description

The following section will be focused on the numerical analysis of the RCIC system of F1D2 in order to estimate the RCIC system behavior in general, and the RCIC turbine in special. The analysis will be based on the basic energy and mass balance of the different elements forming the system and will consider both, single and two-phase flow scenarios either with or without the addition of the degradation coefficient developed in Chapter 2 using the HEM and NHEM.

The RCIC system basic diagram is displayed in **Figure 3-5**.

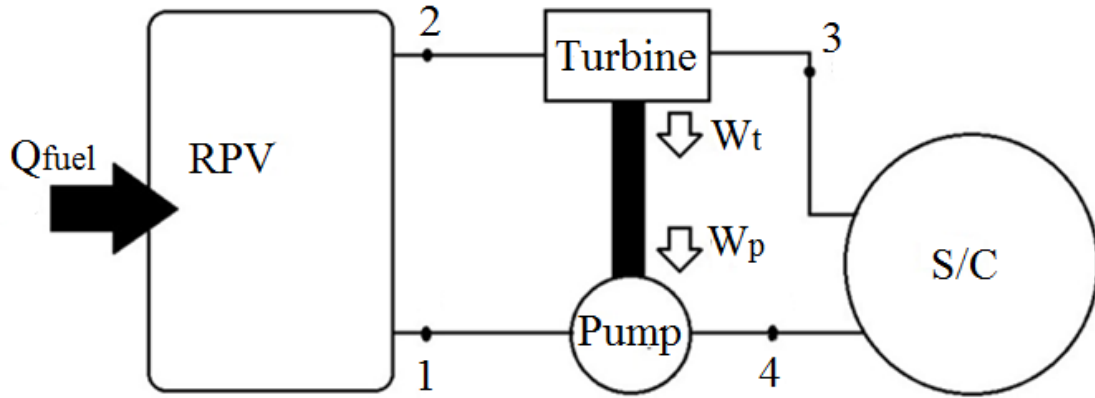
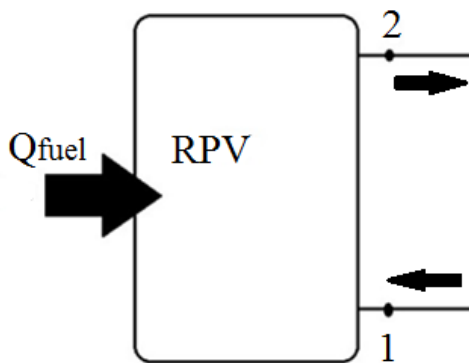


Figure 3-5 RCIC system thermal hydraulic diagram

In this diagram, the main RCIC components are described; the RPV, the turbine, the pump and the suppression chamber along with the control point used in the analysis. The system can be reduced to a simple Rankine cycle by using the RPV as a boiler heating up the water pumped by the RCIC pump until saturated conditions and the S/C as a heat exchanger or heat sink where the steam coming from the RPV is cooled down by the water inventory. One especial condition of this system is the presence of a turbine-driven pump, forcing the pump and the turbine to move at the same speed by connecting them by a shaft making the turbine generated power to be equal to the pump received power.

- RPV :



The energy balance in the RPV is described in equation 3.1

$$Q = \dot{m} * \Delta h \text{ [kW]} \quad (3.1)$$

Where:

Q : Is the energy provided by the fuel (Q_{fuel}). [kW]

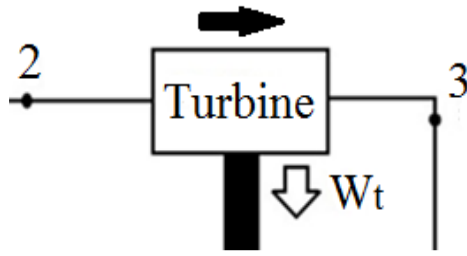
\dot{m} : Is the mass flow rate in the RPV (\dot{m}_{RPV}). [kg/s]

Δh : Is the enthalpy difference between the inlet (1) and the outlet (2). [kJ/kg]

Using all the previous considerations, equation 3.1 can be rewritten into

$$Q_{fuel} = \dot{m}_{RPV} * (h_2 - h_1) \text{ [kW]} \quad (3.2)$$

- Turbine:



The energy balance in the RCIC turbine is described in equation 3.3

$$W_t = \dot{m} * \Delta h \text{ [kW]} \quad (3.3)$$

Where:

W_t : Is the turbine generated work. [kW]

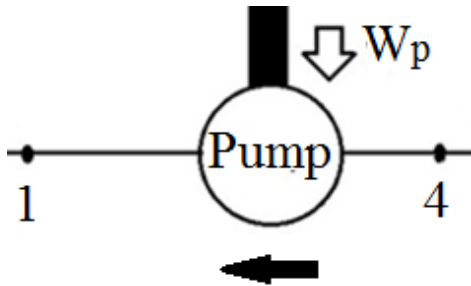
\dot{m} : Is the mass flow rate through the turbine (\dot{m}_t). [kg/s]

Δh : Is the enthalpy difference between the inlet (2) and the outlet (3). [kJ/kg]

If an isentropic expansion is assumed when calculating the Δh , then an isentropic efficiency (η_{ist}) must be added. Equation 3.3 becomes.

$$W_t = \dot{m}_t * (h_3 - h_2) * \eta_{ist} \text{ [kW]} \quad (3.4)$$

- Pump:



The energy balance of the pump is completely analogous to the turbine being described in equation 3.5

$$W_p = \frac{\dot{m}_p * (h_1 - h_4)}{\eta_{isp}} \text{ [kW]} \quad (3.5)$$

Equation 3.5 can be rewritten using the hydraulic power transferred to the fluid by the pump.

$$W_p = \dot{m}_p * \frac{H * g}{\eta_p * 1000} \text{ [kW]} \quad (3.6)$$

Where:

\dot{m}_p : Is the mass flow rate through the pump. [kg/s]

η_p : Is the pump efficiency.

H : Is the pump head. [m]

g : Is the gravity. [m/s²]

Prior to analyze the RCIC system response during the F1D2 accident conditions, the different efficiencies have to be estimated. In order to estimate them, a single phase

analysis will be performed under the RCIC specification sheet resumed in **Table 1-1** and using one of the RCIC limitation conditions expressed in equation 3.7.

$$W_p = -W_t \rightarrow \frac{\dot{m} * (h_1 - h_4)}{\eta_{isp}} = -\dot{m} * (h_3 - h_2) * \eta_{ist} * \eta_{shaft} \quad (3.7)$$

Where:

η_{shaft} : Is the shaft efficiency (0.9 from literature [23-24]).

3.3.2- Accident analysis

The F1D2 accident analysis would be done considering a mixture of steam/water through the turbine. The assumptions made for the analysis are based on the data measured and gathered by TEPCO [11];

- The fluid properties at each point of control would be calculated by using the TEPCO measured RPV and Drywell pressure displayed in **Figure 3-1** and **Figure 3-2** to properly recreate the accident conditions. [11]
- According with TEPCO data and experiments, the water level in the RPV was constant during RCIC operation time as displayed in **Figure 3-4**. [11] This condition forces all the mass flow rates to be equal $\dot{m}_p = \dot{m}_t = \dot{m}_{RPV} = \dot{m}$
- $\eta_p, \eta_{ist}, \eta_{shaft}$ are already known and assumed constant
- Since the RCIC operation is after scram, $Q_{fuel} = Q_{decay\ heat}$ shown in **Figure 3-3** [11]

The equation system use to describe the RCIC behavior during the accident is based on the energy balance of the equations 3.2, 3.4, 3.6, in conjunction of the system mass balance based on the assumptions previously described.

The resulting equation system is displayed in the following equations.

RPV energy balance

$$Q_{decay\ heat} = \dot{m} * \Delta h \rightarrow Q_{decay\ heat} = \dot{m} * [(h_{2v} * x + h_{2l} * (1 - x)) - h_1] \quad (3.8)$$

Generated turbine – received pump work equivalency

$$\frac{\dot{m} * H * g}{\eta_p * 1000} = -\dot{m} * [h_3 - (h_{2v} * x + h_{2l} * (1 - x))] * \eta_{ist} * \eta_{shaft} \quad (3.9)$$

RCIC mass balance

$$\dot{m}_p = \dot{m}_t = \dot{m}_{RPV} = \dot{m} \quad (3.10)$$

Steam mass flow rate in the turbine

$$\dot{m}_{t-steam} = x * \dot{m} \quad (3.11)$$

Where:

$\dot{m}_{t-steam}$: Is the steam mass flow rate in the turbine. [kg/s]

Under the specified conditions, the unknown parameters of this equation system are the mass flow rates and the quality on the Main Steam Line (MSL).

The equation system previously described does not consider the turbine factor previously developed in Chapter 2. If the degradation is to be included, the equation 3.9 then has to be modified; in case of the HEM, equation 3.9 becomes

$$\frac{\dot{m}_p * H * g}{\eta_p * 1000} = -\dot{m}_t * \Delta h_{s=const} * \eta_{ist} * \eta_{shaft} * \eta_{HEM} \quad (3.12)$$

Where:

η_{HEM} : Is the degradation coefficient developed by applying the homogeneous equilibrium model described in equation 2.25.

Analogous to HEM, if the NHEM is to be applied, equation 3.9 becomes

$$\frac{\dot{m}_p * H * g}{\eta_p * 1000} = -\dot{m}_t * \Delta h_{s=const} * \eta_{ist} * \eta_{shaft} * \eta_{NHEM} \quad (3.13)$$

Where:

η_{NHEM} : Is the degradation coefficient developed by applying the non-homogeneous equilibrium model described in equation 2.26.

The equation system is evaluated on each time step during the 70h of RCIC operation time recorded by TEPCO [11]. The analysis process is shown in the flow chart in **Figure 3-6**.

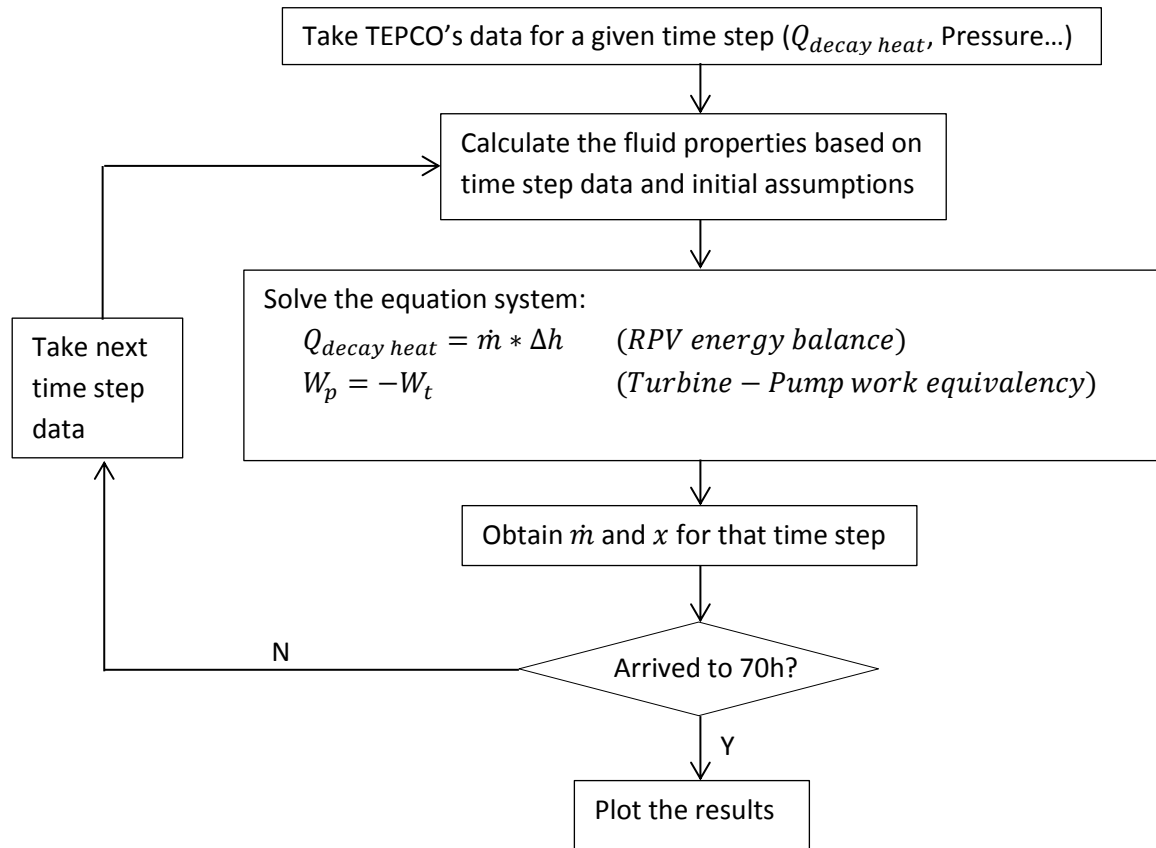


Figure 3-6 RCIC system numerical analysis flow chart

3.3.3- Analysis results and discussion

In this section, the results from all the previously described scenarios will be presented and discussed. For the first case, the results of the basic analysis without any degradation coefficient applied to the turbine are displayed in **Figure 3-7**.

The figure shows the flow quality as a function of time applying the previous equations without considering any type of turbine degradation. As can be observed, despite the equation system has a solution; this solution is only numerical, with no agreement with the initial assumptions of two phase flow stated previously. Since the flow quality is negative, there is no reason to try to find the steam flow rate. The fact of non-real solution agrees with the stated assumption of some degradation due to the water kinetic energy loss and the corresponding reduction on the energy of the moisture.

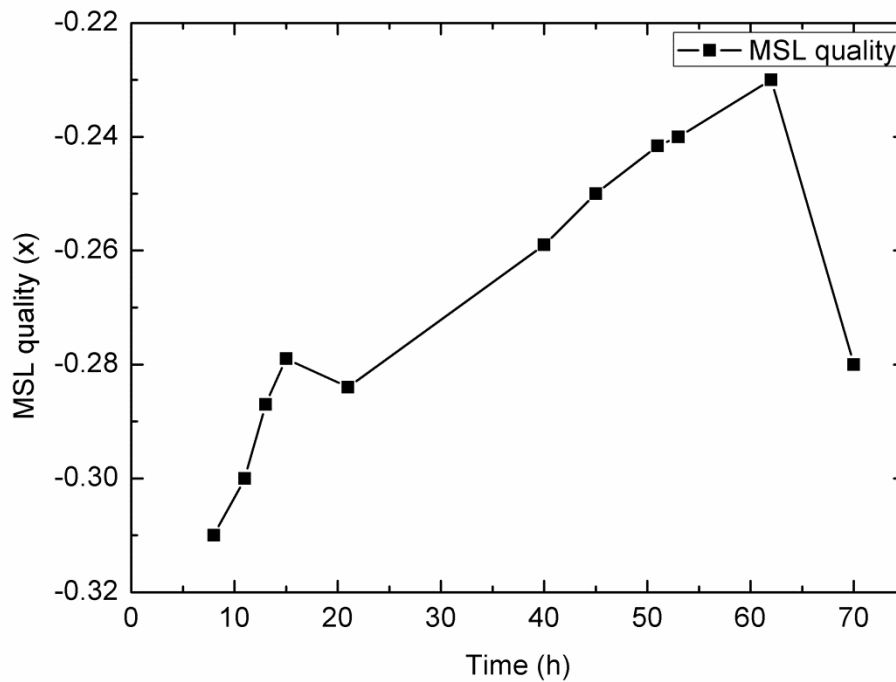


Figure 3-7 MSL quality without turbine degradation

The following figures show the results of the RCIC behavior when the turbine degradation is considered. The results of the HEM case can be observed in **Figure 3-8** which shows that the stream through the turbine is, indeed, a two-phase flow, being a mixture of water and steam. Despite the results agree with the initial assumptions and boundary conditions one thing must be reminded, the HEM limitations.

As mention in Chapter 2, the HEM is a model that assumes a perfect mixture in which both, steam and water, phases are in perfect equilibrium moving at same velocity. Despite it can be true at high qualities, where the small water droplets can be carried by the steam flow with little interferences, it becomes inaccurate at low qualities where the water phase becomes dominant and cannot be carried by the steam.

Unfortunately, the results on **Figure 3-8** estimate a low quality stream (around 13% - 19%). In this situation, the application of the NHEM proved to be a logic improvement.

The results of NHEM scenario are plotted in **Figure 3-9**, which shows that the stream through the turbine is, again, a two-phase flow, being a mixture of water and steam

agreeing with the initial assumptions. In this case, though, the flow quality increases from 6% during the first hours to ending around 14%.

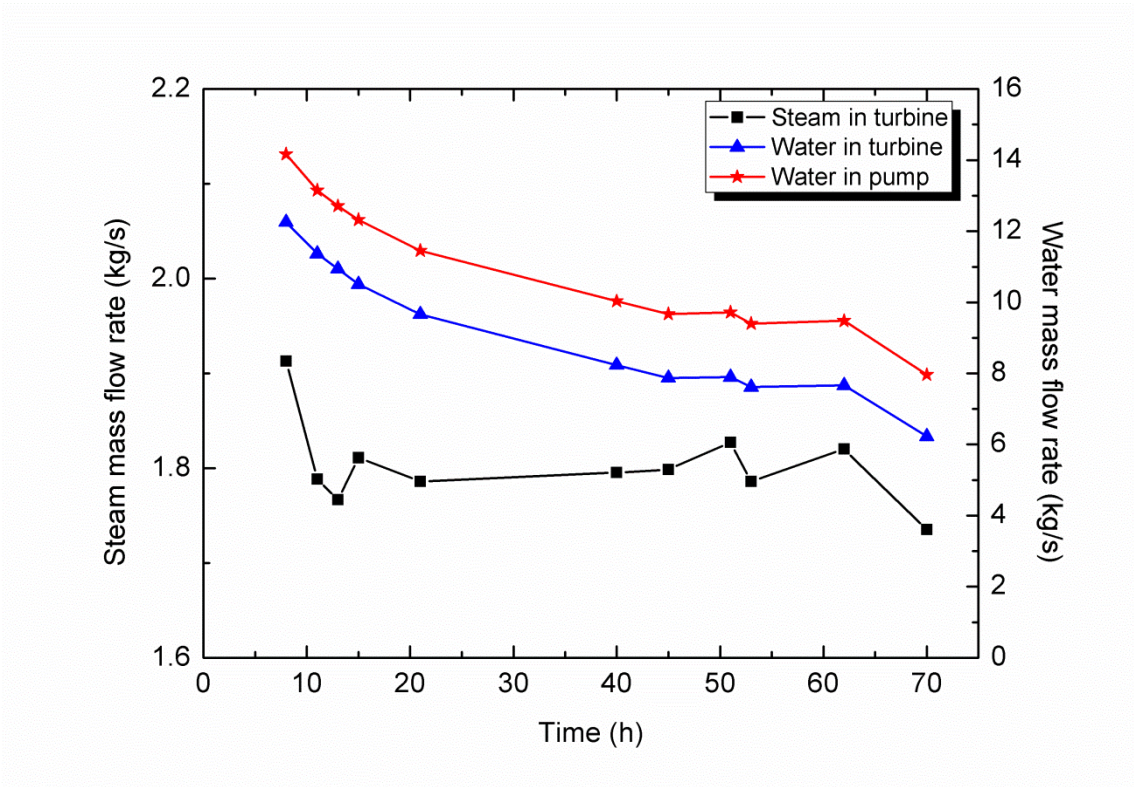


Figure 3-8 RCIC mass flow rates applying HEM coefficient

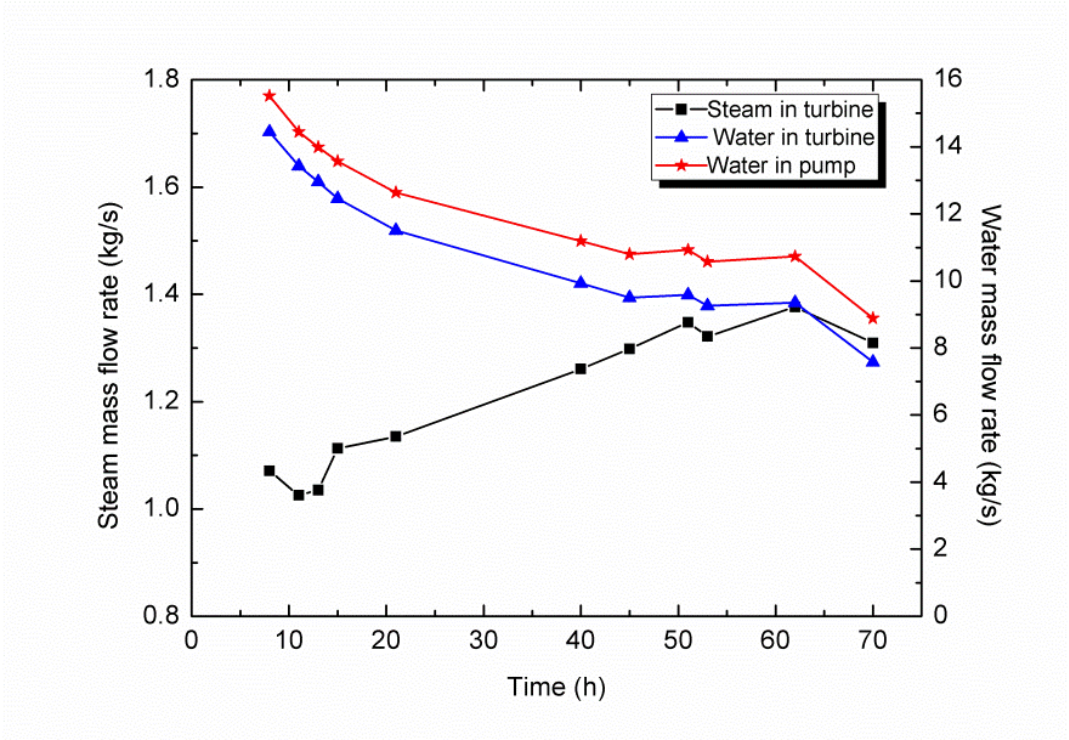


Figure 3-9 RCIC mass flow rates applying NHEM coefficient

Despite presenting a similar behavior both cases, HEM and NHEM also show some differences being the most relevant the reduction of the steam flow through the turbine in NHEM scenario. Although this reduction could seem strange it agrees with the theory behind the models themselves. In one hand, the HEM assumes that all the mixture is moving at one unique velocity, being this one an average between both, steam and water speeds depending on the quality.

On the other hand, the NHEM uses two different speeds for the two phases resulting in a faster steam phase and a slower water phase. In order to obtain a similar energy, and assuming that the kinetic energy of a fluid is depending on the mass flow rate and the velocity, is completely reasonable to see a mass flow reduction if the speed of that flow is increased.

Although most of the companies related with Fukushima analysis projects do not take into consideration the RCIC turbine itself, the IAE also analyzed the two phase flow scenario by using energy and mass balance and considering some degradation in the turbine due to the water presence.

Despite using the same concept, IAE analysis differs from the one presented here in its boundary conditions and initial assumptions. In their model, fully explained in [24], is considered that only the steam is creating positive work in the turbine meanwhile all the water is applying a negative effect. The consideration of the steam flashing phenomena due to the rapid expansion is also included. The resulting mass flow rates obtained by IAE are shown in **Figure 3-10**.

The mass flow rates found by IAE have a similar behavior than the ones obtained by both models, especially with NHEM as can be appreciated in **Figure 3-11**. Some discrepancy appears during the first hours mainly due to the CST operation; during the first 13h, the water was injected to the RPV from the CST instead from the SC which is not included in the present analysis making the data of the first hours non-accurate.

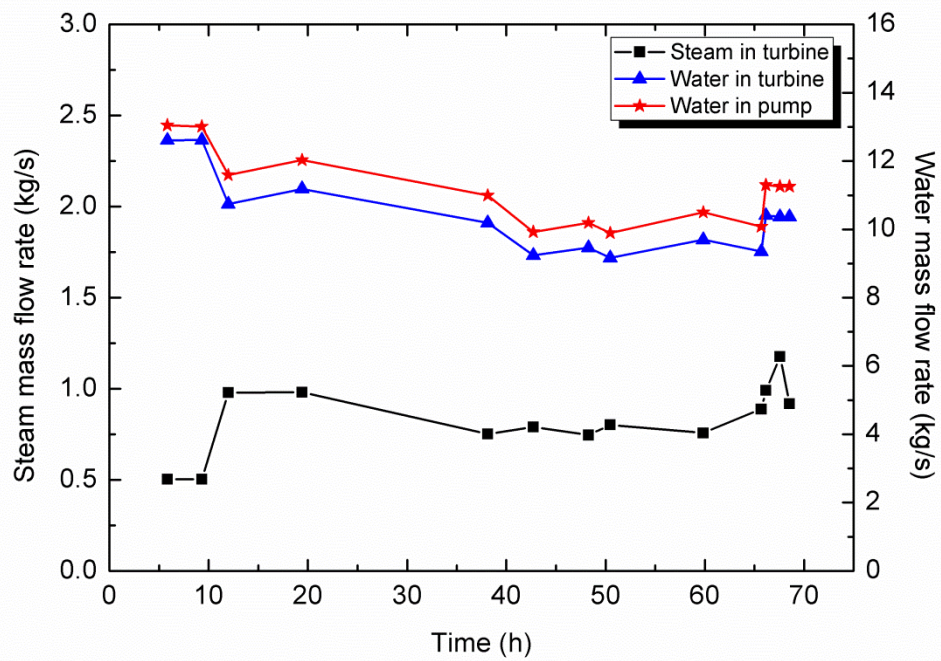


Figure 3-10 RCIC mass flow rates applying by IAE [24]

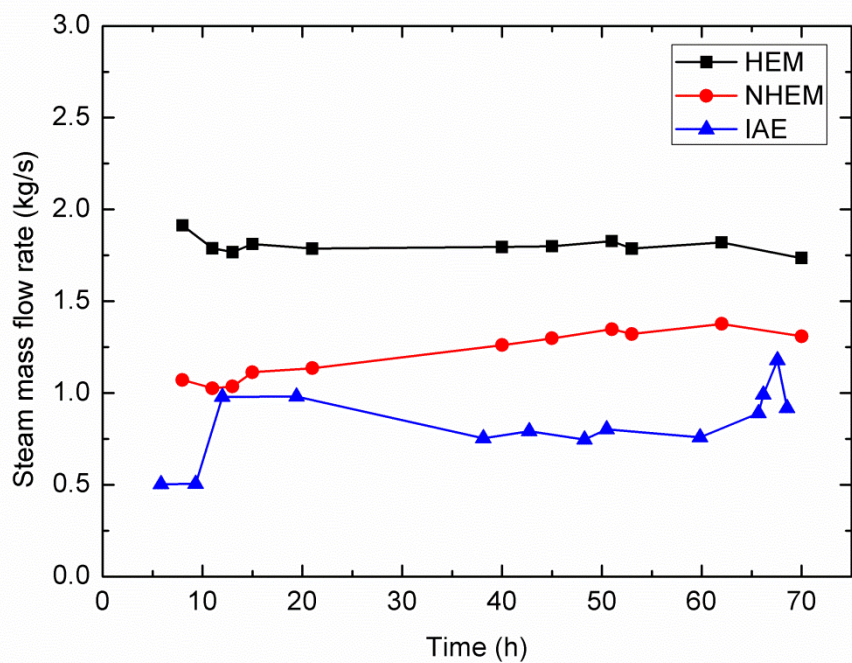


Figure 3-11 RCIC turbine steam mass flow rates comparison

Despite giving close values to the NHEM model, the IAE equations show lower quantities of steam along the RCIC operation time.

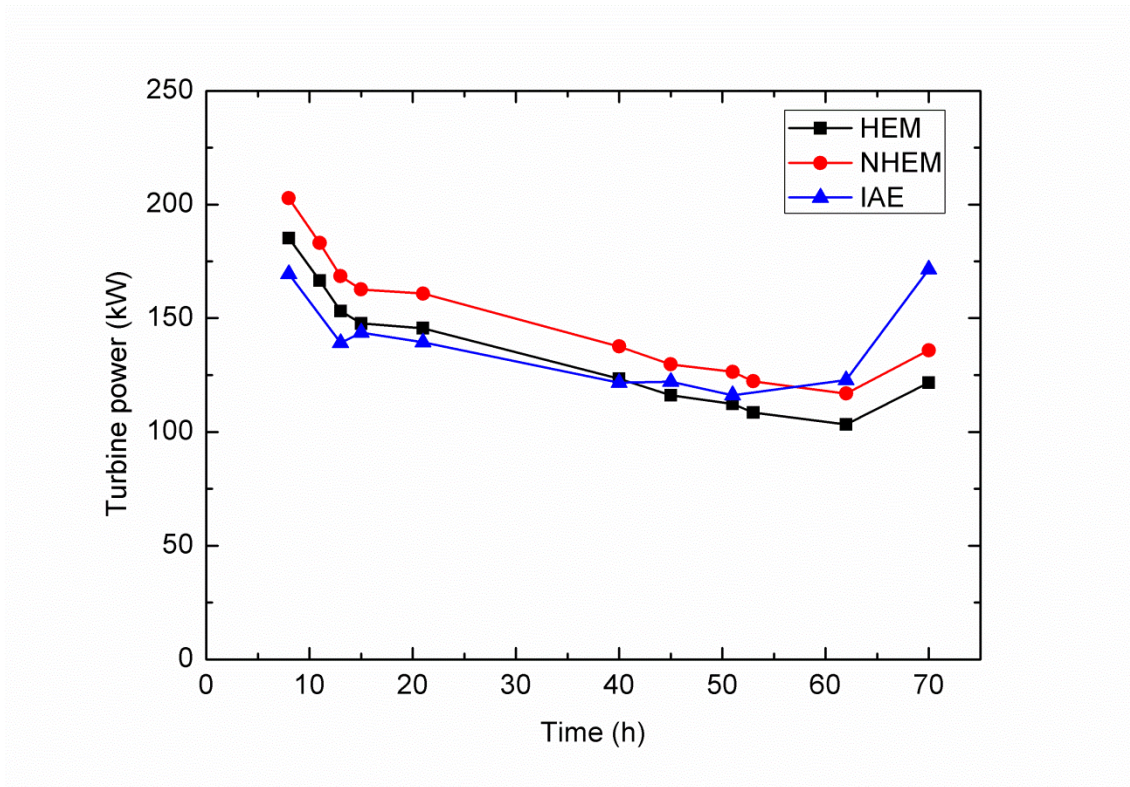


Figure 3-12 RCIC turbine power comparison

Figure 3-12 shows the turbine output power during the RCIC operational time considering the effect of HEM and NHEM models and comparing them with IAE results, all 3 presenting almost and exact behavior. Despite having a reduced steam flow rate, the NHEM shows a higher output power mainly caused by the increment of the overall flow rates.

For comparison purposes, the degradation coefficient developed and used by IAE in their SAMPSON analysis is described in equation 3.14. [42]

$$\eta_{\alpha} = 1 + 0.32 \log(0.9\alpha + 0.1) \quad (3.14)$$

Where:

α : Is the flow void fraction

As can be observed, the IAE degradation coefficient is a logarithmic function based on the fluid void fraction far away from the HEM and NHEM previously described.

For a more visual comparison, **Figure 3-13** shows the values of the IAE and the NHEM degradation coefficient at different flow qualities.

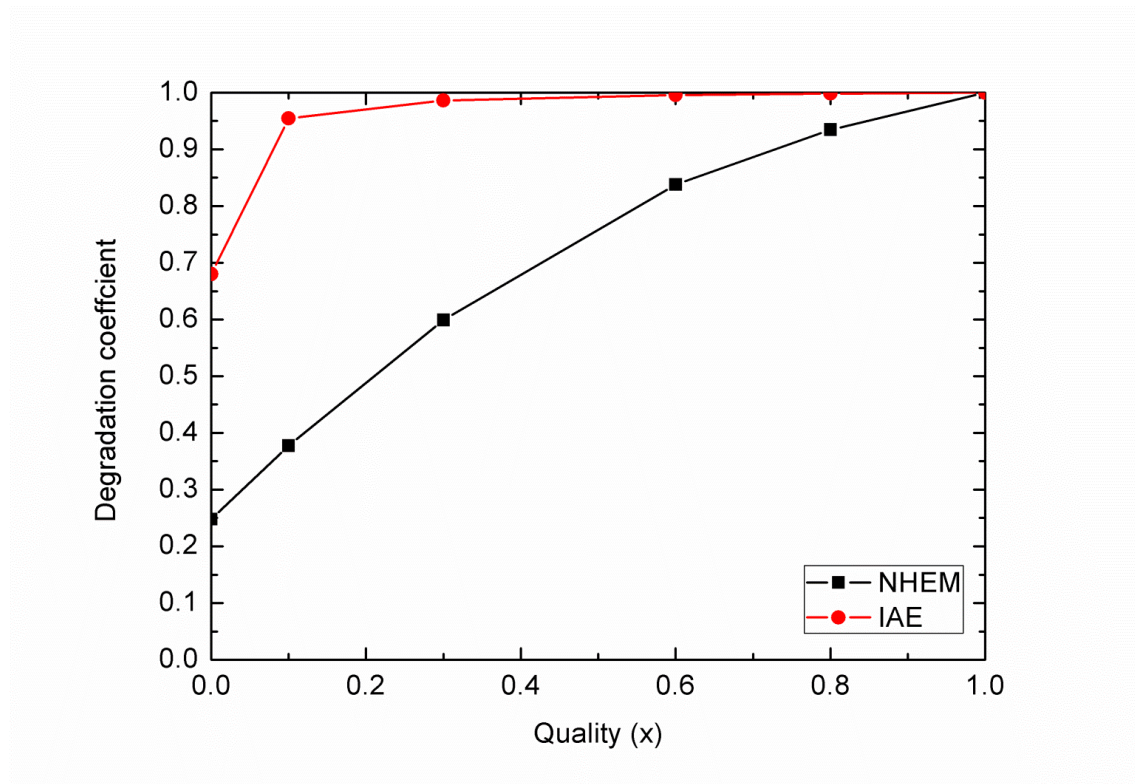


Figure 3-13 IAE-NHEM comparison

The divergence observed between the IAE and NHEM degradation coefficient in **Figure 3-13** is the main reason between the differences on the numerical analysis results. The degradation developed and applied in this dissertation is based on the steam turbine design equations and the critical flow models which provide a quantitative explanation about the turbine power behavior in two-phase flow scenarios. The IAE coefficient, on the other hand, is a iteration-generated parameter with the objective to match the analysis results to the onsite measurements without being based on any model.

A further explanation about why the results with no degradation were only a numerical solution meanwhile the ones with the application of the HEM and NHEM show a realistic behavior might be done. The results can be explained by the essence of the RCIC system itself; a closed loop system where the turbine performance at time step t will affect its own performance in time step $t+dt$. If the turbine generates more power due to the water presence, the pump receives more power, pumping more water at the same time and,

consequently, increasing the RPV water level furthermore and injecting more water to the turbine at the same time.

The data displayed in **Figure 3-14** shows the mass flow rates in the pump and the turbine at a given RPV pressure with either, with or without turbine degradation, at several turbine flow qualities. The black line shows the hypothetical maximum, critical, flow rate that can pass through the turbine at a given qualities meanwhile the red and blue lines represent the water mass flow rate in the pump computed using equation 3.9 (no degradation) and equation 3.13 (NHEM degradation).

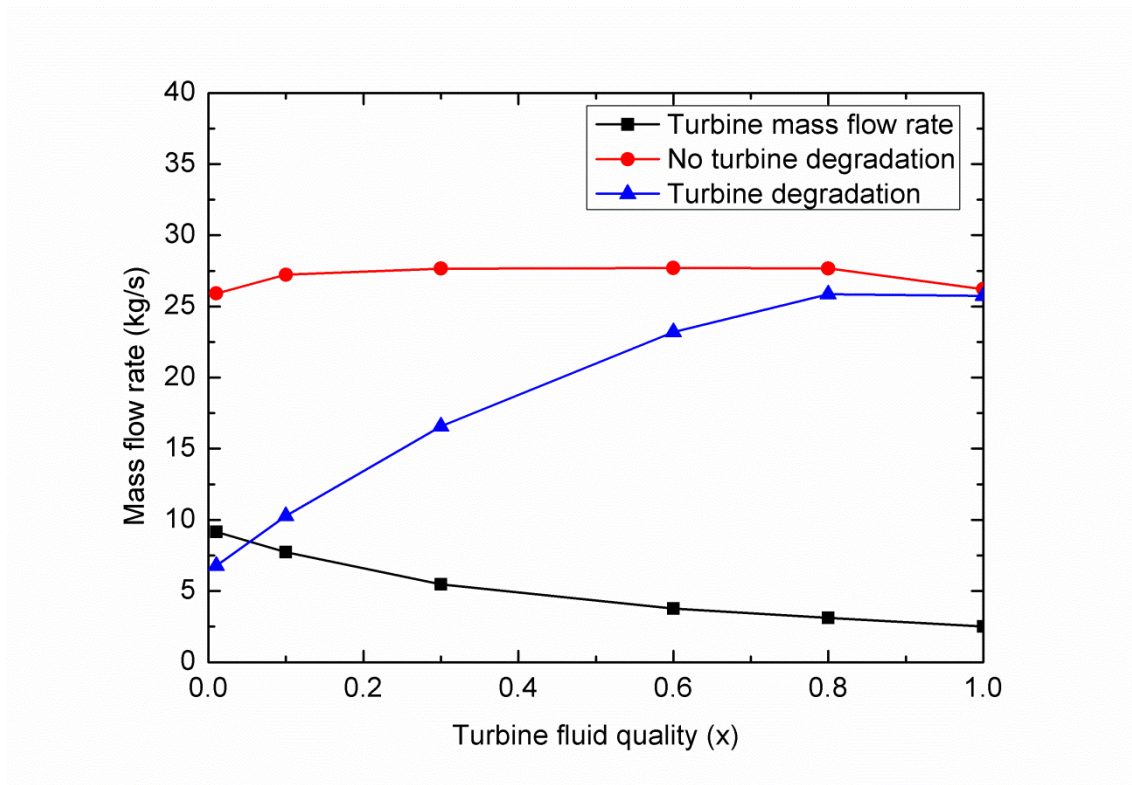


Figure 3-14 RCIC pump-turbine mass balance

As can be observed, in the case of no degradation, it does not matter the flow quality because the black and red lines will never intersect. This means that the system will be always unbalanced causing the RPV water level to increase without control. On the other hand, with turbine degradation, it is a balance point in the intersection between the blue and black lines. At this point, the mass extracted from the RPV and the mass injected to the RPV will be the same and the water level will remain constant. The intersection point will change depending on the system conditions (RPV and S/C pressure)

Agree with the previous explanation, TEPCO's data shown that the water level remained constant after reaching the MSL, as can be appreciated in **Figure 3-14**, meaning that the turbine power suffered a reduction in order to balance the inlet/outlet mass in the RPV. [23-24]

3.4- Summary

The present Chapter describes the Fukushima Daiichi Unit 2 nuclear power plant and accident progression caused by the earthquake and the consequent tsunami showing the major event log.

The data recorded by the operators during the accident is used to create the assumptions used in the RCIC numerical analysis. The analysis considers a two phase flow in the RCIC turbine and present several scenarios in order to best estimate the turbine behavior.

A basic scenario with no turbine degradation shows results that, despite being a numerical solution of the equation system, only correspond to subcooled water and it has no fitting with the initial assumptions made.

Other analyses are carried on by including a turbine degradation based on the degradation coefficient developed in Chapter 2 using the HEM and NHEM critical flow models. Those analyses present, not only a numerical solution but, a realistic solution accorded to the assumptions. In this case, once compared, the NHEM results are more accurate due to the low quality of the predictions. The NHEM will be the model applied to RELAP/Scdap code in future chapters.

The results are also compared with the predictions of the IAE and present a similar flow rates and turbine power behavior. The discrepancy in the results is caused by how the degradation coefficient is obtained in both analysis as well as the initial assumptions.

Chapter 4 RELAP/ScdapSIM

The RELAP/ScdapSIM is one of the severe accident codes developed by the U.S. Nuclear Regulatory Commission (NRC) to describe the overall reactor coolant system (RCS), fission product generation and transport, core damage evolution and thermal-hydraulic response in severe accident scenarios.[14]

The code was initially developed at the Idaho National Laboratory (INL) under the sponsorship of the Office of Nuclear Regulatory Research of the NRC as a part of the international Scdap development and training program (SDTP).

The two primary modules of RELAP/Sdap severe accident code are the RELAP5 module, acronym for Reactor Excursion and Leak Analysis Program, and the Scdap module, acronym for Severe Core Damage Analysis Package. The RELAP5 part takes care of the overall RCS thermal-hydraulics, reactor kinetics, non-condensable gases transport and the control system interactions calculations. It is based on a two-fluid model solved either by a semi-implicit or nearly-implicit numerical processes to allow economical calculations of system transients with unequal temperatures and velocities of the different phases.

On the other hand, the Scdap module is related to the core behavior during a severe accident. The module includes calculations for the fuel rod heat-up, deformation and rupture, oxidation, fission product generation and transport, Zirconium-Uranium interactions, flow and freezing of molten fuel and cladding, and debris formation processes.

The RELAP/ScdapSIM nodalizations are commonly developed by the interaction between the different component models that the code includes. Those component models include fuel and control rods, pumps (either normal or jet), turbines, ECC mixers, separators, heat structures, valves, reactor kinetics, pipes, annulus, and the control logic needed to operate all of them.

Those component models are coupled with special process models which include the abrupt area change, form losses, choked flow, boron tracking and non-condensable gases. The data needed to use all of the previous models is widely described in the several user manuals of the code. [14][34-36]

4.1- Code architecture

RELAP5 module is based on a modular top-down structure. The three principal blocks which englobe all the subroutines, where the models and procedures are located, are the input (INPUT), transient/steady-state (TRNCTL), and the stripping (STRIP) as described in **Figure 4-1**. [36]

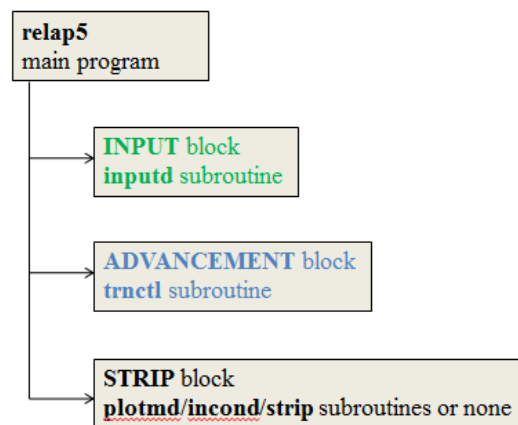


Figure 4-1 RELAP/ScadpSIM main blocks [36]

- The INPUT block processes the input. It calls the r-level subroutines to process the input cards used in the input deck. The r-level processing mainly consists on extracting the data in their format (integer, real, ...) and place it into the appropriate RELAP5 databases. INPUT block also calls the i-level subroutines to check the linkage between the models and initialize them.
- The transient/steady-state block (TRNCTL) handles both transient and the steady-state options. It computes the time step advancement based on the time step control and all the system properties based on the governing equations of each component. If the advancement process is not completed for a given time step before the simulated time stipulated in the input block, the simulation ends with an error alert. Is in this block where the source code modifications are done and it will be deeper described in the following section.
- The strip block (STRIP) extracts simulation data from a restart plot file for convenient passing of RELAP5 simulation results to other computer programs.

4.1.1- Transient/steady-state (TRNCTL) block

The complexity of the advancement block is described in **Figure 4-2**, the main subroutine TRNCTL is divided into three lower level subroutines. First, subroutine TRNSET performs the initial procedures for the time advancing calculations and establishes the memory space needed for them. Then subroutine TRAN, the driver, controls the advancement of the properties of the all the component and processes based on the driving equations. It is a high memory demanding process and almost all the computational time is spent here. At last, the TRANFIN releases the space for the dynamic data blocks that are no longer needed. [36]

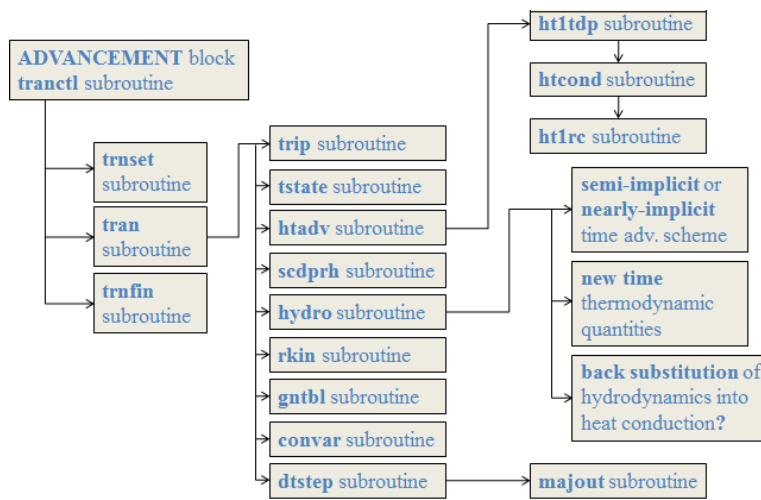


Figure 4-2 Transient block main subroutines [36]

The different modules called at each time step by the subroutine TRANS are listed below. [36]

- The trip system module (TRIP) evaluates logical statements. Each trip statement is a simple logical statement that has a true or false result.
- The equation of state boundary volume module (TSTATE) calculates the thermodynamic state of the fluid in each hydrodynamic boundary volume (time-dependent volume). This subroutine also computes velocities for the time-dependent junctions.

- The heat structure module (HTADV) advances heat conduction/transfer solutions. It calculates heat transferred across solid boundaries of hydrodynamic volumes.
- The hydrodynamics module (HYDRO) advances the hydrodynamic solution.
- The reactor kinetics module (RKIN) advances the reactor kinetics of the code. It computes the power in the reactor by assuming space independent approximation.
- The control system module (CONVAR) provides the capability of simulating control systems typically used in hydrodynamic systems.
- The time step control module (DTSTEP) determines the time step size, controls output editing, and determines whether the transient advancements should be terminated.

The modules relevant for the current research are the hydrodynamic and heat structure modules; the hydrodynamic is used to compute the fluid properties through the RCIC system components including the turbine and is where the modifications in the code will be done, the heat structure module is used in the S/C to simulate the heat exchange between the inside and the outside during the torus room flooding sensitive analysis.

4.1.2- Heat structure model

Heat structures are one of components available in RELAP5 which provide the opportunity to calculate the heat transferred across solid boundaries between hydrodynamics volumes. The principal modeling heat structures capabilities include the option to reproduce fuel pins of plates with nuclear or electrical heating, heat transfer across steam generator tubes, and the heat transfer from pipes and vessel walls. [14]

Heat structures are usually represented by one dimensional heat conduction in rectangular, spherical or electrical geometry. The heat structure is based on a non-constant spacing mesh system where each different mesh point can have different properties providing the capability of simulate complex geometries such as the fuel rod, gap and clad with accuracy. The different material thermal conductivities and volumetric heat capacities are provided in tabular or functional form either from built-in or user-supplied data.

If internal heat source is used, it can be calculated from the reactor kinetics equations, from a power vs time tables or from a control system variable.

Equation 4.1 describes the integral form of the heat conduction equation used in RELAP5. [14]

$$\iiint_V C_{p,v}(T, \vec{x}) \frac{\partial T}{\partial t}(T, \vec{x}) dV = \iint_S k(T, \vec{x}) \nabla T(T, \vec{x}) \cdot d\vec{s} + \iiint_V S(\vec{x}, t) dV \quad (4.1)$$

Where:

k: Is the thermal conductivity. [W/mK]

s: Is the contact surface. [m²]

S: Is the internal volumetric heat source [W/m³]

t: Time [s]

T: Is the temperature. [K]

V: Volume. [m³]

x: Is the space coordinate in the x-axis. [m]

C_{pV}: Is the volumetric heat capacity. [J/m³K]

Regarding the boundary conditions, RELAP includes the capability to reproduce symmetric or insulated conditions taking the data from correlation package or user-specified tables which relates the thermal properties with time or temperature. In case of a heat structure representing the wall between two hydrodynamic volumes (steam generators tubes or the S/C with the surrounding room) the correlation packages contains models for convective, nucleate boiling, transition and film boiling heat transfer from the wall to water and reverse transfer from water to wall, including condensation.

4.1.3- Hydrodynamic model

The RELAP5 hydrodynamic model computes the fluid properties by solving eight field equations, one for each of the model primary dependent variables. These primary dependent variables are the pressure (P), the phasic specific internal energies (U_g, U_f), the void fraction (steam volume fraction) (α_g), the phasic velocities (v_g, v_f), the non-condensable gases quality (X_n) which is defined in equation 4.2, and the boron density (ρ_b). The independent variables used for calculation are time (t) and distance (x). [14]

$$X_n = \frac{M_n}{M_n + M_s} \quad (4.2)$$

Where:

M_n : Is the mass of non-condensable gases. [kg]

M_s : Is the mass of steam. [kg]

There are also secondary dependent variables used in the field equations, those are; phasic densities (ρ_g, ρ_f), phasic temperatures (T_g, T_f), saturation temperature (T^s), and, in case of multiple non-condensable gases, non-condensable specie mass fraction (X_{ni}) in non-condensable gas phase described in equation 4.3. [14]

$$X_{ni} = \frac{M_{ni}}{\sum_{i=1}^N M_{ni}} = \frac{M_{ni}}{M_n} \quad (4.3)$$

Where:

M_{ni} : is the mass of the i -th non-condensable in the gaseous phase. [kg]

M_n : is the total mass of non-condensable gas in the gaseous phase. [kg]

N: is the number of non-condensable.

The basic field equations for the two-fluid non-equilibrium model consist of two phasic mass continuity equations, two phasic momentum equations, and two phasic energy equations.

4.1.3.1- Mass continuity

The phasic mass conservation equations are described in equation 4.4 for the vapor and in equation 4.5 for the liquid:

$$\frac{\partial}{\partial t}(\alpha_g \rho_g) + \frac{1}{A} \frac{\partial}{\partial x}(\alpha_g \rho_g v_g A) = \Gamma_g \quad (4.4)$$

$$\frac{\partial}{\partial t}(\alpha_f \rho_f) + \frac{1}{A} \frac{\partial}{\partial x}(\alpha_f \rho_f v_f A) = \Gamma_f \quad (4.5)$$

This equations does not include either flow source or sink, leading to the requirement that the liquid generation has to be the negative form of the vapor generation as it is described in equation 4.6 in order to accomplish the overall flow continuity

$$\Gamma_g + \Gamma_f = 0 \quad (4.6)$$

4.1.3.2- Momentum conservation

Such as the mass continuity, two momentum equations are used in the hydrodynamic model. Equation 4.7 shows the momentum conservation equation for the vapor phase meanwhile equation 4.8 shows the momentum conservation equation for the liquid phase. [14]

$$\begin{aligned} & \alpha_g \rho_g A \frac{\partial v_g}{\partial t} + \frac{1}{2} \alpha_g \rho_g A \frac{\partial v_g^2}{\partial x} = \\ & - \alpha_g A \frac{\partial P}{\partial x} + \alpha_g \rho_g B_x A - (\alpha_g \rho_g A) FWG(v_g) + \Gamma_g A(v_{gt} - v_g) \\ & - (\alpha_g \rho_g A) FIG(v_g - v_f) - C \alpha_g \alpha_f \rho_m A \left[\frac{\partial(v_g - v_f)}{\partial t} + v_f \frac{\partial v_g}{\partial x} - v_g \frac{\partial v_f}{\partial x} \right] \end{aligned} \quad (4.7)$$

$$\begin{aligned} & \alpha_f \rho_f A \frac{\partial v_f}{\partial t} + \frac{1}{2} \alpha_f \rho_f A \frac{\partial v_f^2}{\partial x} = \\ & - \alpha_f A \frac{\partial P}{\partial x} + \alpha_f \rho_f B_x A - (\alpha_f \rho_f A) FWF(v_f) + \Gamma_f A(v_{ft} - v_f) \\ & - (\alpha_f \rho_f A) FIF(v_f - v_g) - C \alpha_f \alpha_g \rho_m A \left[\frac{\partial(v_f - v_g)}{\partial t} + v_g \frac{\partial v_f}{\partial x} - v_f \frac{\partial v_g}{\partial x} \right] \end{aligned} \quad (4.8)$$

Where:

B_x : Is the body force

FIG : Is the vapor phase interface frictional drag. [s^{-1}]

FIF : Is the liquid phase interface frictional drag. [s^{-1}]

FWG : Is the vapor phase wall friction drag. [s^{-1}]

FWF : Is the liquid phase wall friction drag. [s^{-1}]

The momentum conservation equations used in RELAP5 are based on the one-dimensional phasic momentum equation with some assumptions and simplifications; the Reynolds stresses are neglected, both phases and interfacial pressures are assumed to be equal (except in case of stratified flow), covariance terms, interfacial momentum storage and phasic viscous stresses are all neglected. The interface force terms are computed from both, pressure and viscous stresses meanwhile the normal wall forces are assumed adequately modeled by the variable area momentum flux formation. [14]

The terms FWG and FWF presented in the momentum equations are part of the wall frictional drag, which are linear in velocity, and are products of the friction coefficient, the frictional reference area per unit volume, and the magnitude of the fluid bulk velocity. The interfacial velocity in the interface momentum transfer term is the unit momentum with which phase appearance or disappearance occurs. The coefficients FIG and FIF are computed by using two different models, drift flux and drag coefficient models, depending on the flow regime.

Analogous to mass conservation equations, the conservation of momentum at the interface requires that the force terms associated with interface mass and momentum exchange sum to zero as described in equation 4.9.

$$\begin{aligned} & \Gamma_g A v_{gI} - (\alpha_g \rho_g A) FIG (v_g - v_f) - C \alpha_g \alpha_f \rho_m A \left[\frac{\partial (v_g - v_f)}{\partial t} \right] \\ & - \Gamma_g A v_{fI} - (\alpha_f \rho_f A) FIF (v_f - v_g) - C \alpha_f \alpha_g \rho_m A \left[\frac{\partial (v_f - v_g)}{\partial t} \right] = 0 \end{aligned} \quad (4.9)$$

Equations 4.10 and 4.11 show the general assumption that the interface momentum transfer due to friction and due to mass transfer independently sum to zero.

$$v_{gI} = v_{fI} = v_I \quad (4.10)$$

$$\alpha_g \rho_g FIG = \alpha_f \rho_f FIF = \alpha_g \alpha_f \rho_g \rho_f FI \quad (4.11)$$

Where:

FI: Is the global interfacial friction coefficient

Flow regime map

If two different phases coexist in the same component, the momentum conservation equations are influence by the interphase drag coefficients which depend on the flow regime in that component.

RELAP5 has different flow regimes estates based on the component properties and geometry; vertical flow regime, horizontal flow regime, ECC mixer flow regime and junction flow regime. In case of the present research, the RCIC turbine is nodalized in RELAP5 as a horizontal component. [14]

The horizontal flow regime map used in RELAP5 is applied to volumes with an elevation angle Θ such that $0 < \Theta < 45^\circ$. The map used is similar to the vertical flow regime map and consist to 5 different flow regimes; horizontally stratified, bubbly, slug, annular-mist, and mist pre-CHF. The flow regimes corresponding to post-CHF are not included in the horizontal flow map. [14]

Figure 4-3 represents the schematic of the horizontal flow regime map with the transition between the different regimes based on the velocity, mass flux and void fraction increment.

In the schematic, the flow regime can vary both, horizontally or vertically. Horizontally the flow regime depends on the fluid void fraction passing through bubbly, slug, annular mist and pre-CHF regimes.

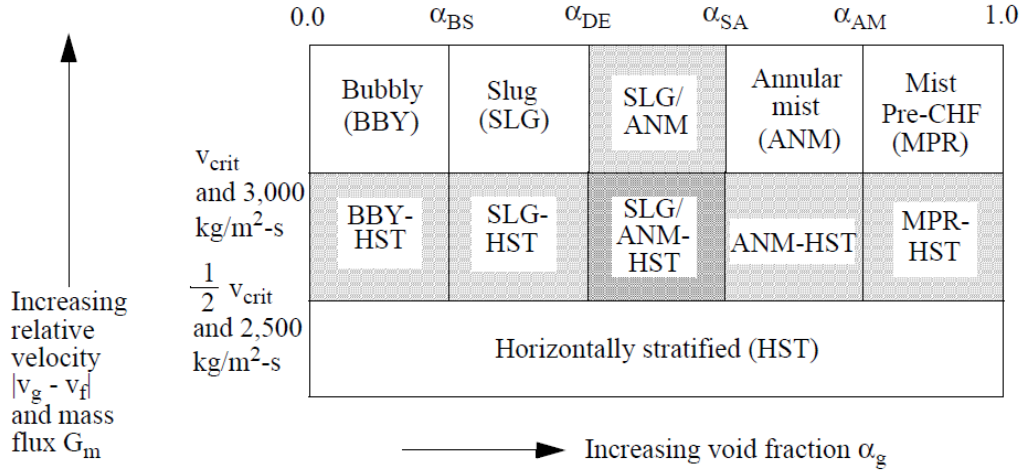


Figure 4-3 Horizontal pipe flow regimes [14]

The minimum void fraction needed for transition between the bubbly and slug regimes (α_{BS}) is mainly influenced by the mass flux as can be observed in equation 4.12.

$$\begin{aligned} \alpha_{BS} &= 0.25 & G_m &\leq 2000 / \frac{kg}{m^2 s} \\ &= 0.25 + 0.00025 * (G_m - 2000) & 2000 < G_m < 3000 \text{ kg/m}^2 s \\ &= 0.5 & G_m &\geq 3000 \text{ kg/m}^2 s \end{aligned} \quad (4.12)$$

The minimum void fraction for annular mist flow (α_{AS}) is constant.

$$\alpha_{AS} = 0.8 \quad (4.13)$$

The transition between annular mist flow and slug is a region corresponding to a fluid with a void fraction between $\alpha_{DE} < \alpha_g < \alpha_{AS}$, where α_{DE} is defined as a constant by equation 4.14.

$$\alpha_{DE} = 0.75 \quad (4.14)$$

At last, the final flow regime, the pre-CHF, is reached when the fluid void fraction is almost the unity.

$$\alpha_{AM} = 0.9999 \quad (4.15)$$

Vertically, the regime depends on the velocity and the mass flux and the flow rate can move from horizontal stratified to the rest of the available regimes. The criterion to define

the horizontal stratified regime is based on the one developed by Taitel and Dukler[14]. According to the model, the flow regime is horizontal stratified if the vapor velocity is lower than a critical velocity, as explained in equation 4.16

$$|v_g| \leq v_{crit} \quad (4.16)$$

Where:

v_{crit} : Is the gas velocity above which the horizontal interphase waves will grow. [m/s]

$$v_{crit} = \frac{1}{2} \left[\frac{(\rho_f - \rho_g)g\alpha_g A}{\rho_g D \sin\theta} \right]^{\frac{1}{2}} (1 - \cos\theta) \text{ [m/s]} \quad (4.17)$$

Where:

A : Is the pipe cross-section area. [m²]

D : Is the pipe diameter. [m]

θ : Is related to the liquid level with respect to the bottom of the volume. [degrees] **Figure 4-4** shows the relationship between the angle and the void fraction [14]

$$\alpha_g \pi = \theta - \sin\theta \cos\theta \quad (4.18)$$

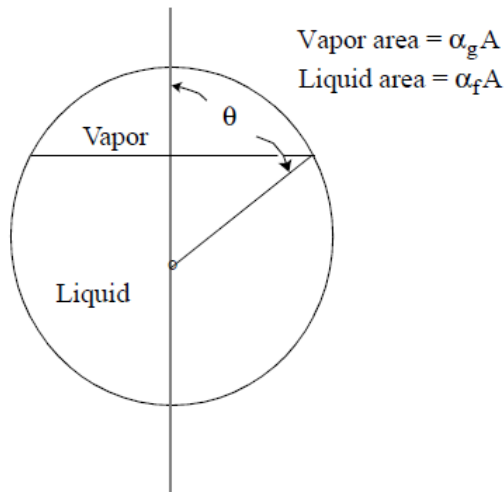


Figure 4-1 $\theta - \alpha_g$ relationship [14]

This initial condition is modified in the RELAP5 code to handle situations where the flow is stratified but the liquid is not stagnant as was assumed in the study by Taitel and

Dukler[14]. Then, equation 4.16 is modified and the flow is horizontally stratified if the phasic velocity difference satisfies the condition expressed in equation 4.19.

$$|v_g - v_f| \leq v_{crit} \quad (4.19)$$

The velocity condition described in equation 4.19 is coupled with the requirement of a mass flux $G_m \leq 3000/kg/m^2s$ in order to establish the horizontal stratified flow regime boundaries.

If both conditions are accomplished, the flow undergoes to a horizontal stratified regime, if the conditions are not satisfied, the fluid undergoes to a transition to a bubbly, slug, annular mist or pre-CHF regimes based on its void fraction. As can be appreciated in **Figure 4-3**, the lower transition limits are $|v_g - v_f| = 1/2 v_{crit}$ and $G_m \leq 2500/kg/m^2s$.

Once the flow regime is computed based on the fluid properties, the code selects one of the two different models availables to calculate the interphase drag coefficients used in the momentum equations 4.7 and 4.8; drift flux and drag coefficient models

Drift flux

The first model available correspond to the drift flux model; an approximation used only in the bubbly and slug regimes in vertical flows. The model specified the distribution coefficient and the vapor drift velocity. Then, these two quantities must be converted into a constitutive relation for the interfacial frictional force per unit volume in order to compute the global interfacial friction coefficient (FI). The process to accomplish the conversion is divided into two steps.[14]

- The first one considers the effect of the phasic wall frictional force on the relative velocity between the vapor and liquid phases
- The second step computes the interfacial friction force per unit volume from the drift flux parameters

Drag coefficient

The drag coefficient model is the model used to calculate the interphase drag force when the drift flux is not used; in all the flow regimes except for the slug and bubbly in vertical flows. This model has been included in the code since the early version of RELAP5, when it was used for all the regimes, and is based on the correlations for drag coefficients and for the computation of the interfacial area density. [14]

Equation 4.20 describes the relation for the frictional force between a moving body and the surrounding fluid.

$$F = \frac{1}{2} \rho v^2 C_D A \text{ [N]} \quad (4.20)$$

Where:

F : Is the drag force. [N]

ρ : Is the fluid density. [kg/m³]

v : Is the velocity of the body relative to the fluid. [m/s]

C_D : Is the drag coefficient

A : Is the projected area of the body. [m²]

If the moving body is constituted by a group of bodies moving through a fluid (bubbles moving through fluid or droplet moving through vapor), the equation 4.20 is modified to represent the frictional force developed for each body into equation 4.21.

$$F_i = \frac{1}{8} \rho_c |v_g - v_f| (v_g - v_f) C_D S_F a_{gf} = C_i |v_g - v_f| (v_g - v_f) \quad (4.21)$$

Where:

F_i : Is the force per unit volume of fluid

C_i : $\frac{1}{8} \rho_c C_D S_F a_{gf}$

ρ_c : Density of continuous phase

a_{gf} : Is the interfacial area per unit volume

S_F : Is the shape factor

The additional factor of $\frac{1}{4}$ between equation 4.20 and 4.21 comes from the conversion of the projected area of spherical particles into the interfacial area, meanwhile, the shape factor is included to consider the non-spherical particles. Once the parameters of continuous density, shape factor, interfacial area density and drag coefficient are found for a given regime, the interfacial force is computed using equation 4.21 from which the global interfacial friction coefficient (FI) can be calculated using equation 4.22 assuming $F_{ig} = F_{if} = F_i$

$$FI = \frac{\left(\frac{F_{ig}}{\alpha_g \rho_g} + \frac{F_{if}}{\alpha_f \rho_f} \right)}{\rho_m (v_g - v_f)} \quad (4.22)$$

4.1.3.3- Energy conservation

At last, the two phasic thermal energy equations used by the hydrodynamic model are described in equation 4.23 and 4.24.

$$\begin{aligned} \frac{\partial}{\partial t}(\alpha_g \rho_g U_g) + \frac{1}{A} \frac{\partial}{\partial x}(\alpha_g \rho_g U_g v_g A) = \\ -P \frac{\partial \alpha_g}{\partial t} - \frac{P}{A} \frac{\partial}{\partial x}(\alpha_g v_g A) + Q_{wg} + Q_{ig} + \Gamma_{ig} h_g^* + \Gamma_w h_g' + DISS_g \end{aligned} \quad (4.23)$$

$$\begin{aligned} \frac{\partial}{\partial t}(\alpha_f \rho_f U_f) + \frac{1}{A} \frac{\partial}{\partial x}(\alpha_f \rho_f U_f v_f A) = \\ -P \frac{\partial \alpha_f}{\partial t} - \frac{P}{A} \frac{\partial}{\partial x}(\alpha_f v_f A) + Q_{wf} + Q_{if} + \Gamma_{if} h_f^* + \Gamma_w h_f' + DISS_f \end{aligned} \quad (4.24)$$

Analogous to the momentum conservation equations, the energy equations are based the one-dimensional phasic thermal energy equations with the following simplifications:

- Reynolds heat flux is neglected
- Covariance terms are universally neglected (unity assumed for covariance multipliers)
- Interfacial energy storage is neglected
- Internal energy storage is neglected

The phasic energy dissipation terms, $DISS_g$ and $DISS_f$, are the sums of wall friction and pump effects. The dissipation effects due to interface mass transfer, interface friction, and virtual mass are neglected. This is a reasonable assumption since these terms are small in magnitude in the energy equation. In the mass and momentum equations, interface mass transfer, interface friction, and virtual mass are important and are not neglected. The wall friction dissipations are defined in equations 4.25 and 4.26. [14]

$$DISS_g = \alpha_g \rho_g FWG v_g^2 \quad (4.25)$$

and

$$DISS_f = \alpha_f \rho_f FWF v_f^2 \quad (4.26)$$

The phasic energy dissipation terms satisfy the relation expressed in equation 4.27.

$$DISS = DISS_g + DISS_f \quad (4.27)$$

Where:

$DISS$: Is the energy dissipation. When a pump component is present, the associated energy dissipation is also included in the dissipation terms.

4.2- RELAP RCIC system nodalization

RELAP/ScdapSIM has been widely used since its earliest versions to simulate accident progression in both, PWR and BWR. **Figure 4-5** describes one of the most used BWR nuclear power plant nodalization corresponding to the BWR/5 reactor of Laguna Verde (Mexico). Laguna Verde input model has been used for preliminary assessments for Fukushima accident [37].

The Laguna Verde input model was initially developed by CNSNS and it is provided with a high level of detail. It represents all the important features of the core, RPV, associated emergency cooling systems and the containment. The core is based on a four groups or representative BWR assemblies which differ in their properties; burnup histories and power levels and the associated control blade/channel boxes. Each group has associated a

flow channel to describe the flow within it and an additional flow channel representing the flow in the bypass regions outside the channel boxes and surrounding the control blades.

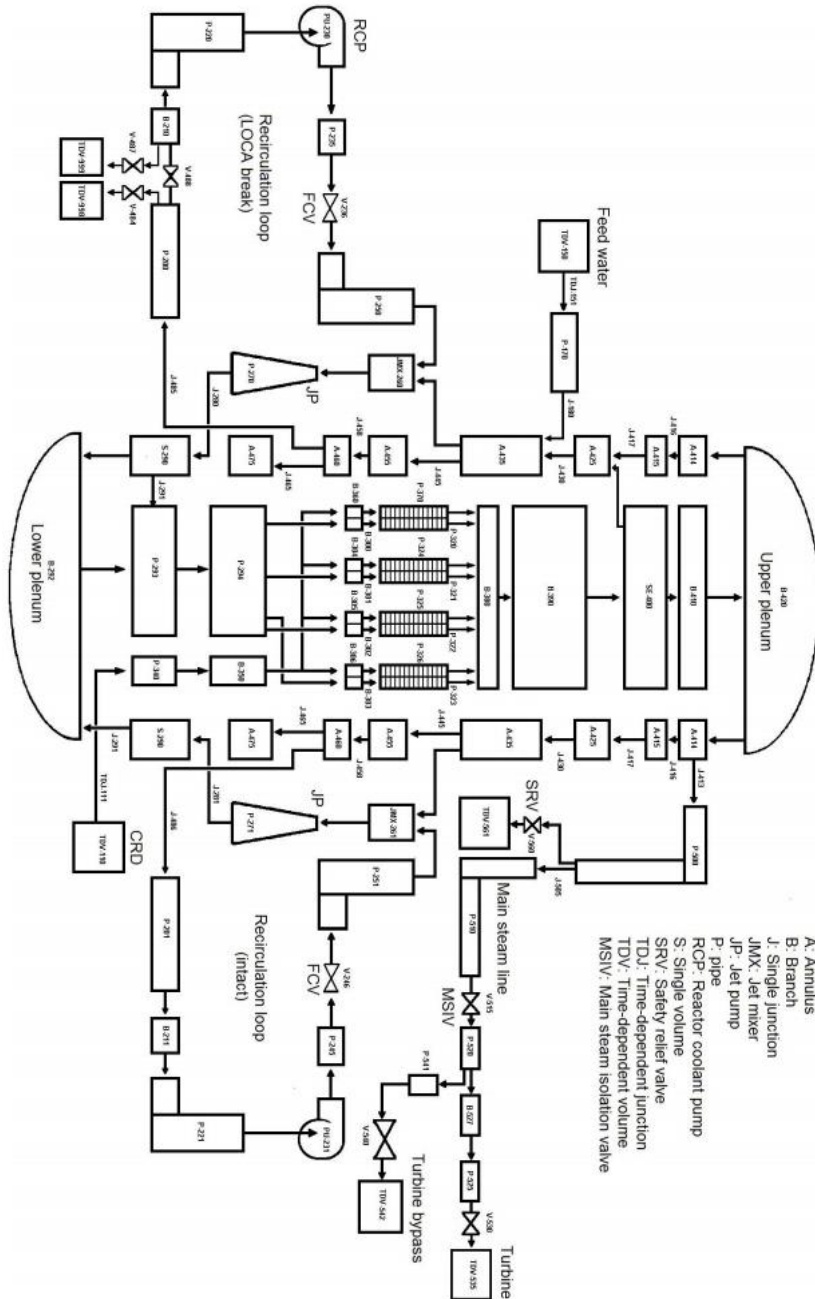


Figure 4-5 Laguna Verde nodalization [37]

Each representative assembly in each group includes a fuel rod bundle, Zircaloy channel box and a B₄C control blade. Fuel rods and channel box have been created using the corresponding Scdap models for fuel rod and channel box/control blade component. The corresponding axial and radial peak factors are based on the Fukushima Daiichi records. [37]

Figure 4-6 displays the RCIC function in the Laguna Verde input deck. As can be observed, the RCIC system is reduced to a water injection from the upper region of the upper dome. The corresponding steam mass flow to the RCIC turbine is included in the MSL and used to regulate the amount of water injected by the system described in the figure.

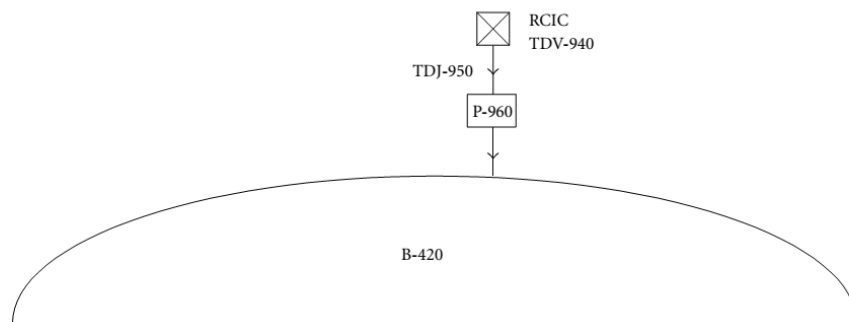


Figure 4-6 Laguna Verde RCIC system nodalization [37]

This simplification can be affordable in normal accident progression where the RCIC system operates in cycles, being open until the water level in the RPV raises enough and then being turned off. In F1D2 this simplification is not enough, as explained in Chapter 3, the RCIC operated for almost 70h without stopping, taking a major role in the accident progression.

The main reasons why the RCIC is usually simplified can be divided in two:

- The turbine model: In RELAP5, the turbine model requires a lot of data which is usually not available for the user. Despite RELAP/ScdapSIM manuals offer generic values for the unknown parameters, the resulting model is quite sensible and can easily crash terminating the simulation suddenly. This is the main reason why, as can be noticed in the nodalization in **Figure 4-5**, not only the RCIC turbine but all

the turbines are represented by time-dependent volumes instead of turbine components.

- The pump model: The pump model in RELAP5 requires a specific set of parameters called the homologous curves which are difficult to compute if the data is not available. The RCIC pump and the homologous curves generation will be discussed deeply later.

The RCIC system nodalization created for this study has passed for an iteration process having several versions while gaining in complexity and detail. The early version was mainly a description of the three basic elements of the RCIC system; RCIC turbine, S/C and RCIC pump. During the iteration process displayed in **Figure 4-7**, secondary systems such as the vacuum breakers to connect the S/C and the drywell, the RHR system and the CST were added. Due to the assumptions made of the accident progression, where the torus room was considered to be flooded by the tsunami affecting the S/C pressure and temperature, a heat exchanger structure was created to simulate the S/C wall in order to compute the heat transfer at several outside conditions.

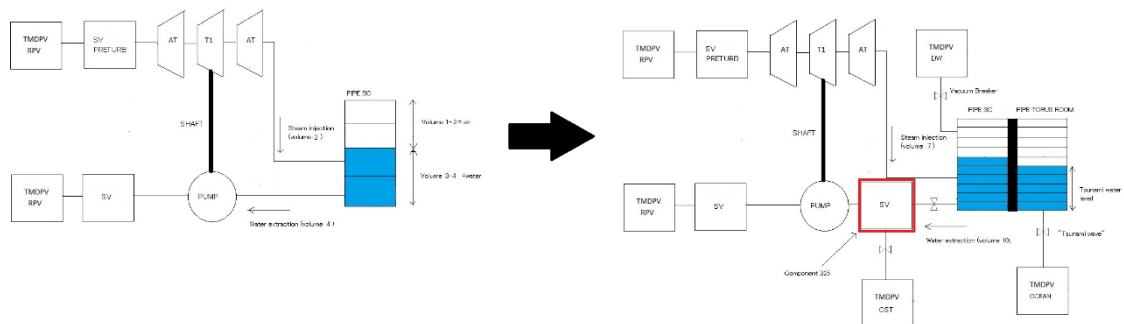


Figure 4-7 Iteration of RCIC system nodalization

Figure 4-8 shows in detail the final nodalization used to represent the RCIC system. The steam is extracted from the MSL region of the RPV represented by the time-dependent volume 210; time-dependent volumes are infinite flow volumes used in RELAP5 to simulate the entrance and exits of the nodalized system, they are used to establish the flow boundary conditions at each time step.

The steam is moved by the piping system through the turbine stage group represented by the actual turbine and the initial/final artificial turbine used only for computational purposes without any kind of effect in the final results []. The steam then, reaches the

suppression chamber, represented by an annulus component (A-415) with ten vertical nodes.

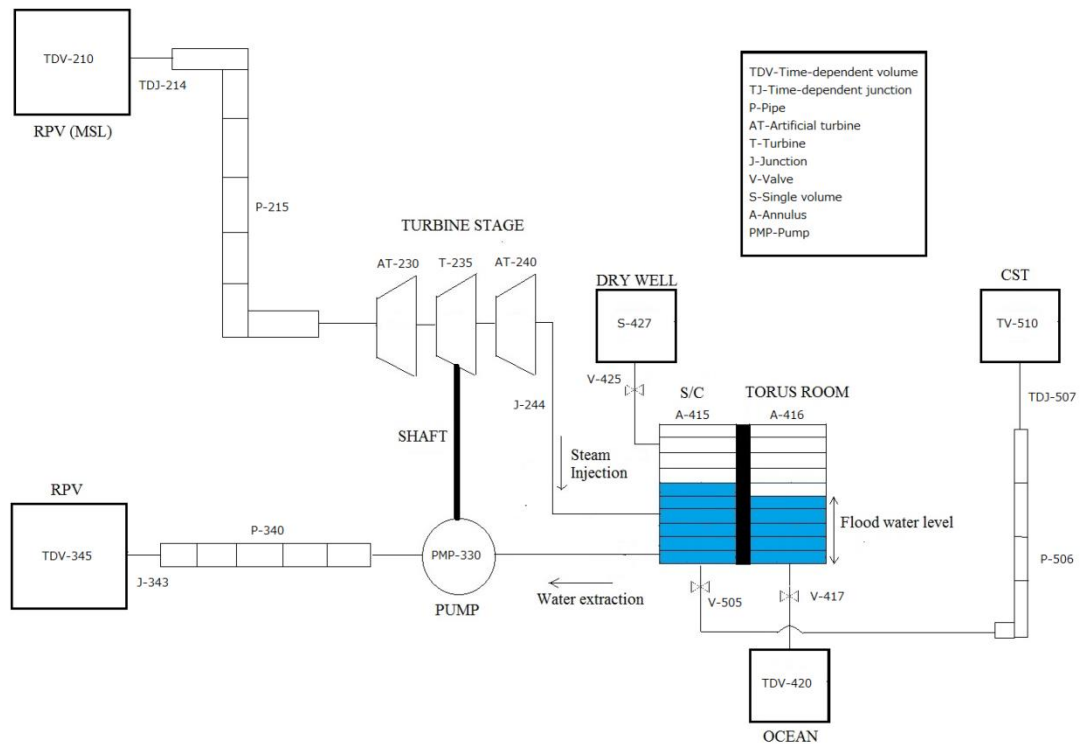


Figure 4-8 Final version of the RCIC nodalization

The upper nodes are filled with air, assumed non-condensable gas in RELAP5, while the bottom six nodes are filled with water representing the S/C water inventory of around 3000m^3 .

The nodes are used to reproduce the thermal stratification phenomenon that happens in the S/C when the hot steam injection interacts with the cold water of the pool. As can be observed in **Figure 4-7** the number of nodes has been increased from the early iterations, the reason behind this decision is to avoid the computation oscillations caused when a water node is depleted due to the water extraction and replaced with non-condensable gas. As the nodes are larger, the resulting oscillation becomes larger.

The S/C is connected to the surrounding room (A-416) by a heat structure used to evaluate the heat transfer between the inside and outside of the S/C. The reproduction of the heat structure has to take into consideration the special shape of the suppression pool; a toroid chamber. Since toroid volumes cannot be reproduced in RELAP5 some considerations have to be taken in order to obtain accurate simulation results.

Figure 4-9 shows how the volume and heat transfer surface continuity that must be preserved when a toroid volume is converted into a cylindrical-shape component. In other words, each of the nodes has to have the same volume and transfer surface in the RELAP5 nodalization than they have in the real volume

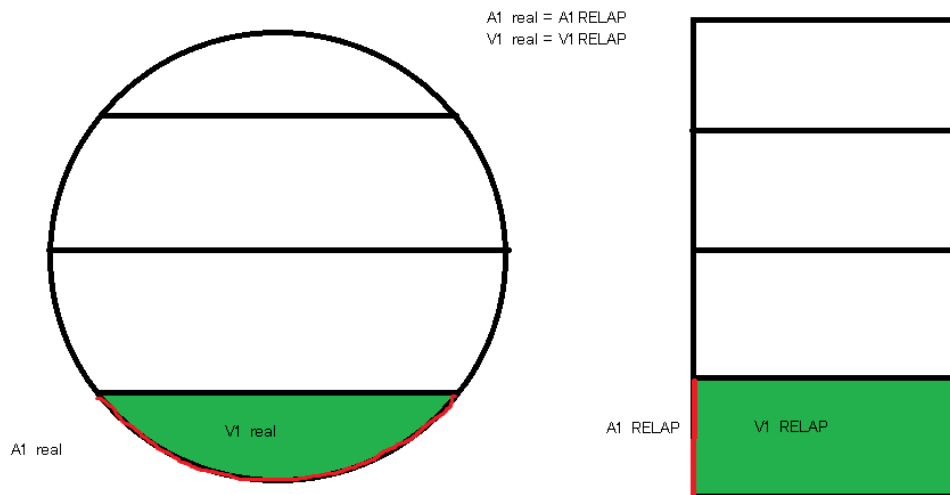


Figure 4-9 Heat structure volume and area conservation

The S/C surrounding room, A-416, is also divided into ten vertical nodes and connected to a time-dependent volume by a valve. This subsystem is used to simulate the effect of the tsunami and can be applied to different water flooding heights.

The mass is extracted from the S/C by two ways:

- Cold water is extracted from the bottom node and pumped back to the RPV by the RCIC pump (PMP-330). The pump is directly connected to the turbine by a shaft.
- Once the pressure inside the suppression chamber exceeds the drywell pressure by 25psia, the vacuum breaker valves are opened to equalize the pressure between them.

The CST is the last subsystem nodalized, it is represented by a time-dependent volume and the amount of water injected to the system is regaled by the CST valve (V-505), regarding TEPCO data [], CST of F1D2 injected 1000T during the first 13 hours so the corresponding control logic is set up to reproduce that behavior in the simulations.

Since the RHR system was not operational during the accident, it has been not included in the current RCIC nodalization.

This current RELAP5 RCIC nodalization is able to work either being connected to a larger nodalization such as the Laguna Verde NPP shown in **Figure 4-5** or alone.

To work alone only up to three variables are needed to run the simulation; the RPV pressure, the MSL flow quality and, optionally, the RPV temperature. Those values are used as boundary conditions in volumes TDV-210 and TDV-245. This kind of simulations have the benefit of being faster than the ones including more complex input decks and in cases where the RPV pressure profile is available such as the F1D2 accident progression.

4.3- RELAP code modifications

The modifications presented in this chapter will be applied into the RELAP5 turbine model in order to improve the model performance under two-phase flow scenarios. The modifications are the turbine degradation coefficient developed in Chapter 2 and the steam flashing phenomenon.

4.3.1- Turbine degradation coefficient

The NHEM turbine degradation coefficient developed in Chapter 2 and described in equation 2.26 will be applied into the turbine power calculation. In RELAP5, the turbine power is computed in the `turbst.ff` subroutine which is included in the `vexp.ff` and `vimp.ff` subroutines which, at the same time, are part of the hydrodynamic model.

The previous volume continuity equations presented early in this chapter are used for the stage group, assuming a nozzle throat area for the inlet and the last stator nozzle throat discharge area for the outlet. Unlike, mass and energy continuity equations, the momentum conservation equations in the turbine component are modified by the work extracted in the rotating blades system of each stage group.

The development of these modified equations is started assuming a steady-state total energy balance for a homogeneous fluid passing through the volume, as described in **Figure 4-10**, and then, that general equation is extended to be used for the two-fluid system.

Equation 4.28 represents the total energy balance between the inlet (1) and outlet (2) (Figure 4-10) cross-sections in a steady-state situation. [14][35]

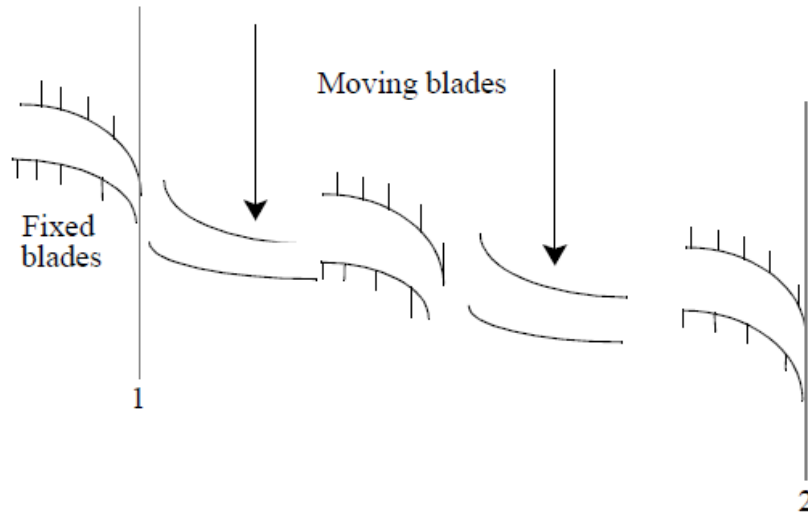


Figure 4-10 Turbine stages diagram [14]

$$\left[\rho v A \left(\frac{1}{2} v^2 + h \right) \right]_1 = \left[\rho v A \left(\frac{1}{2} v^2 + h \right) \right]_2 + (\rho v A)_1 W \quad (4.28)$$

Where:

ρ : Is the density. [kg/m³]

v : Is the velocity. [m/s]

h : Is the enthalpy. [J/kg]

A : Is the cross-sectional area. [m²]

W : Is the shaft work per mass flow rate extracted from the fluid. [W]

In this ideal situation the heat loss is neglected and, for continuity considerations, $\rho v A$ is considered constant. Diving equation 4.28 by $\rho v A$ the energy balance is converted into an equivalent force balance (power=force x velocity) as displayed in equation 4.29.

$$\frac{1}{2} v_2^2 - \frac{1}{2} v_1^2 = -(h_2 - h_1) - W \quad (4.29)$$

In the ideal isentropic process, if the external heat loss and internal dissipation are neglected, the enthalpy difference is equal the specific volume times the pressure difference ($dh = 1/\rho dp$). [14][35]

$$h_2 - h_1 = \frac{1}{\rho} (p_2 - p_1) \quad (4.30)$$

The actual work produced per unit of mass flow by the fluid as the momentum changes is calculated as an efficiency factor times the isentropic enthalpy change across the stage as described in equation 4.31. [14][35]

$$W = -\eta \int_{S=const} dh = -\eta \int_{S=const} \frac{1}{\rho} dp \quad [W/kg s^{-1}] \quad (4.31)$$

Where:

η : Is the stage group efficiency

If constant efficiency and density are assumed for each stage group, equation 4.31 can be approximated as displayed in equation 4.32.

$$W = -\eta \frac{1}{\rho} \Delta p \quad [W/kg s^{-1}] \quad (4.32)$$

In the unmodified RELAP5 turbine model, when equations 4.30 and 4.32 are substituted into equation 4.29 the resulting equation (equation 4.33) corresponds to the momentum equation for the analyzed steady-state case. Equation 4.33 shows that only a small fraction, corresponding to $(1-\eta)$, of the pressure gradient contributes to changes in the fluid kinetic energy. The larger fraction, η , of the pressure gradient results in turbine work.

$$\frac{1}{2} v_2^2 - \frac{1}{2} v_1^2 = -\left(\frac{1-\eta}{\rho}\right) (p_2 - p_1) \quad (4.33)$$

If the momentum conservation equation for the steady-state is expanded to contemplate two-phase fluid scenarios, the resulting momentum equation for each phase will be as the formulas described, in differential form, in equations 4.34 (for the vapor) and 4.35 (for the liquid).

$$(\alpha_g \rho_g) \left(\frac{dv_g}{dt} + v_g \frac{dv_g}{dx} \right) = -\alpha_g (1-\eta) \frac{dp}{dx} - \alpha_g \rho_g HLOSSG v_g - \alpha_g \rho_g FIG (v_g - v_f) \quad (4.34)$$

$$(\alpha_f \rho_f) \left(\frac{dv_f}{dt} + v_f \frac{dv_f}{dx} \right) = -\alpha_f (1 - \eta) \frac{dp}{dx} - \alpha_f \rho_f HLOSSL v_f - \alpha_f \rho_f FIL (v_f - v_g) \quad (4.35)$$

Where:

$HLOSSG, HLOSSL$: Are vapor and liquid frictional losses. [m/s]

The model modification will take place once the turbine power is computed. This way, equation 4.32 will be modified with the NHEM degradation coefficient displayed in equation 2.26. Equation 4.36 shows the turbine power calculated with the inclusion of the new parameter.

$$W' = W \eta_{NHEM} \rightarrow W' = \left[-\eta \int_{S=const} \frac{1}{\rho} dp \right] \eta_{NHEM} [W/kg s^{-1}] \quad (4.36)$$

Where:

$$\eta_{NHEM}: -0.623x^2 + 1.357x + 0.248$$

Then equation 4.36 will be rewritten to consider the new parameter

$$\frac{1}{2} v_2^2 - \frac{1}{2} v_1^2 = - \left(\frac{1 - \eta * \eta_{NHEM}}{\rho} \right) (p_2 - p_1) \quad (4.37)$$

Analogously, the momentum conservation equations presented in equations 4.34 and 4.35 are modified considering the NHEM turbine degradation.

$$\begin{aligned} (\alpha_g \rho_g) \left(\frac{dv_g}{dt} + v_g \frac{dv_g}{dx} \right) = \\ -\alpha_g (1 - \eta * \eta_{NHEM}) \frac{dp}{dx} - \alpha_g \rho_g HLOSSG v_g - \alpha_g \rho_g FIG (v_g - v_f) \end{aligned} \quad (4.38)$$

$$\begin{aligned} (\alpha_f \rho_f) \left(\frac{dv_f}{dt} + v_f \frac{dv_f}{dx} \right) = \\ -\alpha_f (1 - \eta * \eta_{NHEM}) \frac{dp}{dx} - \alpha_f \rho_f HLOSSL v_f - \alpha_f \rho_f FIL (v_f - v_g) \end{aligned} \quad (4.39)$$

Generally, there are several guidelines used for turbine calculations in RELAP5 that have to be considered.

- Generally, due to the low amount of water in the turbine it is recommended to use the homogeneous option in all axial junctions. If it is desired, the condensation effect can be included in the stage efficiency
- The fluid path through the turbine is very tortuous making the wall friction meaningless. Wall friction in turbine should be set at 0, if it is desired, the wall friction can be included in the user-specified form loss
- The area changes in a turbine are gradual, so the smooth junction option should be used

In RELAP5, the efficiency coefficient that appears in the equations 4.31 to 4.39 can be computed by using three different models depending on the data available. Those formulas affect the simulated turbine output power and will be discussed deeper in the next chapter along with the sensitivity analysis.

As observed in Chapter 2, the turbine torque and power are related by the Euler equation. In RELAP5, the torque is computed by the formula displayed in equation 4.40

$$\tau = (\rho v A) W \frac{R}{v_t} = (\rho v A) \frac{\eta}{\rho} (p_2 - p_1) \frac{R}{v_t} [Nm] \quad (4.40)$$

Where:

R : Is the mean stage radius at the nozzle. [m]

v_t : Is the tangential or rim velocity of the moving blades. [m/s]

With the modification to include the turbine degradation, equation 4.40 becomes

$$\tau = (\rho v A) W' \frac{R}{v_t} = (\rho v A) \frac{\eta * \eta_{NHEM}}{\rho} (p_2 - p_1) \frac{R}{v_t} [Nm] \quad (4.41)$$

4.3.2- Steam Flashing

Steam flashing, or flash evaporation, is a phenomenon that occurs when saturated liquid flow at high pressures is discharged into a low pressure volume by passing through a throttling valve or equivalent device. If the liquid is a single-component liquid such as water, a fraction of it directly flashes into vapor. [38]

There is the assumption, made by some of the investigation reports [24], that the liquid phase suffered the process when moving through the RCIC turbine during the F1D2 accident. This phenomenon drastically increases the flow quality and eventually influences on the power developed by the turbine; if the both, turbine degradation and steam flashing are considered, the developed power by the turbine is higher than if only the degradation coefficient is applied.

The amount of steam generated by the steam flashing can be easily deduced based on the upstream and downstream conditions (RPV and S/C in case of the RCIC turbine) as it is displayed in equation 4.42.

$$w = \frac{(h_{il} - h_{fl})}{h_{fe}} \quad (4.42)$$

Where:

w : Is the ratio of flash vapor generated [kg of vapor/kg of condensate]

h_{il} : Is the initial liquid enthalpy (upstream conditions). [kJ/kg]

h_{fl} : Is the final liquid enthalpy (downstream conditions). [kJ/kg]

h_{fe} : Is the final evaporation enthalpy (downstream conditions). [kJ/kg]

Observing the equations used in the turbine model in RELAP5, there is no information about the possibility of phase change due to the expansion suffered by the fluid. The change in the quality will modify the liquid and vapor void fractions and, consequently, affect the momentum equations described in equations 4.34 and 4.35. In case to consider both, degradation and steam flashing, the modifications will also affect the degradation coefficient itself.

Assuming that the initial quality of a fluid is $x = M_g/M_t$ where M_g is the initial vapor mass and M_t is total initial fluid mass, after the expansion, the quality changes to $x' = M_g'/M_t'$ where M_g' and M_t' are the vapor and total masses after the flashing. Then, assuming mass conservation where $M_t' = M_t$, the relationship between the initial and final qualities can be calculated.

$$\begin{aligned} \frac{M_g'}{x'} &= \frac{M_g}{x} \rightarrow \frac{(M_g + wM_w)}{x'} = \frac{M_g}{x} \rightarrow x' = x \frac{(M_g + wM_l)}{M_g} \rightarrow \\ \rightarrow x' &= x \frac{(M_g + w(M_t - M_g))}{M_g} \rightarrow x' = x \frac{(M_g + w(\frac{M_g}{x} - M_g))}{M_g} \rightarrow x' = x + w - wx \end{aligned} \quad (4.43)$$

Where:

M_l : Is the initial liquid mass. [kg]

w : Is the ratio of flash vapor generated [kg of vapor/kg of condensate]

Generally, the void fraction is computed using the quality-void fraction relationship by equation 4.44.

$$V_g \rho_g = M_g \rightarrow \alpha_g V_t \rho_g = x M_t \rightarrow \alpha_g = x \frac{\rho_t}{\rho_g} \quad (4.44)$$

Where:

V_g : Is the vapor volume. [m³]

V_t : Is the volume of the fluid. [m³]

ρ_t : Is the density of the fluid. [kg/m³]

The void fraction change due to the steam flashing evaporation is described in equation 4.45 rearranging equations 4.44 and 4.43

$$\alpha_g' = x' \frac{\rho_t}{\rho_g} \rightarrow \alpha_g' = (x + w - wx) \frac{\rho_t}{\rho_g} \rightarrow \alpha_g' = \alpha_g + w \frac{\rho_t}{\rho_g} - w \alpha_g \quad (4.45)$$

4.4- RCIC Pump

Unlike the turbine, in the RCIC pump there is no two-phase flow study to be done, the pump is always pumping water unless the S/C or the CST are completely depleted during the operation time.

On the other hand the pump requires a specific set of data called the homologous curves in order to be simulated by RELAP/Scdap with precision. The main objective of this section is to generate those curves from the RCIC specification data from **Table 1-1**

4.4.1- Description

The RCIC pump is a horizontal, turbine-driven, single stage, centrifugal impulse pump. The centrifugal pump is one of the most used types of pump around the world. The principle behind is really simple, well-described and widely tested, the resulting pump is robust, effective and relatively cheap to produce. Despite the wide range of variations on the basis of the centrifugal pump, all of them have the same basic hydraulic parts. [39]

The basic principle behind the centrifugal pump is the increment of the fluid pressure due to the increment in its velocity caused by the centrifugal force; the fluid flows from the inlet to the impeller center and out along its blades receiving the mechanical energy generated by the motor (turbine in case of RCIC) through the rotating impeller. **Figure 4-11 [40]** shows an example of the fluid path.

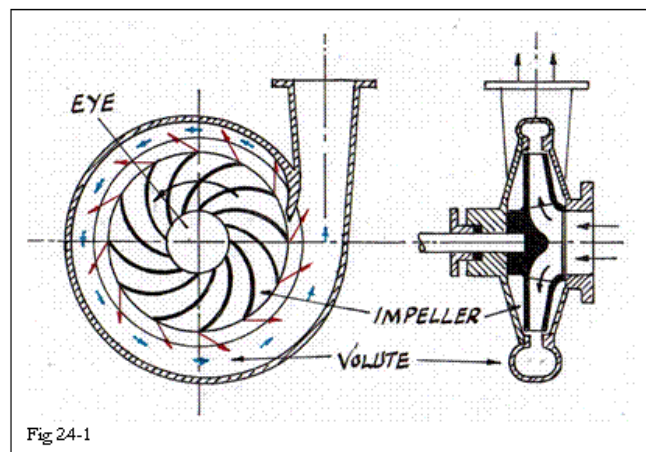


Figure 4-11 Flow path [40]

Figure 4-12 [41] Shows a cutaway view of a centrifugal pump where the common hydraulic elements of a centrifugal pump can be observed. The main hydraulic elements of this type of pump are listed below. [39-40]

- Inlet/outlet flanges: the pump is usually connected to the piping system through its inlet and outlet flanged which design depends on the pump purpose. If the pump is

already submerged in the fluid the inlet flange can be removed. The main function of the inlet flange is to guide the fluid to the center of the impeller (impeller eye). The inlet depends of the pump design being the most common ones the inline, endsuction, doublesuction and inlet for submersible pumps.

- Impeller: The key element, the impeller transferees the mechanical energy from the motor to the fluid converting it into kinetic energy and pressure increment. The fluid is sucked into the impeller at the impeller eye and moved in the radial axis through the impeller channels formed by the blades between the shroud and the hub. The design of the impeller is based on the pressure, flow rate and application specifications being the primary element determining the overall pump performance. The simply change of the impeller changes completely the pump; radial impellers are those which outlet diameter is larger than the inlet meanwhile the axial are those where both diameters are the same.

Another critical factor in the impeller performance, and eventually the overall pump, is the number of blades which depends on the requested performance and noise as well as the solid particle seize in the fluid. Impellers with 5-10 blades are usually applied to non-particles fluid while impellers with 2, 3, and 4 are used for high density solid particles fluid such waste water.

- Coupling and drive: In the RCIC the pump impeller is connected to the steam turbine by a shaft creating a weak point due to the difficult of sealing a rotating shaft. In the RCIC system the coupling corresponds to a dry runner pump where the turbine and pump are separated by a long shaft and seal.
- Impeller seal: this seal is mounted in order to prevent a leakage in the gap between the rotating impeller and the static housing when the pump is under operation. The leak ratio depends on the design of the gap and the impeller pressure increment specifications. Since the leak flow will return to the impeller eye, the impeller has to pump both, the leak and the main flow.
- Cavities and axial bearings: Depending on the impeller design, the volume of the cavities will vary affecting the flow around the impeller and capability of the pump to handle small particles such sand and dust. The impeller rotation generated two types of flows in the cavities; primary and secondary that can be observed in **Figure 4-13 [39]**. These flows affect the pressure distribution on the outside of the impeller hub and shroud affecting the axial thrust (sum of all the forces in the axial

axis). The absorption of the axial thrust is the main objective of the axial bearings in order to ensure the balance of the impeller.

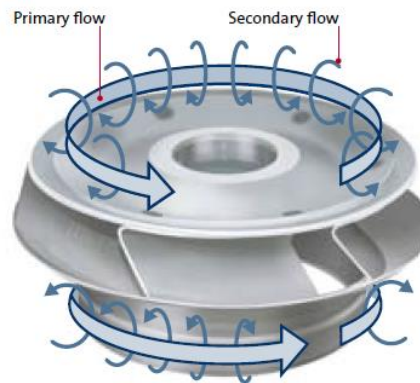


Figure 4-13 Primary and secondary flows at the impeller [39]

- Volute casing, diffuser and outlet flange: The main function of the volute casing is to collect the fluid from the impeller and drive it into the outlet flange. The volute casing converts the dynamic pressure into static pressure using the diffuser; the gradually velocity reduction along with the cross sectional area increment.

Since the RCIC pump is a single stage it does not have a return channel and outer sleeve which are mainly used in multistage pumps to move the fluid from the outlet of the last stage to the outlet flange.

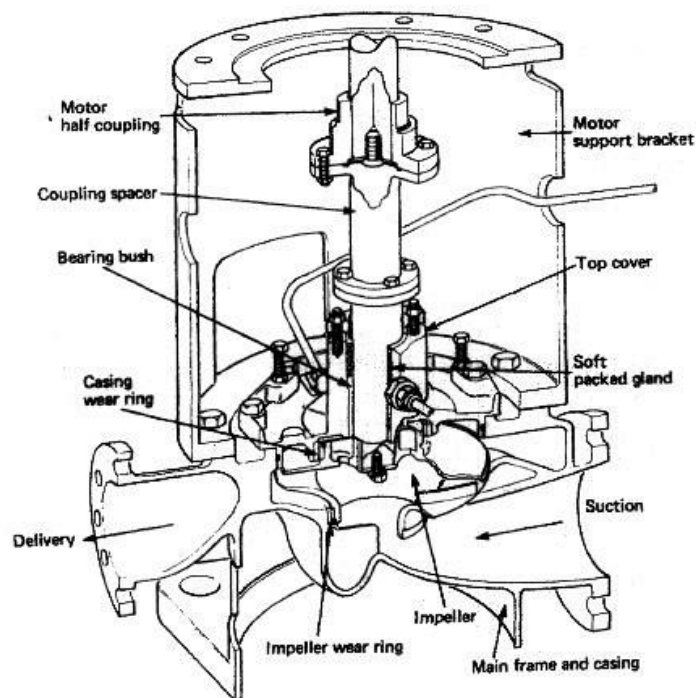


Figure 4-12 Centrifugal pump cutaway view [41]

Specific speed parameter

As mentioned before, the impeller is the key element that modifies the overall pump performance making its identification mandatory. To classify the pumps depending on their impeller the specific speed ($N_q[\text{min}^{-1}]$) is used, a model number based on the designed values of speed, volumetric flow rate and head. The equation used is. [39]

$$N_q = N_r * \frac{Q_r^{0.5}}{H_r^{0.75}} \quad (4.46)$$

Where:

N_r : is the design value of rotational speed [min^{-1}]

Q_r : is the design value of volumetric flow rate [m^3/s]

H_r : is the design value of pump head [m]

Using this parameter not only the impeller geometry can be deduced but also the main curves can be predicted. **Figure 4-14** shows the impeller classification as a function of the specific speed parameter

Pumps with low specific speed have a radial-shaped impeller with a much large difference between the outer and inner diameter. The corresponding head curves (QH curves) are relatively flat and the power curves are positives in the entire flow area

On the contrary, high N_q pumps, correspond to an axial impeller having both, inlet and outlet diameter, of a similar size and small compared to the width of the impeller. The head curves are usually descending and have the tendency to create saddle points. Its performance decreases along with the flow increment. [39]

Applying equation 4.46 into the RCIC pump using the values found in **Table 1-1** as design values for the speed, flow and head the impeller configuration can be deduced resulting into a radial-shaped impeller.

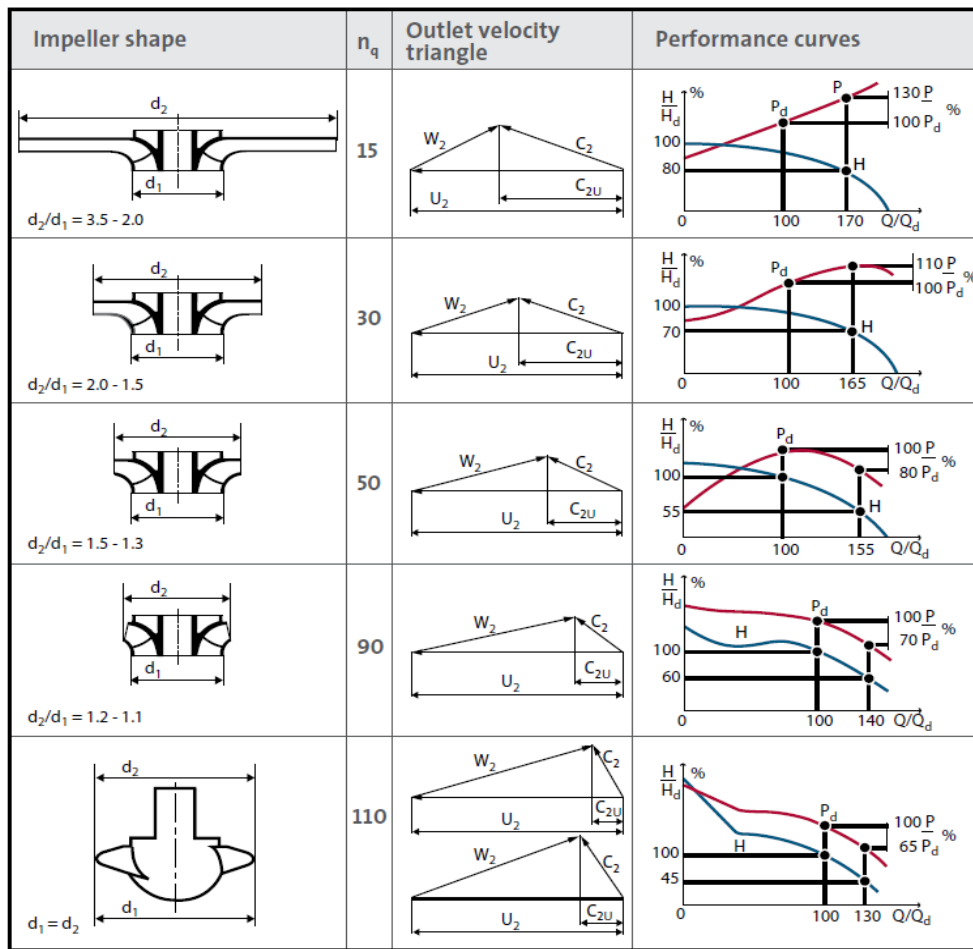


Figure 4-14 Impeller classification [39]

4.4.2- Performance curves

The performance curves are a set of curves which provide information about the pump behavior at a wide range of volumetric flow rates and are used by the customer to select the pump which meets his requirements for a given application.

The curves provide information about the power, the head, the Net Pump Suction Head (NPSH) and the efficiency and are a vital part of the design specifications. Similar curves showing the axial and radial thrust are used for bearing design.

With the specific speed parameter, the performance curves can be roughly estimated but that is not enough, in order to simulate correctly the RCIC pump in RELAP/Scdap code, the exact head curves must to be calculated with precision.

Head-flow performance curve (QH curve)

The most important data for the present study corresponds to the head curve (QH) which is usually provided by the manufacturer, unfortunately the RCIC pump QH curve data is not available so it has to be created from the RCIC specification data shown in **Table 1-1** which, for convenience, has also been included in this chapter (see **Table 4-1**)

Table 4-1 RCIC specification data [6]

	RCIC design specifications	
	Upper pressure limit	Lower pressure limit
Pressure [MPa][abs]	7.83	1.14
Power [kW]	373.0	60.0
Speed [RPM]	4500	2000
Pump Head [m]	850.0	160.0
Water mass flow rate injected to RPV [kg/s]	26.0	26.0
Steam mass flow rate extracted from RPV [kg/s]	2.51	2.51

The QH curve shows the head-flow behavior at a given rotational speed; once the pump is started and runs with constant speed, the head starts at maximum value when the flow is 0 (Q=0) and gradually decreases as much as the flow rate increases until a minimum value of 0 (Q=max).

In most of the cases, the pressure difference through the pump is measured and the head (H) is calculated using equation 4.47

$$H = \frac{\Delta p_t}{\rho * g} [m] \quad (4.47)$$

Where:

Δp_t : Total pressure difference between inlet and outlet [Pa]

ρ : Density of the fluid [kg/m³]

g: Gravity acceleration [m/s²]

Despite it seems that the H calculation depends on the fluid density it has been proved that the results using different fluids will obtain the same results; the head only depends on the geometry and speed.

Δp_t is the total pressure difference created in the pump which can be divided into three different components; the static pressure difference Δp_{static} , the dynamic pressure difference Δp_{dyn} and the geodetic pressure difference Δp_{geo} . [39-40]

$$\Delta p_t = \Delta p_{static} + \Delta p_{dyn} + \Delta p_{geo} \text{ [Pa]} \quad (4.48)$$

The static pressure difference can be measured directly with a differential pressure sensor, or a pressure sensor can be placed at the inlet and outlet of the pump. In this case, the static pressure difference can be found by the following equation. [39-40]

$$\Delta P_{static} = p_{outlet} - p_{inlet} \text{ [Pa]} \quad (4.49)$$

The dynamic pressure is generated due to the difference in the kinetic energy per unit of volumetric flow between the inlet and outlet. [39-40]

$$\Delta p_{dyn} = \frac{1}{2} \rho V_{out}^2 - \frac{1}{2} \rho V_{in}^2 \text{ [Pa]} \quad (4.50)$$

In practice, the dynamic pressure and the flow velocity before and after the pump are not measured during test of pumps. Instead, equation 4.51 describes how the dynamic pressure difference can be calculated as a function of the flow rate (Q) using the inlet/outlet diameter. [39-40]

$$\Delta p_{dyn} = \frac{1}{2} \rho \left(\frac{Q}{\pi/4} \right)^2 \left(\frac{1}{D_{out}^4} - \frac{1}{D_{in}^4} \right) \text{ [Pa]} \quad (4.51)$$

If the diameter does not change the dynamic pressures difference is 0.

The geodetic pressure is simply the height difference between the outlet and inlet gauges. If the height is 0, the geodetic pressure is neglected. The geodetic pressure difference is zero when a differential pressure gauge is used for measuring the static pressure difference. The geodetic pressure difference can be calculated using the following expression. [39-40]

$$\Delta p_{geo} = \Delta z g \rho \text{ [Pa]} \quad (4.52)$$

Combining equations 4.48 to 4.52, the equation 4.47 can be rearranged into the following expression. [39-40]

$$H = \frac{\Delta p}{\rho g} + \Delta z + \frac{1}{2} \rho \left(\frac{Q}{\frac{\pi}{4}} \right)^2 \left(\frac{1}{D_{out}^4} - \frac{1}{D_{in}^4} \right) (m) \quad (4.53)$$

Assuming a constant geometry no matter the system conditions, the diameters multiplying the flow rate can be gathered in a constant parameter (c). Then, equation 4.53 becomes.

$$\frac{1}{2} \rho \left(\frac{1}{\frac{\pi}{4}} \right)^2 \left(\frac{1}{D_{out}^4} - \frac{1}{D_{in}^4} \right) = c \rightarrow H = \frac{\Delta p}{\rho g} + \Delta z + c Q^2 (m) \quad (4.53)$$

Using the data from **Table 4-1**, the only unknown parameters are c and Δz . Despite two operation points are described in **Table 4-1** (low pressure and high pressure conditions) they cannot be used directly since their rotational speed is different. Prior to QH curve calculation, the affinity equations related with the control velocity need to be used.

Speed control

The pump can be controlled by regulating the pump rotational speed, then the QH, power and NPSH curves are changed. How the performance curves change due to the speed regulation can be calculated by the application of the affinity equations which are based on the constant proportion of the velocity triangles occurred during the geometrical scaling [39].

The affinity equations are the following for flow rate (Q), head (H), power (P) and NPSH

$$Q_B = Q_A \left(\frac{N_B}{N_A} \right) [m^3/s] \quad (4.54)$$

$$H_B = H_A \left(\frac{N_B}{N_A} \right)^2 [m] \quad (4.55)$$

$$P_B = P_A \left(\frac{N_B}{N_A} \right)^3 [W] \quad (4.56)$$

$$NPSH_B = NPSH_A \left(\frac{N_B}{N_A} \right)^2 [m] \quad (4.57)$$

Index A in the equations describes the initial values, and index B describes the modified values. The equations provide coherent points on an affinity parabola in the QH graph. **Figure 4-15** shows a generic affinity parabola with the corresponding coherent points between three different rotational velocities

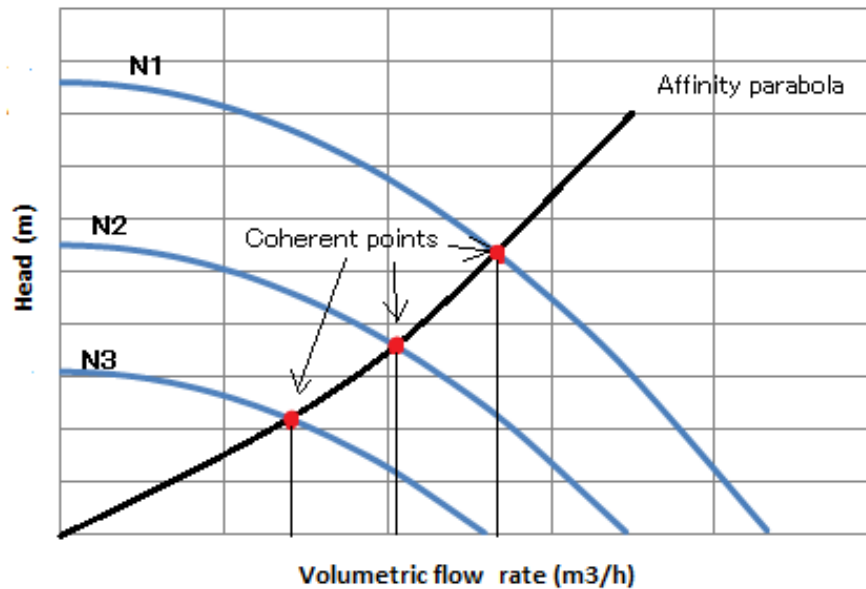


Figure 4-15 Affinity parabola

Applying the affinity equations 4.54 to 4.57 in conjunction with the QH (4.53) curve formula to the RCIC specification data, the QH curve corresponding to the design RCIC pump data described in **Table 4-1** is shown in **Figure 4-16**. The blue dotted line corresponds to the 26kg/s mark, making the intersection with both curves the operation points described in the specification sheet

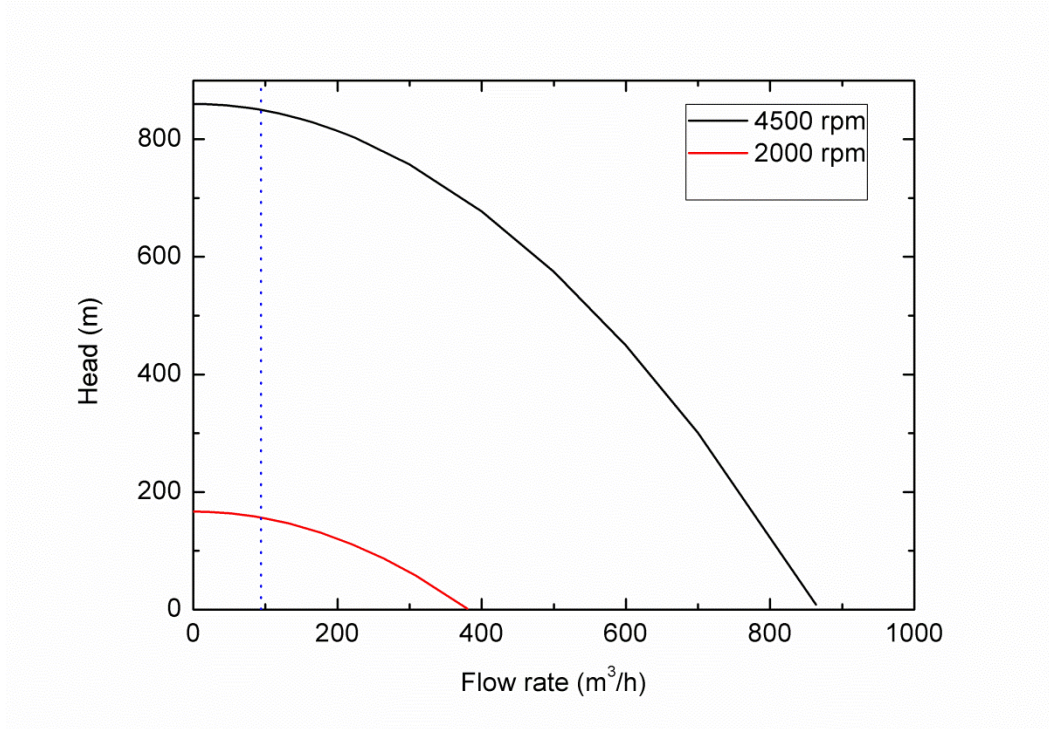


Figure 4-16 F1D2 RCIC pump QH curves

Net Pump Suction Head curve

NPSH is a term related with the cavitation, the phenomenon where small vapor bubbles are created due to local pressure drop. Those small bubbles collapse upon hitting the blades causing deterioration; it is an undesired and harmful effect that has to be avoided.

The extent of cavitation depends on how low the pressure is in the pump and it usually generates noise and vibration starting from the point where the pressure in the pump is lowest, generally the blade edge at the impeller inlet.

The NPSH is also measured in meter like the pump head and can be divided in two types; the available ($NPSH_a$) which is estimation about how close the fluid in the inlet is to the vaporization and the required ($NPSH_R$) which is an expression of the lowest NPSH value required for acceptable operating conditions. [39]

$NPSH_a$ can be calculated using the following equation [39]

$$NPSH_a = \frac{p_{in}}{\rho g} + \frac{v^2}{2g} - \frac{p_{vap}}{\rho g} [m] \quad (4.58)$$

Where:

p_{in} : Is the pressure at the inlet [Pa]

v : is the inlet fluid velocity [m/s]

p_{vap} : The vapor pressure of the fluid at the present temperature [Pa]

If the pump geometry data is not available, the inlet velocity (v) can be found first using the shut-off head formula described in equation 4.59 to find the outer diameter of the impeller (D_{out}) and then use the D_{in}/D_{out} proportion shown in **Figure 4-14** for the corresponding impeller geometry

$$Shut\ off\ Head = (0.012D_{out}N)^2 [m] \quad (4.59)$$

Where:

Shut-off head: Is the maximum head achievable at a given rotational speed (when $Q=0$) [m]

D_{out} : Is the impeller outer diameter [m]

N : is the pump rotational speed [rpm]

Figure 4-17 shows the $NPSH_a$ for the RCIC pump at 4500rpm

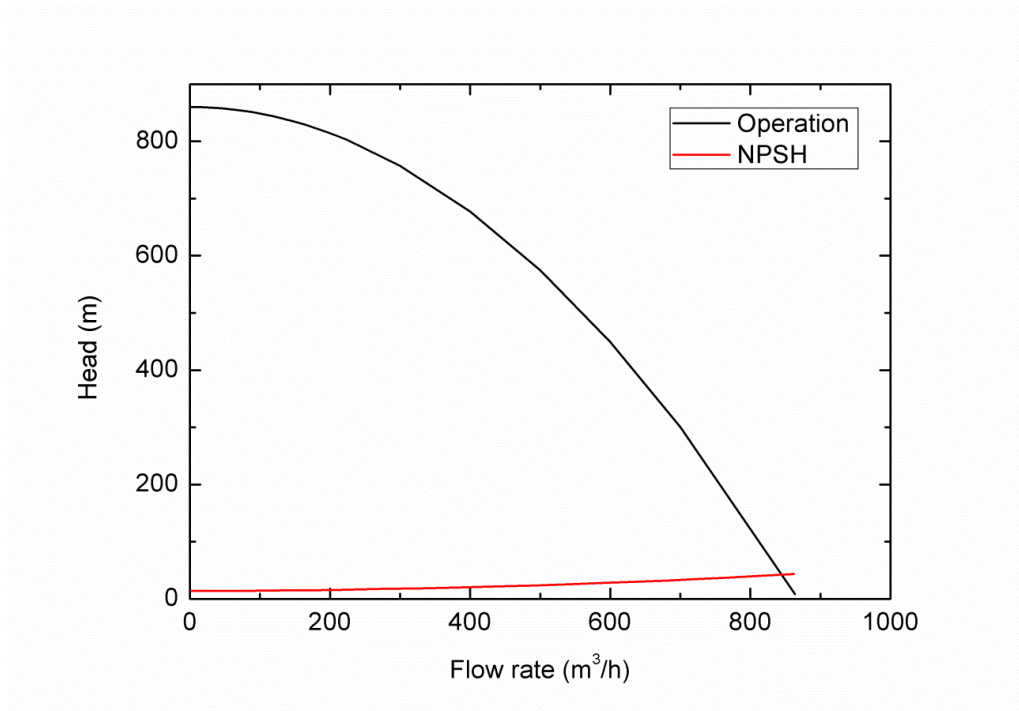


Figure 4-17 F1D2 RCIC pump NPSH curve

$NPSH_r$ is always lower than $NPSH_a$. A minimum safety margin of 0.5 m is recommended but it can vary in function of the application requirements.

The effect of cavitation can be reduced or avoided by: [39-40]

- Lowering the pump level compared to the water level
- Increasing the system pressure (only for closed systems)
- Shortening the suction line to reduce the friction loss
- Increasing the suction line area in order to reduce the fluid velocity and friction
- Avoiding bends and other obstacles in the suction line preventing pressure drops
- Lowering the average fluid temperature to reduce the vapor pressure

4.4.3- Pump homologous curves generation

As mention before, the objective of the chapter is the generation of the homologous curves, an input requirement for RELAP/Scdap code. The complication of the homologous curve generation process is one of the main reasons why the common BWR nodalizations in RELAP does not include a detailed RCIC system nodalization because, despite RELAP/Scdap already has the homologous curves corresponding to several pumps included in its own source code, unfortunately, the RCIC pump is not one of them. [34]

In a random pump, its interaction with the fluid is described by empirically generated curves relating the pump head and torque to the volumetric flow rate and rotational velocity. The performance curves previously described in this chapter are frequently referred to as four-quadrant curves (despite only the first quadrant is usually used) and present the pump information in terms of pump head (H), flow rate (Q), torque (τ) and rotational speed (N). Usually, the data is plotted using the Q and N as axis with lines of constant H or τ

The four quadrants are also called regime mode regions.

- If both, speed and flow are positives (+ Q /+ N): normal pump regime mode
- If negative speed with positive flow (+ Q /- N): reverse pump regime mode
- If negative flow with positive speed (- Q /+ N): dissipation regime mode
- If both, speed and flow are negatives (- Q /- N): turbine regime mode

Figure 4-18 show the head first quadrant (normal pump regime mode) of the RCIC pump obtained using the previous calculated QH curve and the data from **Table 4-1**

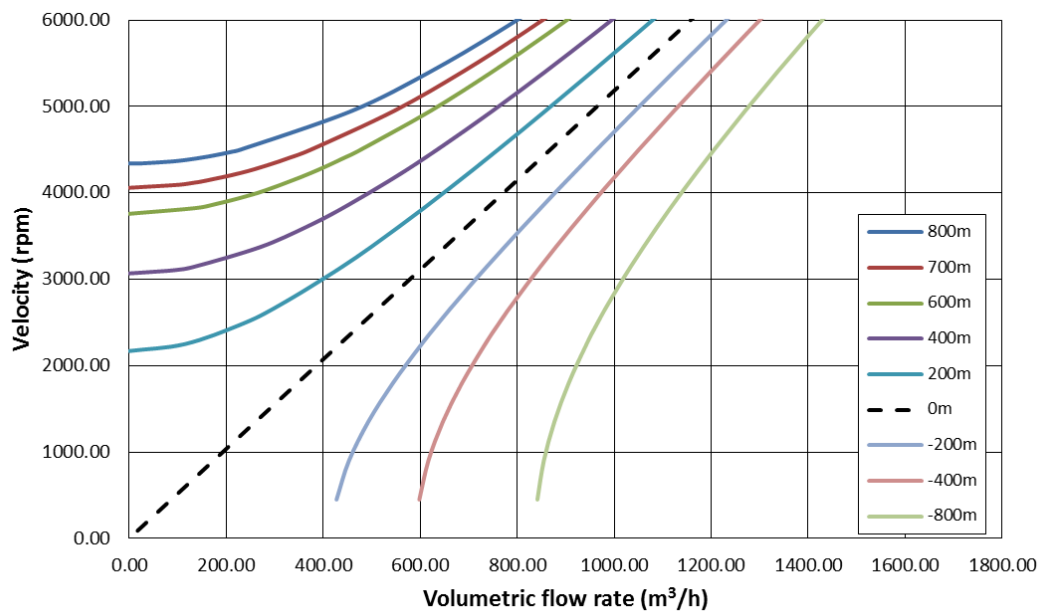


Figure 4-18 Pump head first quadrant map

The same process can be applied to find the torque data as it is shown in **Figure 4-19**

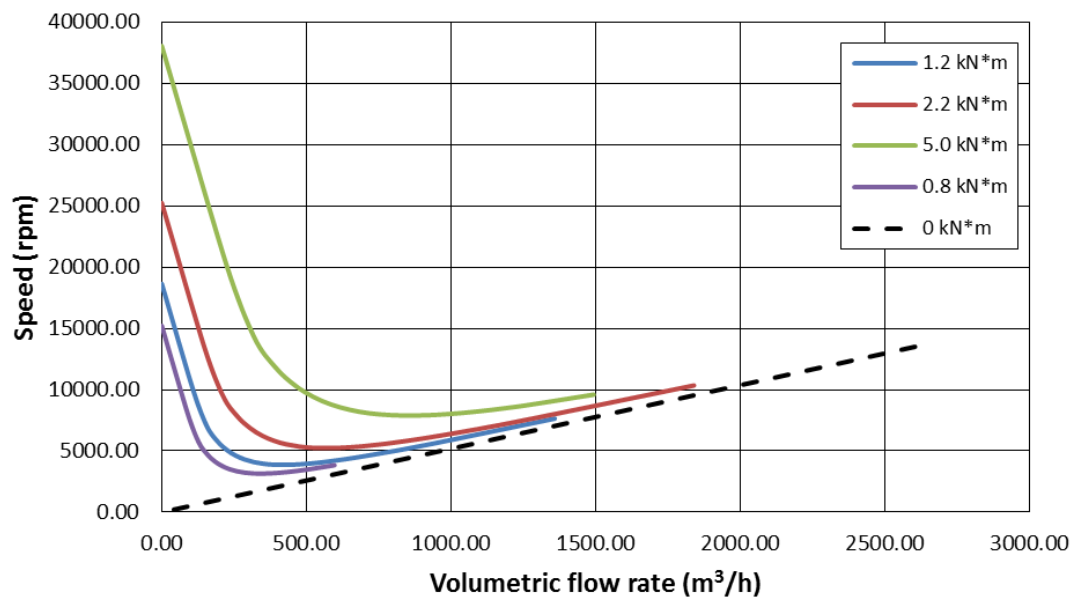


Figure 4-19 Pump torque first quadrant map

This data is used in RELAP/ScdapSIM in a more condensate form, called homologous curves, where the different parameters are converted to non-dimensional ratios (head

ratio, flow ratio, velocity ratio and torque ratio) by dividing them by the corresponding rated values. The rated values are also required in the input deck and correspond to the design values or the maximum efficiency values. [34]

In RELAP/Scdap, the homologous curves are entered in tabular form forming couples of values, being the dependent variable obtained as a function of the independent variable. The curve is generated using those pairs of values along with a table search and linear interpolation scheme.

There is two separate sets of curves, corresponding to head and torque, and each set is divided in four-quadrant of two curves resulting in eight curves, also named octants, for both, head an torque.

Not all the curves musty be entered in the input deck but the simulation will end if the pump moves to an octant not specified in the input.

As mention before, the four-quadrant pump head and torque maps from **Figure 4-18** and **Figure 4-19** are converted into the homologous curves in two steps. First the values become dimensionless by using the rated values applying the following equations. [34]

$$h = \frac{H}{Hr} \quad a = \frac{N}{Nr} \quad v = \frac{Q}{Qr} \quad b = \frac{\tau}{\tau r} \quad (4.60)$$

The rated values for the head, flow and speed are taken from **Table 4-1**. Note, however that the table does not include the rated value for torque. The corresponding rated value (τr) can be obtained by using the hydraulic power transferred to the fluid by the pump, as shown in equation 4.61

$$\tau = \frac{30 * P_{hyd}}{\pi N} [kN * m] \quad (4.61)$$

Where:

P_{hyd} : is the hydraulic power tranferred to the fluid [kW]

$$P_{hyd} = \frac{\rho Q H}{3,6 * 10^6} [kW] \quad (4.62)$$

Once the values have been reduced to non-dimensional parameters they are plotted in terms of the dimensionless independent parameter a/v or v/a and the dependent parameter h/a^2 or h/v^2 for head or b/a^2 or b/v^2 for torque. The independent and

dependent parameters used for plotting depends of which octant is being plotted. The different configurations are shown in **Table 4-2**

Each of the octants is named using a three letters code being the first one the corresponding to which kind of octant is being plotted; head (H) or torque (B), the second letter corresponds to the independent variable used; flow (V) or speed (A). The last letter is referred to the regime mode; Normal, Dissipation, Turbine or Reverse [34]

Figure 4-20 shows the resulting RCIC pump head homologous curves of the first quadrant octants (HAN and HVN)

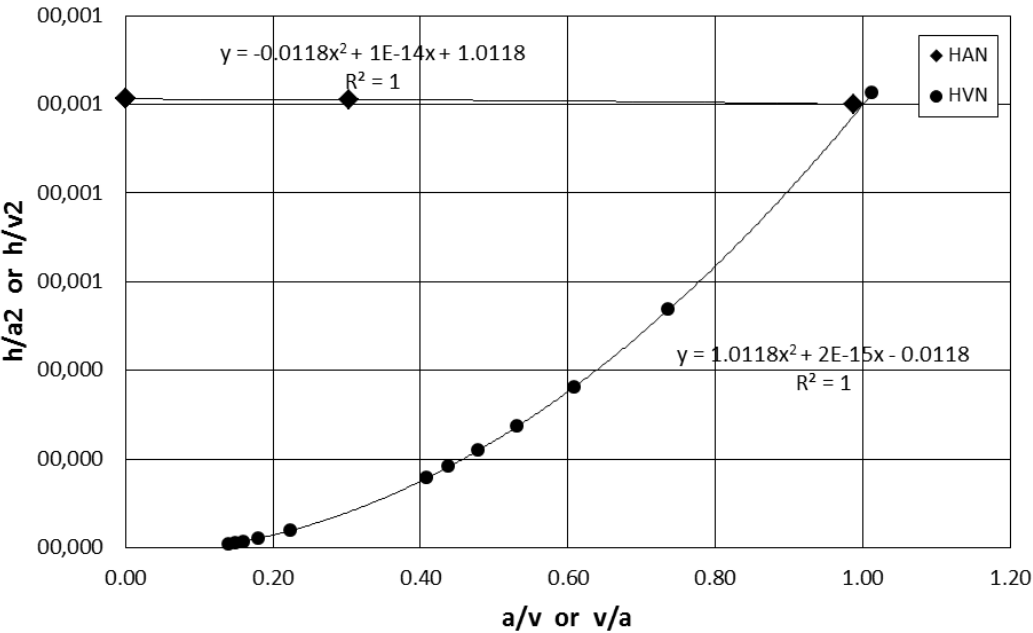


Figure 4-20 Pump head homologous curves

On the same way, **Figure 4-21** shows the torque homologous curves of the two octants (BAN and BVN)

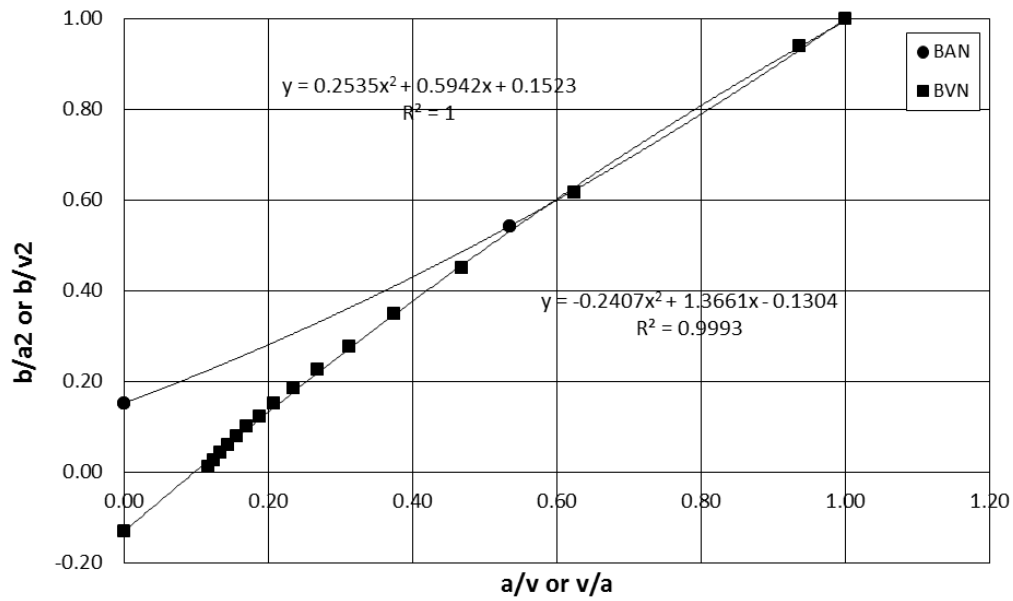


Figure 4-21 Pump torque homologous curves

Figure 4-2 Homologous curves configurations [34]

Regime number	Regime mode ID name	α	v	v/α	Independent variable ^a	Dependent ^a variable head	Dependent ^a variable torque
1	HAN BAN Normal pump	> 0	≥ 0	≤ 1	v/α	h/α^2	β/α^2
2	HVN BVN Normal pump	> 0	≥ 0	> 1	α/v	h/v^2	β/v^2
3	HAD BAD Energy dissipation	> 0	< 0	≥ -1	v/α	h/α^2	β/α^2
4	HVD BVD Energy dissipation	> 0	< 0	< -1	α/v	h/v^2	β/v^2
5	HAT BAT Normal turbine	≤ 0	≤ 0	≤ 1	v/α	h/α^2	β/α^2
6	HVT BVT Normal turbine	≤ 0	≤ 0	> 1	α/v	h/v^2	β/v^2
7	HAR BAR Reverse pump	≤ 0	> 0	≥ -1	v/α	h/α^2	β/α^2
8	HVR BVR Reverse pump	≤ 0	> 0	< -1	α/v	h/v^2	β/v^2

4.5- Summary

In this chapter, the RELAP/ScdapSIM severe accident code has been presented. The code is based into different modules, the RELAP5 which is related with the thermal-hydraulics and the Scdap which is related to the radionuclide behavior. RELAP5 module presents a modular top-down architecture based on consequent levels of specific subroutines.

The problems with the current RCIC nodalizations force the creation of a brand new nodalization for the RCIC. The nodalization has pass through an iteration process from the initial simplified approximations to the final version, which includes all the relevant secondary systems as well as the control logic to simulate the F1D2 accident progression.

The nodalization used has the property of being able to perform simulations either being connected to an RPV such the Laguna Verde or being isolated and using the desired RPV pressure profile and flow quality in the MSL as boundaries conditions.

One of the problems with the RCIC nodalizations is the turbine model which it has been modified for the present study with the inclusion of the degradation coefficient developed in Chapter 2 and the steam flashing phenomenon. Both modifications influence on the turbine generated power and consequently, in the computed momentum equations.

A secondary objective of this section is the generation of the homologous curves prior to use the RCIC nodalization in RELAP/Scdap. The homologous curves are the condensed representation of the pump head and torque characteristic curves.

Prior to the homologous curves generation, the QH curve has to be obtained usually by the manufacturer but not in this case. The QH curve is generated by using the data from the RCIC specifications and the pump theory described in this chapter.

The generation process used in this chapter has some flaws however. Due to the little information available of the RCIC pump only the first quadrant (normal pump regime) homologous curves could be generated. Although it should not be a problem due to regarding the data, the RCIC pump was supposed to run always in that regime. If the simulation crashes before ending, the last time step pump regime should be checked to ensure that assumption.

Chapter 5 Simulation results and discussion

The simulation results will be presented and discussed in this chapter. The nodalization used for the simulation is the one shown in **Figure 4-8** corresponding to the last iteration version of the RCIC system.

The created nodalization has the ability to perform simulations in open or closed loop configurations.

- Open loop: The nodalization is used as presented in **Figure 4-8**. For this configuration, the RPV is reduced to two time-dependent volumes (210 and 345) and the only required boundary conditions are the RPV pressure profile and the flow quality at the MSL. This configuration is useful thanks to its low boundary conditions needed and its simplicity which allows making faster simulations.
- Closed loop: The nodalization can be attached to an RPV nodalization, such as Laguna Verde, in order to physically close the loop. The boundary requirements are changed to the fuel energy, either using the reactors kinetics or the power vs. time table option. This configuration requires more data and its complexity is increased consuming more computational time. It has the advantage to minimize the uncertainties caused in the models by closing the loop.

5.1- Single phase flow analysis

Before starting with the reproduction of the accident itself, a brief single phase simulation analysis should be done to verify the nodalization itself; as mention before, the RCIC nodalization used in this research has been completely created from zero, including the generation of the homologous curves used in the pump model. Thus, it has to be verified that it is supposed to work as intended and it is able to simulate with accuracy, at least, the design points described in the RCIC system specification sheet.[6]

Table 5-1 RCIC specification sheet []

	RCIC design specifications	
	Upper pressure limit	Lower pressure limit
Pressure [MPa][abs]	7.83	1.14
Power [kW]	373.0	60.0
Speed [RPM]	4500	2000
Pump Head [m]	850.0	160.0
Water mass flow rate injected to RPV [kg/s]	26.0	26.0
Steam mass flow rate extracted from RPV [kg/s]	2.51	2.51

Table 5-1 has already presented previously in this paper but it has been included here for convenience. The table shows the expected RCIC behavior at two operation points, high and low pressure limits. In other words, if the RPV pressure is 7.83MPa, the RCIC system is supposed to extract 2.5kg/s of pure saturated steam through the MSL and inject a water amount equal to 26kg/s generating 373kW of power at the turbine rotating a 4500rpm and having a pump head equal to 850m. The description of the system in low pressure limit is analogous to the high pressure.

The objective of the single phase analysis is to analyze the nodalization response using a constant RPV pressure s boundary condition equal to the upper and lower pressure values described in the RCIC specification sheet and verify that the rest of computed parameters match the design values.

The simulations were done assuming a simulation time of 10h, long enough to ensure the steady state achievement.

Figure 5-1 to **Figure 5-3** show the computed results for turbine power, rotational speed and pump head for high pressure (black line) and low pressure (blue line) boundary conditions. The RELAP results are compared with the corresponding values obtained from the specification sheet (red line for high pressure and orange for low)

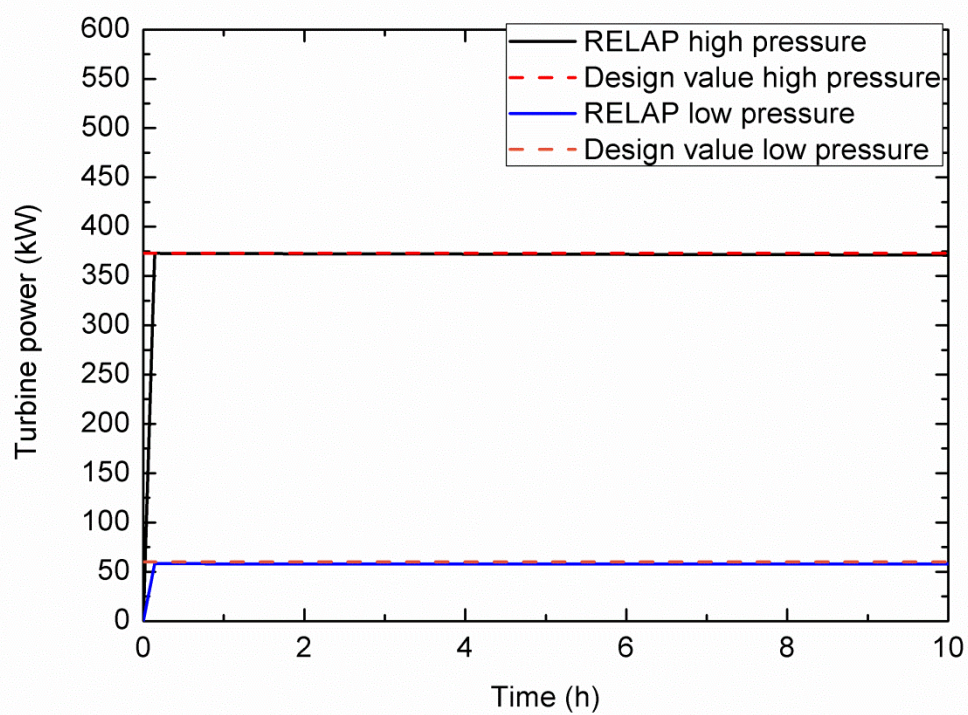


Figure 5-1 RCIC turbine power

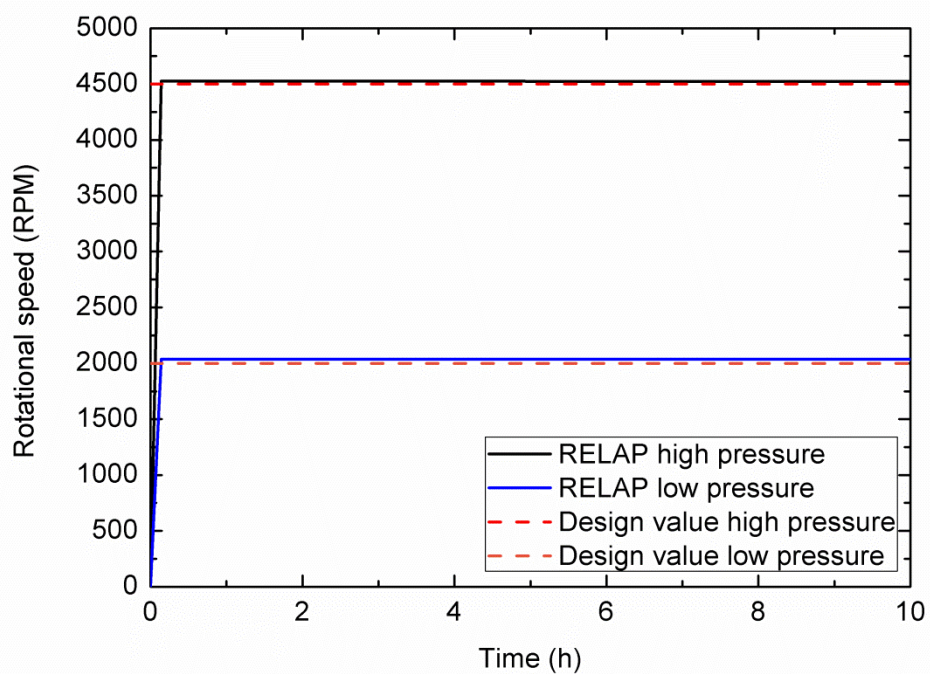


Figure 5-2 RCIC turbine-pump rotational speed

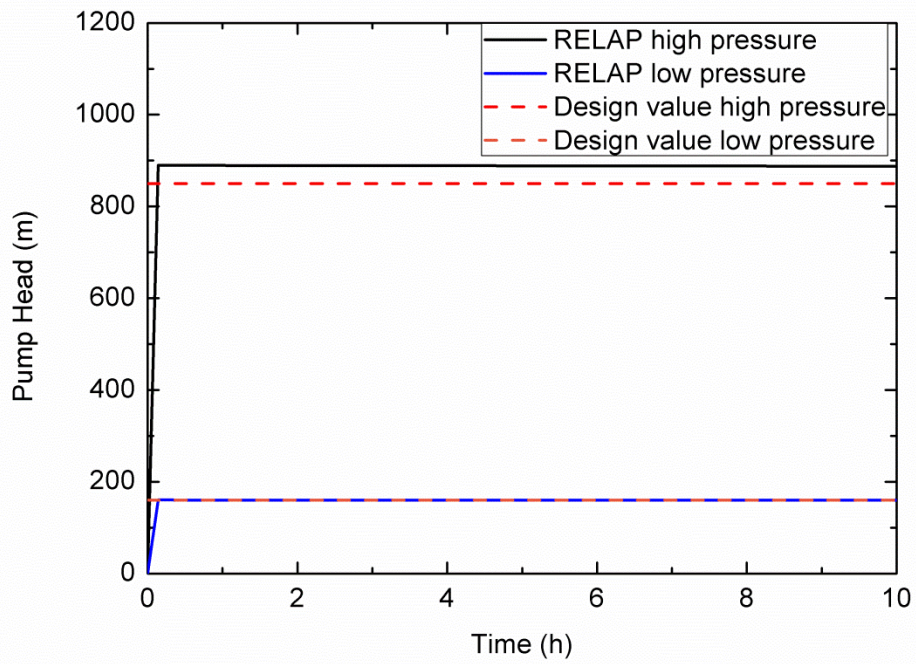


Figure 5-3 Pump head

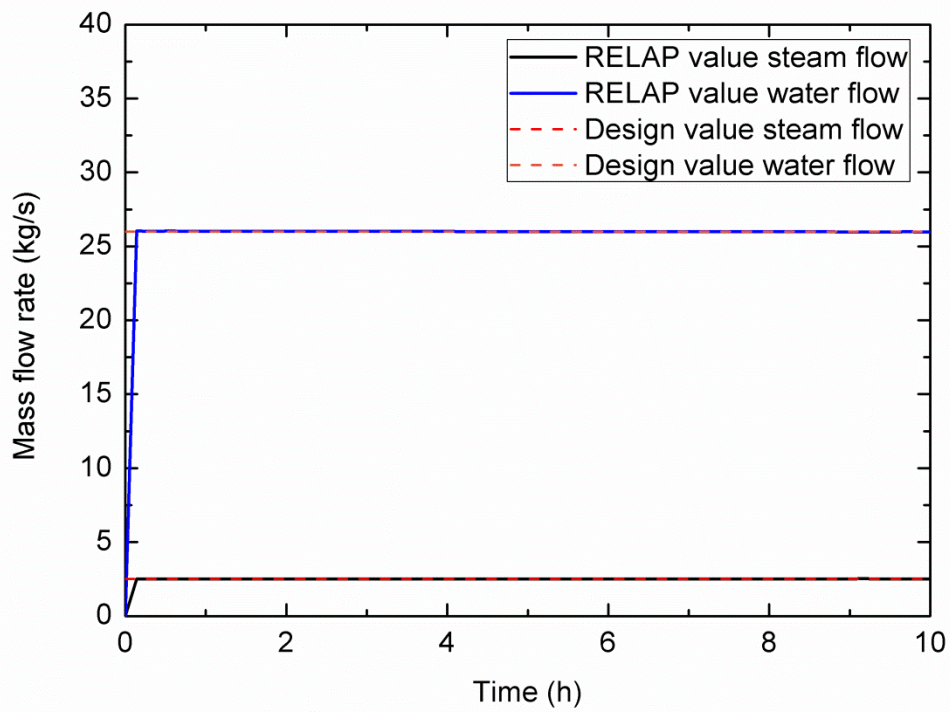


Figure 5-4 High pressure limit mass flow rates

Figure 5-4 represents the computed steam and water mass flow rates corresponding to high pressure limit of 7.83MPa. The computed values are compared with the respective design values.

Analogously, **Figure 5-5** shows the mass flow rates values for low pressure operation point.

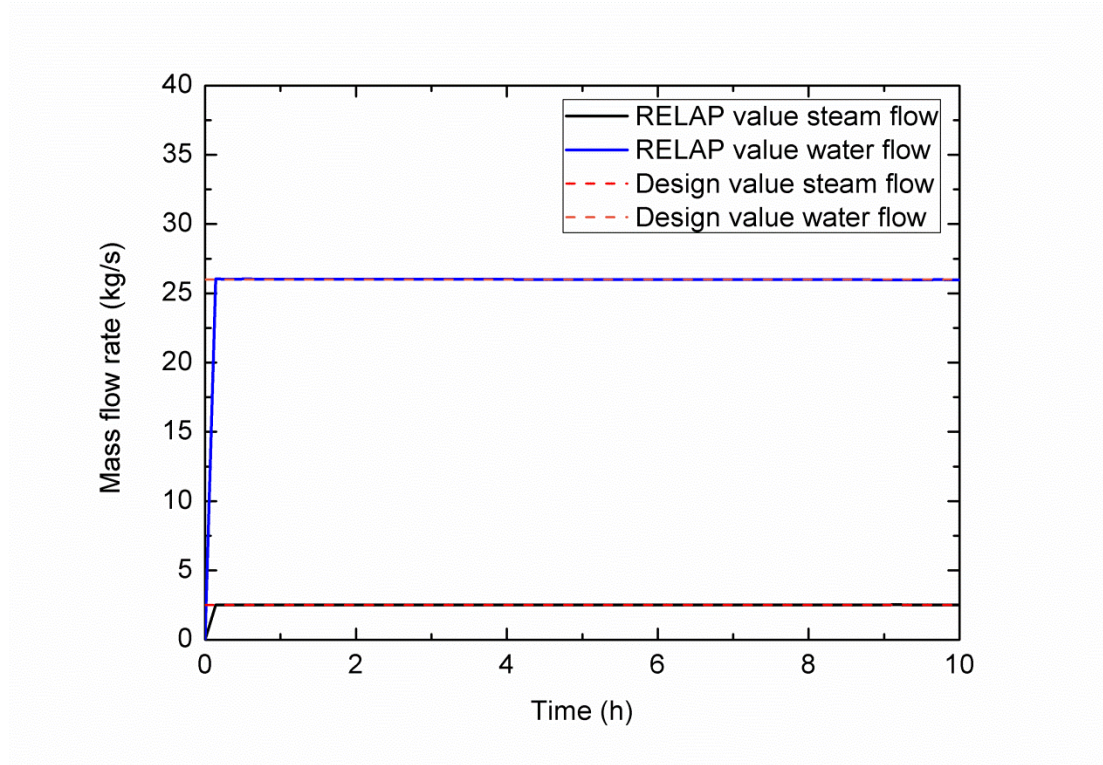


Figure 5-5 Low pressure limit mass flow rates

As can be observed in the previous figures, all the computed parameters show values close to the respective design values allowing concluding the analysis with an overall good accuracy of the RCIC nodalization and, especially, the generated homologous curves.

Once the nodalization has been verified in single phase, the two phase flow analysis can be performed reproducing the F1D2 accident.

5.2- Two-phase flow analysis – Accident progression

5.2.1- Open loop simulations

The first set of simulations considering two-phase flow in the MSL, and consequently in the turbine, are done using the open loop configuration. All the simulations done include the turbine degradation modification explained in the previous chapter. The first data available from TEPCO corresponds to $t=8h$ (**Figure 3-1**), before that single phase has been assumed in the turbine

The open loop configuration simulations use the RPV pressure profile measured by TEPCO (**Figure 3-1**) in conjunction with the mass flow rates calculated with the numerical analysis (**Figure 3-9**).

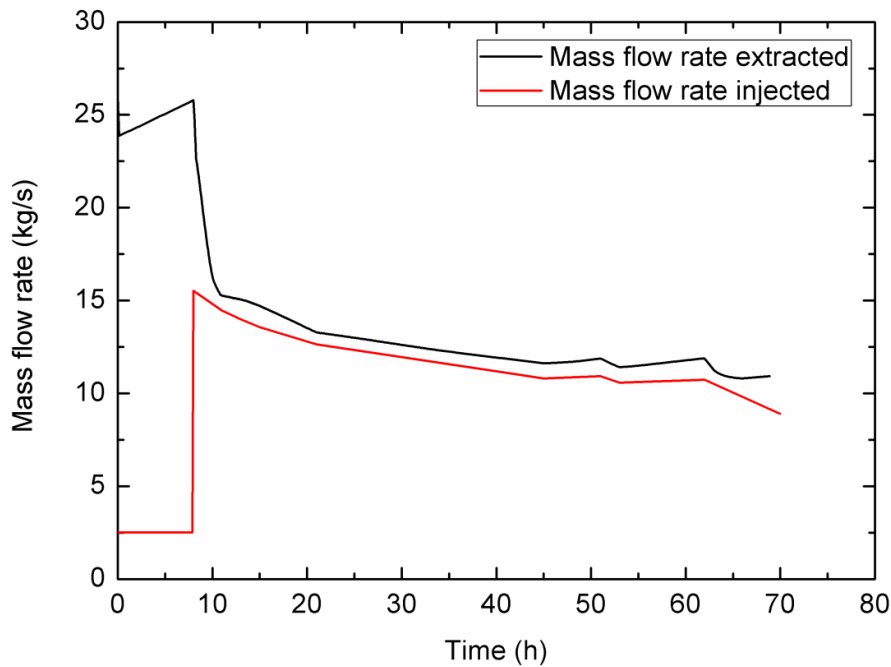


Figure 5-6 Mass flow rates

Figure 5-6 shows the computed values for the mass flow rate extracted from the RPV and the mass flow rate injected back to RPV. The red line shows a single phase period corresponding to the design value of pure steam of 2.5kg/s and then is drastically increased when the water starts to move through the turbine. The presence of water in the turbine leads to a reduction of the amount of water injected to the RPV by the RCIC system until both mass flow rates are coupled leading to a constant RPV water level around the MSL height.

Figure 5-7 describes the suppression chamber water level behavior during the RCIC operation time. The water level is increased during the first 13h due to the use of the CST as a water source. Once the water source is changed at $t = 13\text{h}$, the water starts to decrease mainly due to the actuation of the vacuum breakers which connects the S/C with the drywell

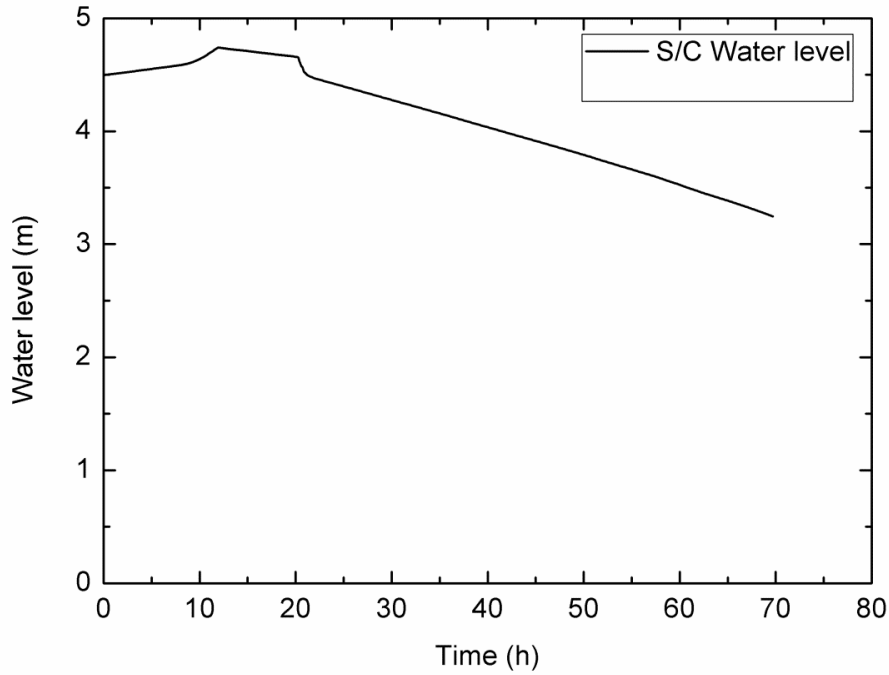


Figure 5-7 S/C water level

The vacuum breakers are set up to be activated when the pressure difference between the S/C and the drywell is higher than 25psia [8-9]. The total mass passing through the vacuum breakers can easily be measured by integrating the data from **Figure 5-8** over the 70h of RCIC operation as described in equation 5.1

$$\dot{m}_{total\ vb} = \int_0^{70} \frac{d\dot{m}_{vb}}{dt} dt \quad (5.1)$$

The computed total mass moved through the vacuum breakers to the Drywell during the RCIC operation time is about 1092kg

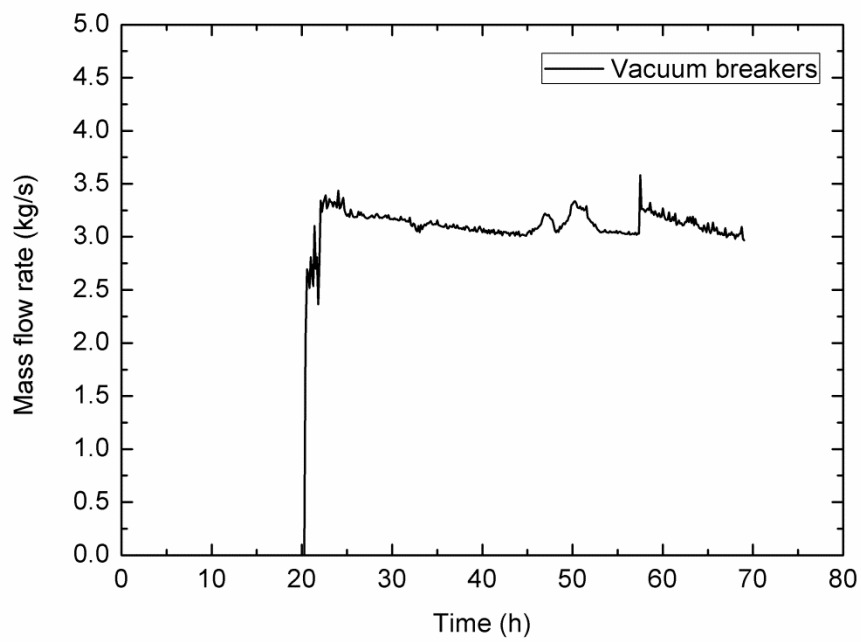


Figure 5-8 Steam mass flow rate through vacuum breakers

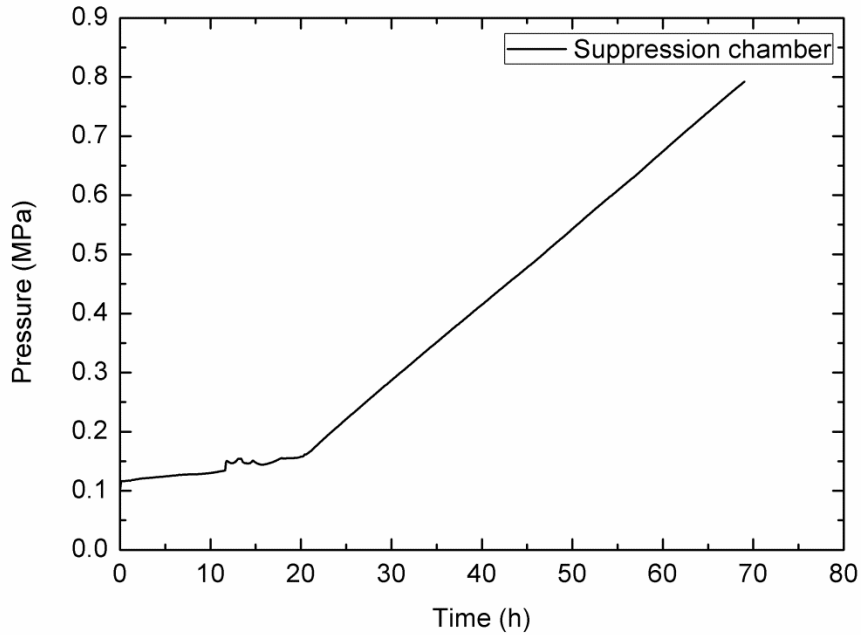


Figure 5-9 S/C pressure

Figure 5-9 and **Figure 5-10** show the pressure and temperature behavior in the suppression chamber during the RCIC operation. The S/C pressure initially slowly increases because the water is absorbing the steam heat. Once the temperature of water at the pool surface reaches the boiling temperature at $t=20\text{h}$ it starts to generate steam causing a much faster pressure increment and a steam extraction through the vacuum breakers to the Drywell. The temperature profiles described in **Figure 5-10** show the temperature at different heights assuming no flooding in the torus room and clearly represent the thermal stratification phenomenon occurred in the S/C due to the fluid injection.

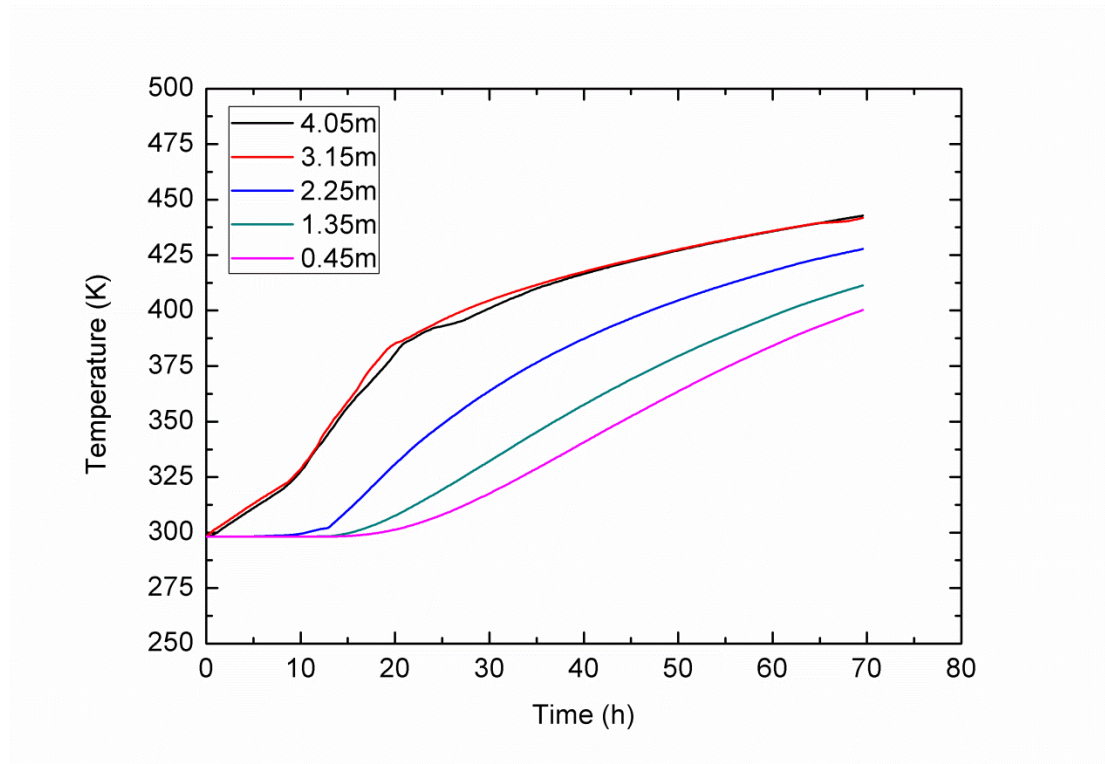


Figure 5-10 S/C temperatures at different heights

Each height corresponds to the middle point of the nodes used to nodalize the suppression chamber. The injection is located between nodes six and seven (red and black lines in the figure) corresponding to the highest temperature values, as far from the injection region, lower the temperatures are.

Figure 5-11 describes the turbine power computed by RELAP. It is compared with the numerical estimation obtained from the numerical analysis of the RCIC and with the computed value of RELAP before the turbine degradation coefficient addition.

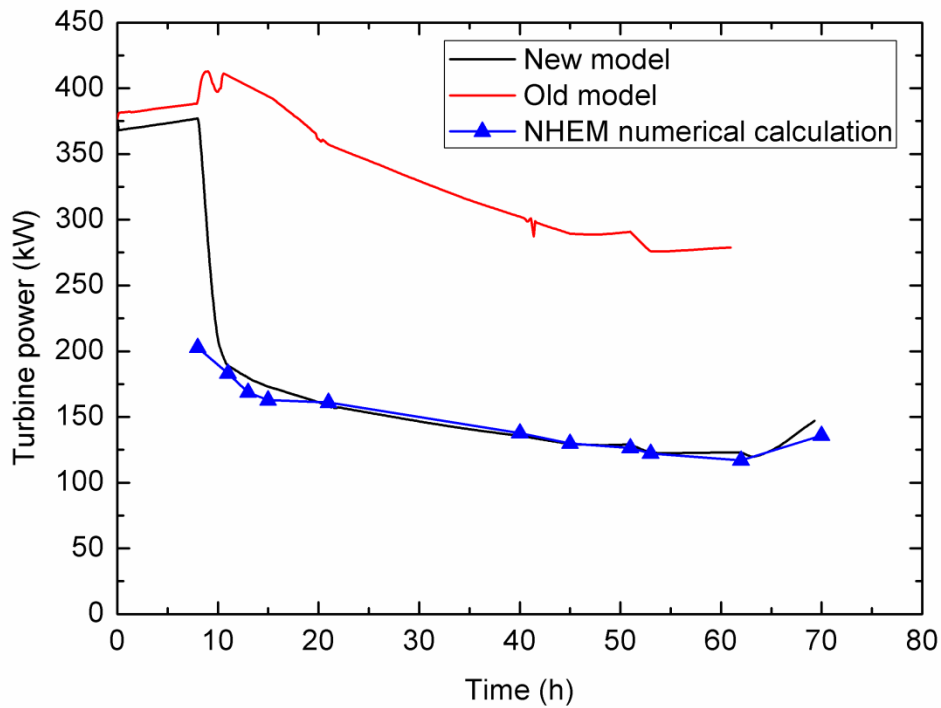


Figure 5-11 Turbine power

As mentioned above, the black line represents the actual computed power including the turbine degradation coefficient developed using the NHEM (new model). It presents a high agreement with the estimated values obtained by the RCIC numerical analysis

The red line, on the other hand, shows the computed value prior the turbine model modification (old mode). It shows a complete different behavior computing larger values even when the two-phase started at 8h.

The turbine response is a key factor on the RCIC system response, if the turbine power is overestimated, the pump will inject larger amount of water and the overall system efficiency will be overpredicted.

Figure 5-12 shows the effects of the turbine power overestimation made by the RELAP model before the modification comparing both mass flow rates pumped back to the RPV under the same boundary conditions. As can be observed, the model previous to the modification computes higher values of water mass flow rate despite to use the same inlet conditions. The conclusions extracted are consequent with the ones extracted from **Figure**

3-13; if no turbine degradation is considered it does not matter the flow quality in the turbine, it will always result in a RPV water level increment.

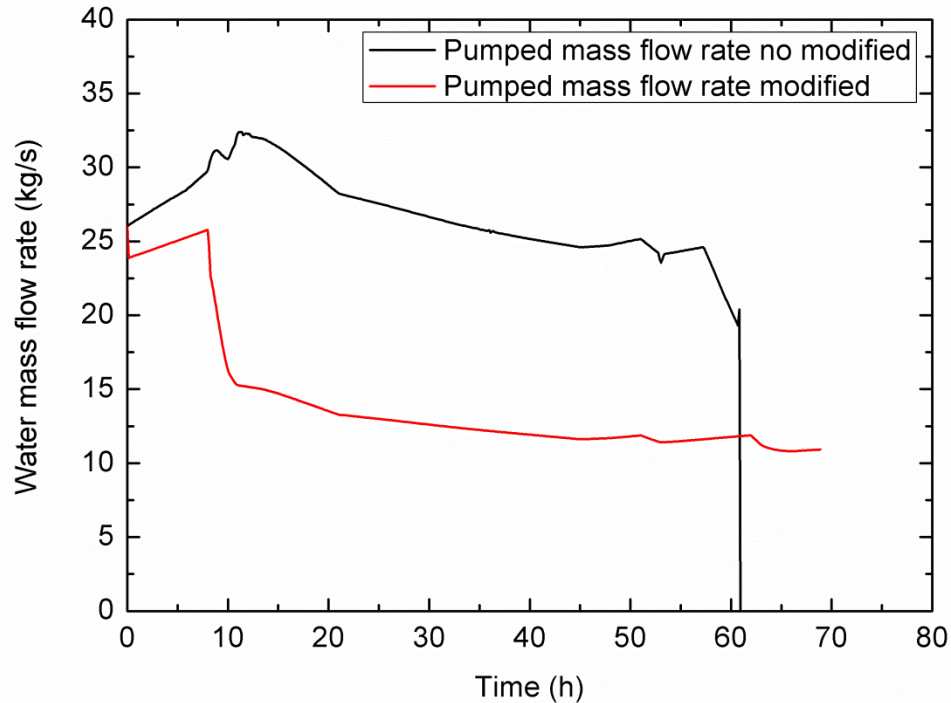


Figure 5-12 Pumped mass flow rate comparison

The black line drastically drops to zero around 60h after the simulation start. It is due to the depletion of the suppression chamber caused by the huge amount of water displaced by the pump. It is clear that the simulation does not agree with the F1D2 event log supporting the initial assumption that some kind of degradation actually occurred in the turbine.

Figure 5-13 shows the computed mass flow rate from the CST. The data from TEPCO [11] suggests an injection of 1000T of water from the CST during the first 13h (marked with dotted line in the figure). The figure also shows, only for comparison purposes, the computed values using the old model (without the turbine degradation included).

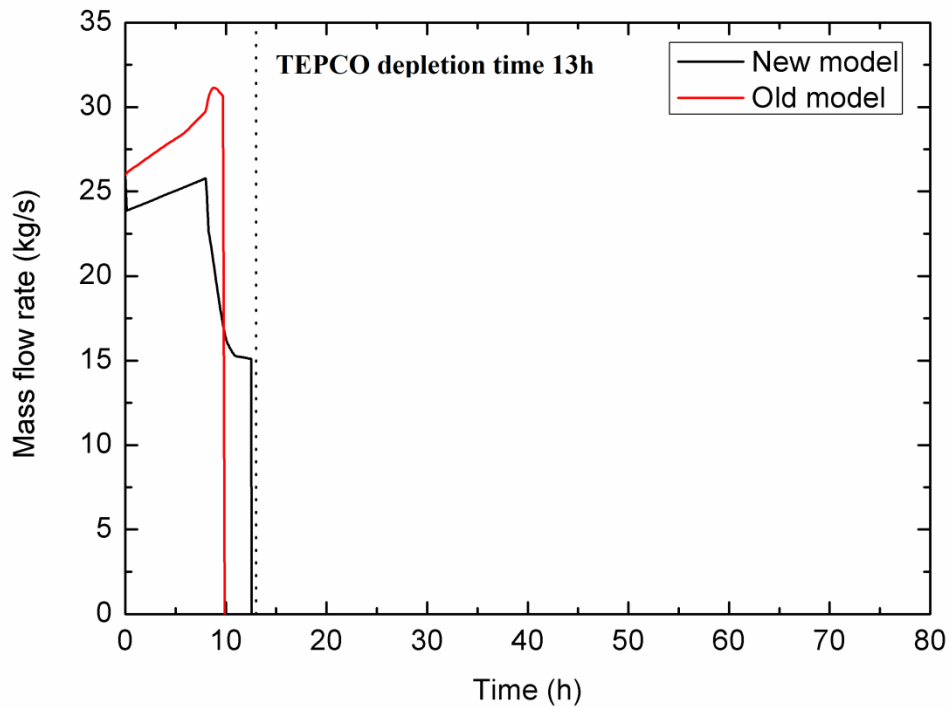


Figure 5-13 CST mass flow rate

The control logic of the nodalization is set up to stop the CST water injection after 1000T have been moved and compute the resulting time. As can be observed, the simulation including the degradation coefficient shows a good agreement with the event log of F1D2 meanwhile the old model is short due to the turbine power overprediction.

5.2.1.1- Torus room flooding

As mention early in this dissertation, one of the assumptions made regarding the RCIC operation was the hypothetical flood of the room where the S/C is located. **Figure 5-9** and **Figure 3-2** show a divergence between the computed and the TEPCO values of the S/C pressure. This difference can be caused by the flooding outside the torus, so a sensitive is done using the flooding control of the nodalization trying several flood levels and observing their influence on the S/C parameters.

The flooding simulation assumes that the wave reaches the torus room suddenly through the service doors 1h after the simulation start meaning no small leakage inside the room is

considered. **Figure 5-14** shows the corresponding water level in the room represented by volume 416 in the nodalization.

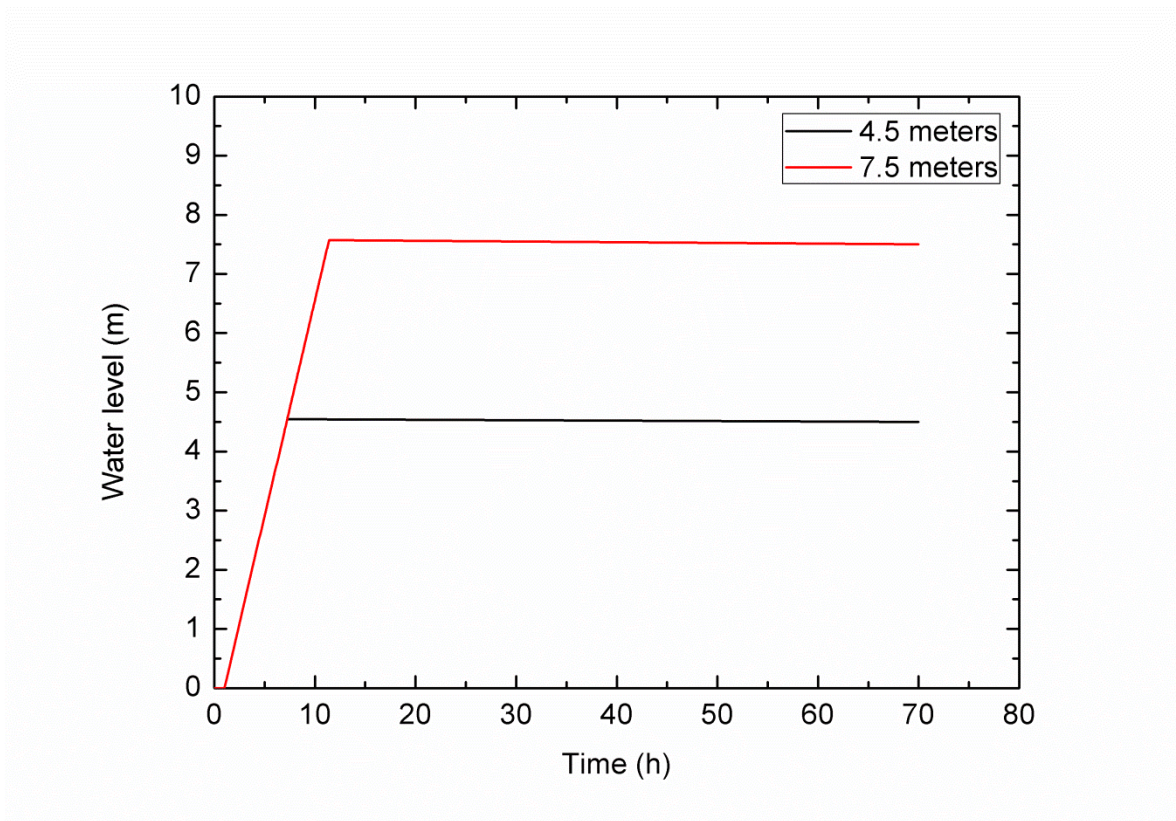


Figure 5-14 Flooding level

The presence of ocean water in the surroundings of the suppression chamber enhances the heat removal from the inside to the outside. **Figure 5-15** shows how the S/C pressure is decreased depending on the water level in the torus room. The dotted line represents the data measured by TEPCO. As can be observed if a flood of the 80% of the S/C height is assumed (water level of 7.5 m), the computed values for the pressure are exactly the same as the measured ones.

The S/C pressure is highly sensitive to the flood level suffering a reduction of almost 50% in the worst flood scenario.

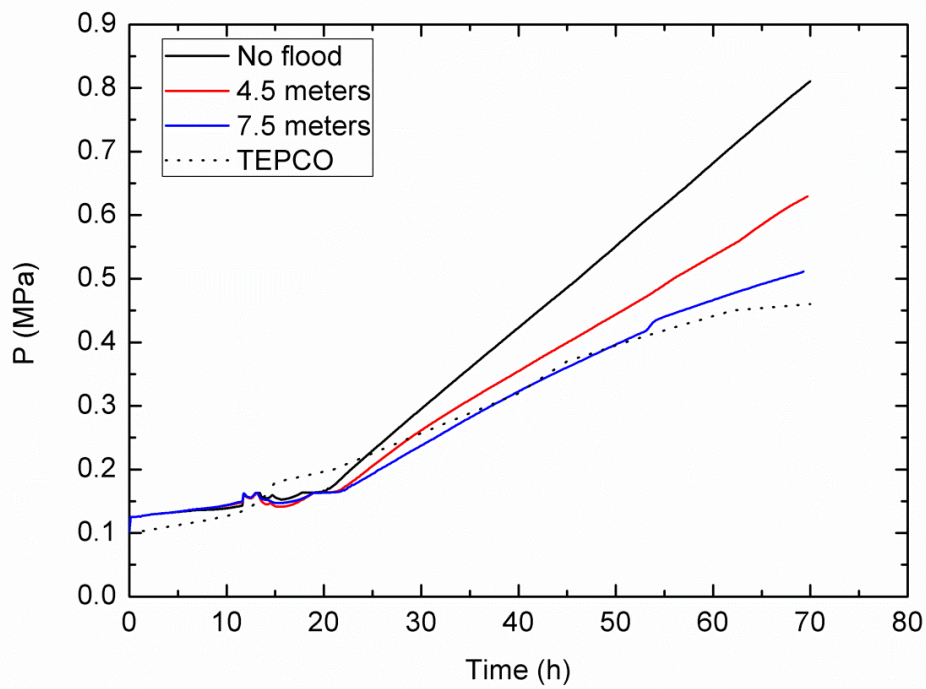


Figure 5-15 Flooding effect on S/C pressure

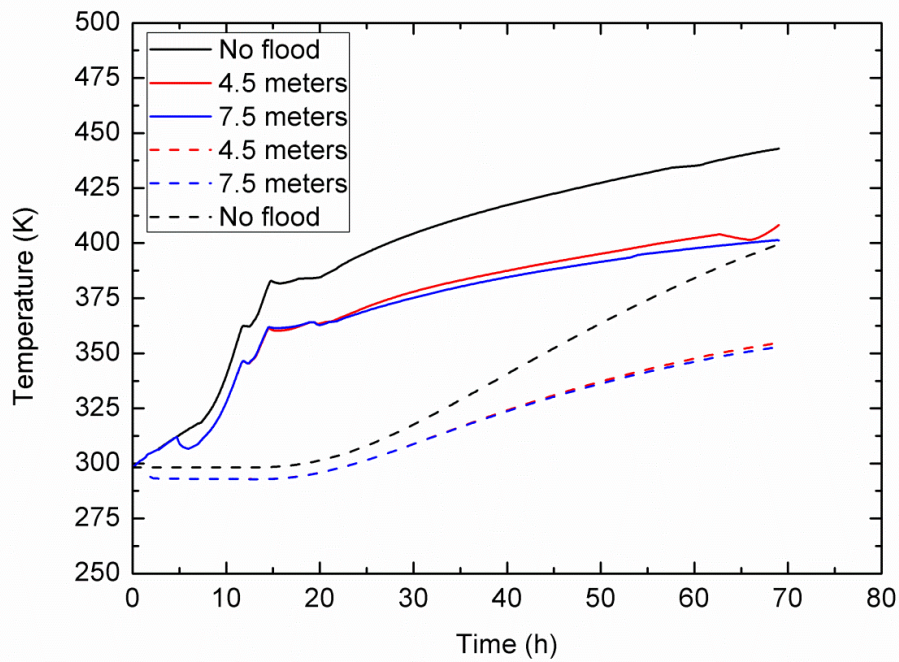


Figure 5-16 Flooding effect on S/C temperature

The presence of water may not only affect the pressure but also the computed temperature on each of the S/C nodes. **Figure 5-16** describes and compares the temperature behavior of the water inside the S/C in two different regions depending on the water level outside.

The flood affects the S/C temperatures, reducing them around 50°C. The solid lines represent the temperature of the water around the injection point. A major decrement in the temperature can be observed in the 4.5 and 7.5 meters case corresponding to the time when the water level outside the S/C reaches the corresponding height.

On the other hand, the dashed lines represent the temperature at the coldest point of the S/C, that it is, the bottom region where the water is extracted. In this region the decrement in the temperature occurs sooner due to its lower height.

An accurate estimation of the S/C conditions is important for the overall RCIC performance since the S/C is considered the exhaust of the turbine and a change in the pool conditions might extend to the turbine performance and, in consequence, to the RCIC system.

Figure 5-17 shows the comparison of the computed turbine power between the simulation with no flood and with flood level of 7.5 meters. As can be observed, despite the changes in the S/C parameters, the RCIC turbine power is almost unaffected.

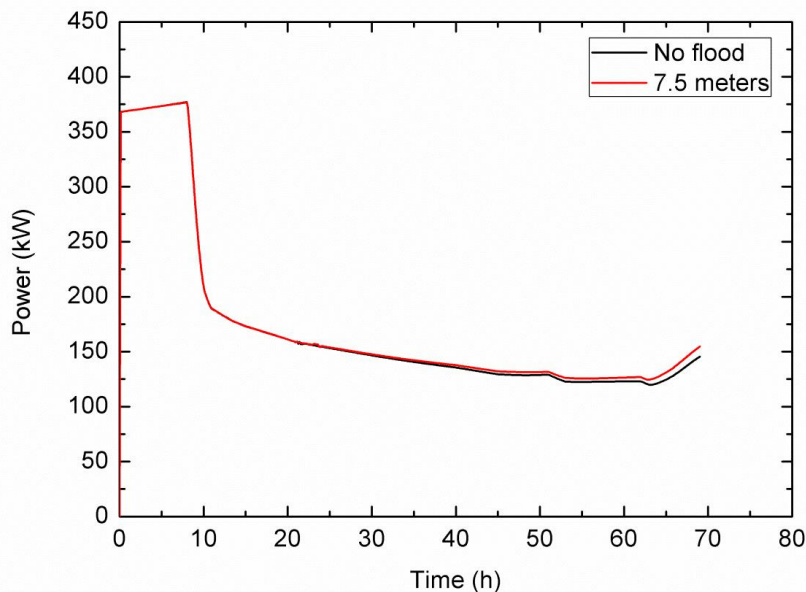


Figure 5-17 Flooding effect on turbine power

The explanation is simple, despite the huge relative reduction in the S/C pressure and temperature; these changes are minor compared with the RPV pressure during the RCIC system operation.

The main conclusion is, regarding RELAP, the flooding cold down the S/C but had no mayor effect on the RCIC system overall performance.

5.2.2- Close loop simulations

The open loop simulation results offer estimation close to the data and the information available of the F1D2 accident but it is not exempt of drawbacks. One of the mayor disadvantages of using open loop configuration is the dependency on the input data; in case of Fukushima Unit 2 that data is the RPV pressure measured by TEPCO.

The main problem with the measured data is the inexactitude on the measurements. As can be observed in **Figure 3-1** the initial pressure measurement is at 8h after the scram signal, during that period no data is available which makes the open loop configuration inaccurate, to solve this a single phase in the turbine has been assumed during that period of time.

The close loop, despite being more complex, allows avoiding such dependency. For the second set of simulations, a simplified version of F1D2 RPV has been included in the nodalization.

Figure 5-18 represents the nodalization used for the RPV used in RELAP/ScdapSIM. The nodalization is connected to the RCIC nodalization shown in **Figure 4-8** by the MSL region for the steam extraction and the lower plenum for the water injection.

For the close loop configuration, the boundary condition is reduced to the F1D2 decay heat profile shown in **Figure 3-3** which is tabulated in a power vs. time table and used in the heat structure used to reproduce the fuel.

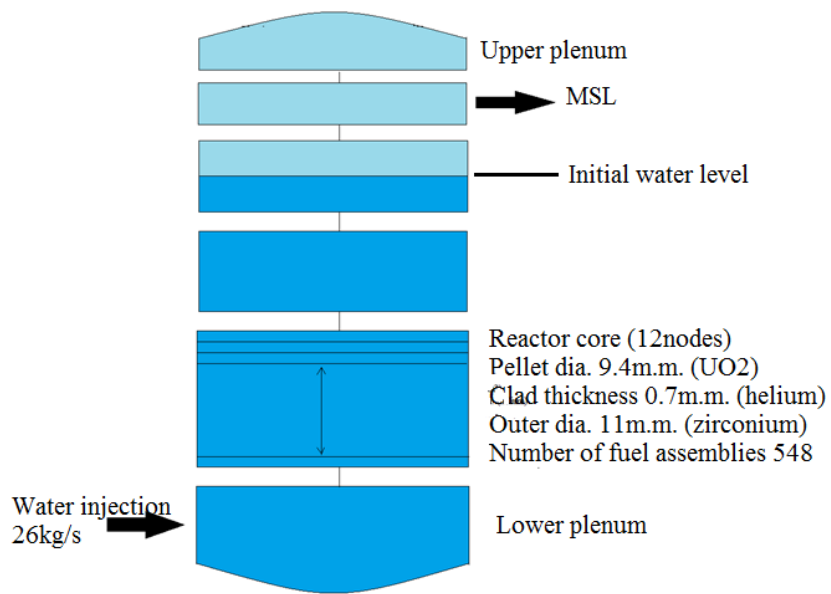


Figure 5-18 RPV nodalization

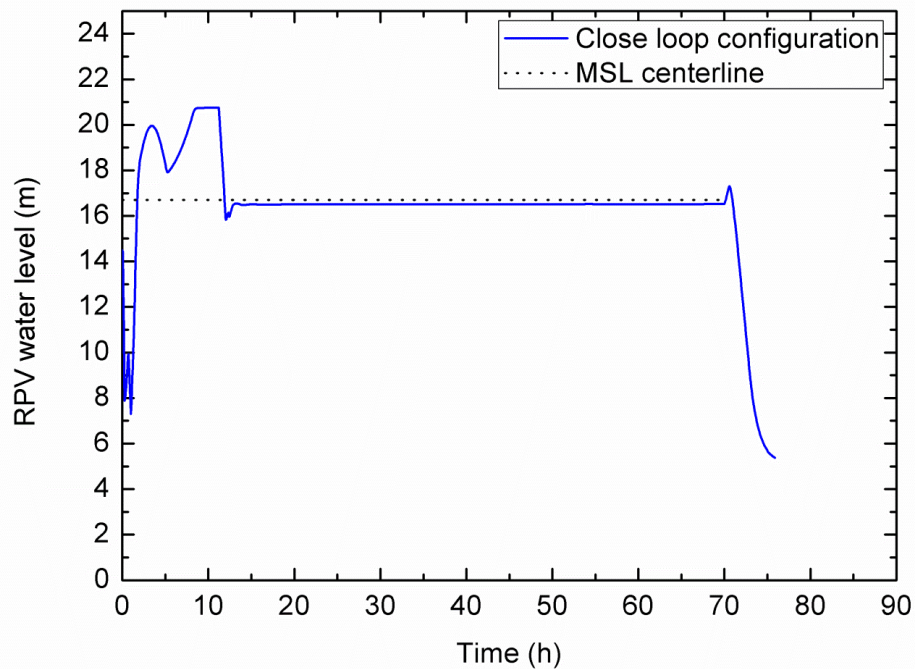


Figure 5-19 Open/close loop RVP water level comparison

Figure 5-19 compares the computed RPV water level simulated by close loop configuration with the height of the centerline MSL. The computed water level agrees with TEPCOs water level measurements and the initial assumptions that the water level reached the MSL. In fact, during the first hours the level exceeded the MSL height causing that only water is extracted from the RPV.

With the close-loop configuration, the RPV pressure changes its condition from user-specified boundary parameter to computed value. **Figure 5-20** shows the resulting RPV pressure obtained by using the close-loop configuration.

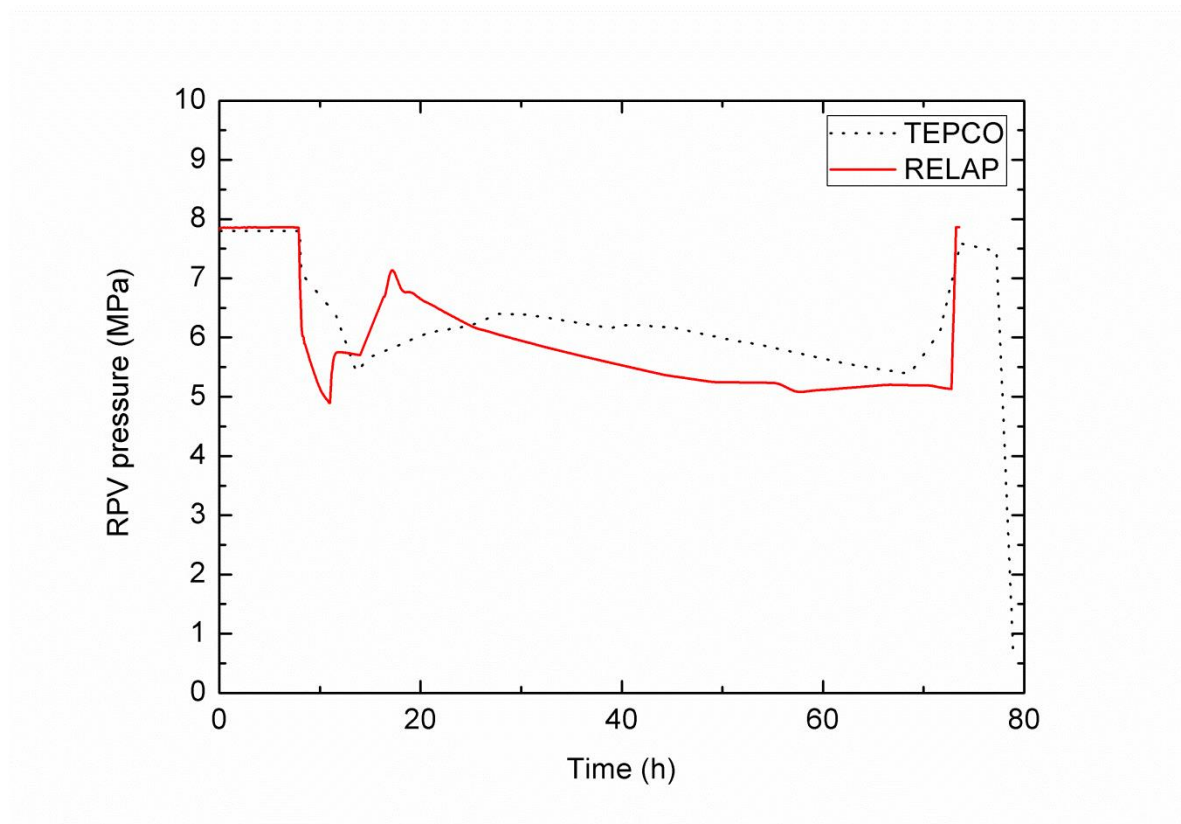


Figure 5-20 RPV pressure

In the figure, the computed value is compared with the measured pressure. The initial pressure suffers a reduction due to the huge amount of cold water injected by the RCIC which also causes the increment of the RPV water level above the MSL height. At this point, the turbine is forced to work with pure water and, hypothetically, suffering a considerable degradation for being working in a beyond-basis scenario.

At the end, the degradation suffered by the turbine causes the reduction of the power generated, reducing, at the same time, the amount of water injected by the RCIC is

reduced causing an increment of the RPV pressure and, eventually, a reduction of the RPV water level.

At some point, the situation naturally stabilizes itself; the water level has been reduced enough which allows the turbine to generate enough power to maintain the water level constant. With this constant flux of hot steam extraction and cold water injection, the RPV pressure starts to decrease gradually. The situation ends with the RCIC failure at 70h mark.

The power developed by the turbine during the simulation also supports the previous explanation as can be observed in **Figure 5-21**. The power initially suffers huge oscillations due to the sudden change from steady-state to transient caused by the aperture of the RCIC valves. The reduction of the output power due to the water presence is clearly described at all stages of the transient.

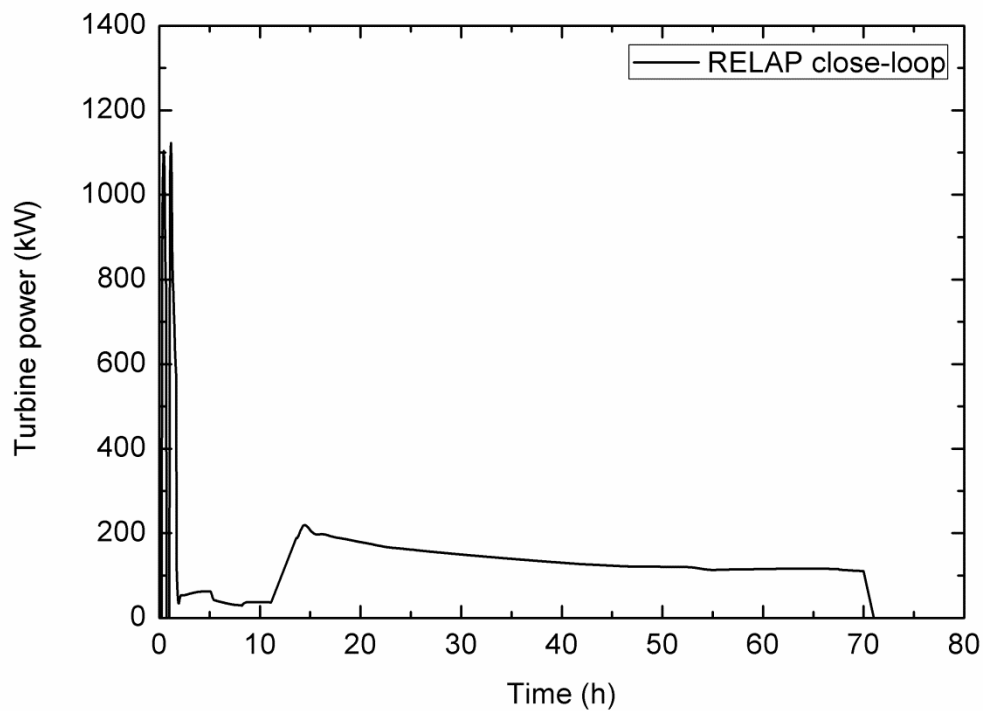


Figure 5-21 Turbine power

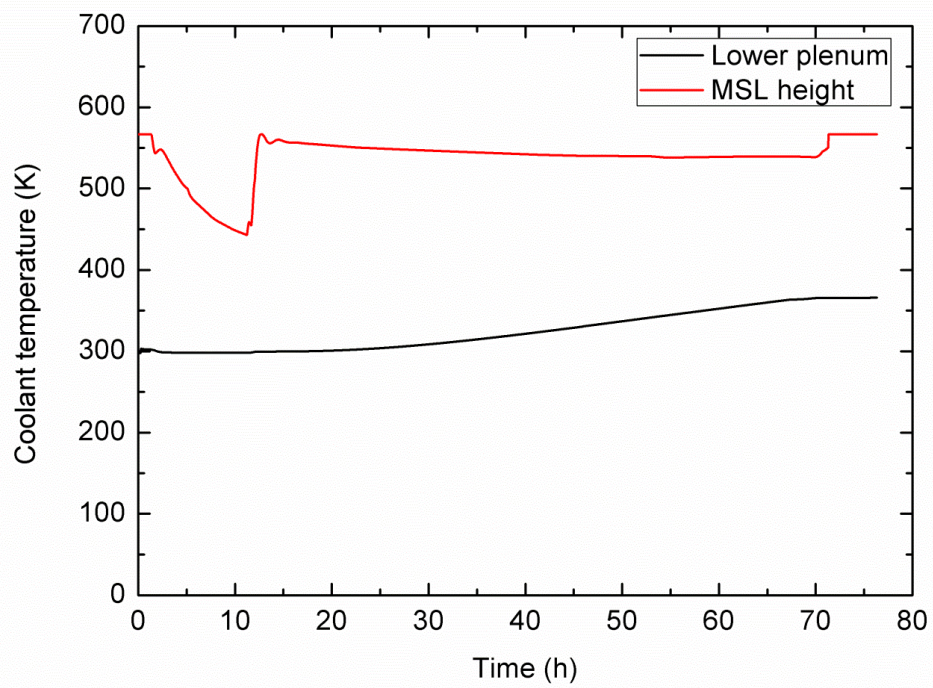


Figure 5-22 Coolant temperatures

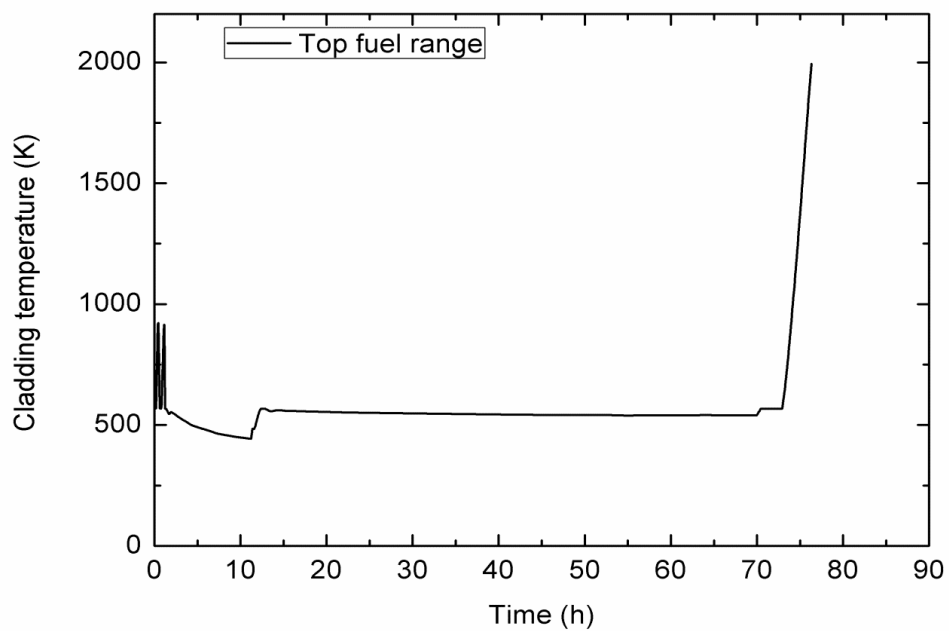


Figure 5-23 Cladding temperatures

Figures 5-22 and **5-23** show the coolant and cladding temperatures behavior respectively. **Figure 5-22** shows the temperatures in the RPV at the lower plenum section and the MSL height. The lower plenum temperature shows a similar behavior than the temperature in the bottom part of the S/C.

On the other hand, the MSL temperature shows a huge initial reduction caused by the huge amount of water injection that also caused the water level increment. Again once the turbine reduces its power and less coolant is injected, the temperature raises just to be cold down again once the situation stabilizes until the RCIC fails.

The cladding temperatures shown in **Figure 5-23** describe a similar behavior than the one explained for the coolant. The clad temperatures are kept far below from its melting point during all the RCIC operation time and only suffer a huge increment to 2000K (melting point of Zircalloy-4 is 2100K) when it fails at 70h

5.2.2.1- Steam flashing phenomenon

As mention early in this study, the instant evaporation of the water fraction can be a relevant phenomenon on the turbine performance and, consequently, on the overall RCIC system behavior.

Figure 5-24 shows the comparison on the fluid quality in the turbine component. As can be observed, the phenomenon causes an overall increase on the quality of around 20-30%. **Figure 5-25** describes the amount of steam generated by the steam flashing phenomenon based on the ratio of flashing vapor (w) calculated in equation 4-42 and the water mass flow rate.

This increment in the fluid quality is translated into an overall increment of the turbine computed power as is described in **Figure 5-26**.

The amount of power incremented depends on the initial quality and follows the tendency of the degradation coefficient shown in **Figure 2-16** and the quality relationship described in equation 4.43; if the initial quality is lower, its increment is larger and eventually the increment in the power is also higher

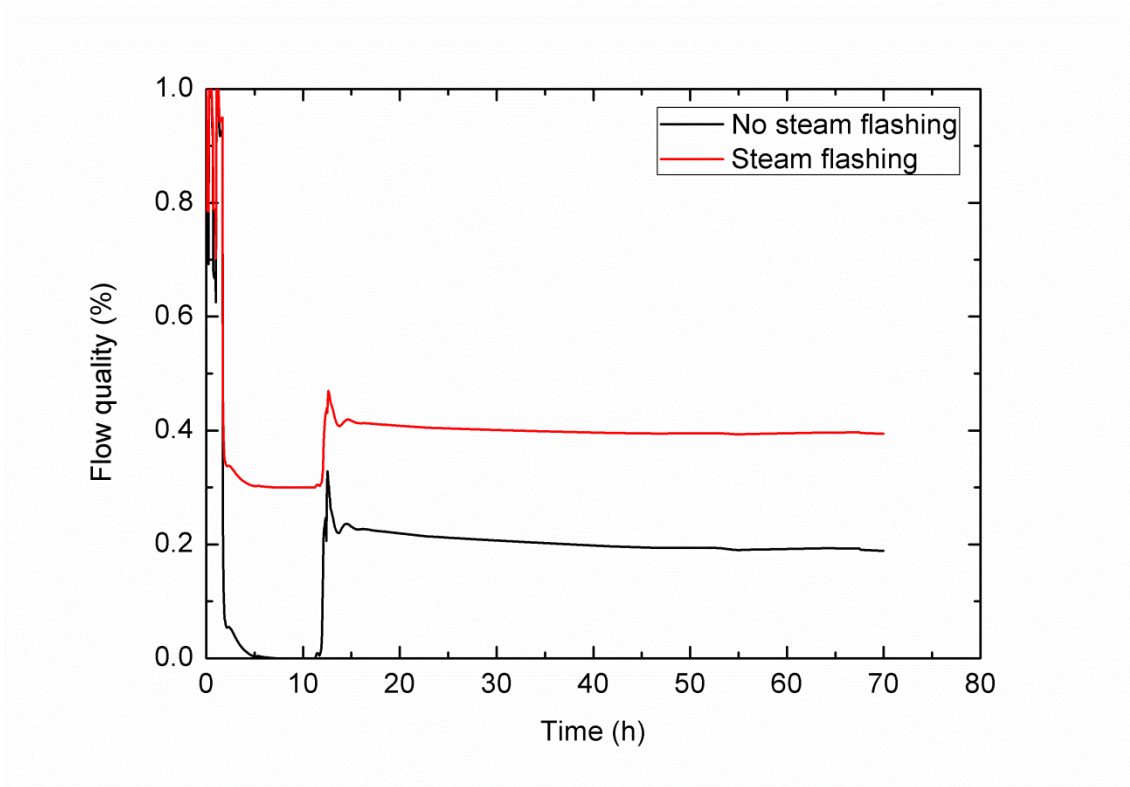


Figure 5-24 Steam flashing effect on turbine fluid quality

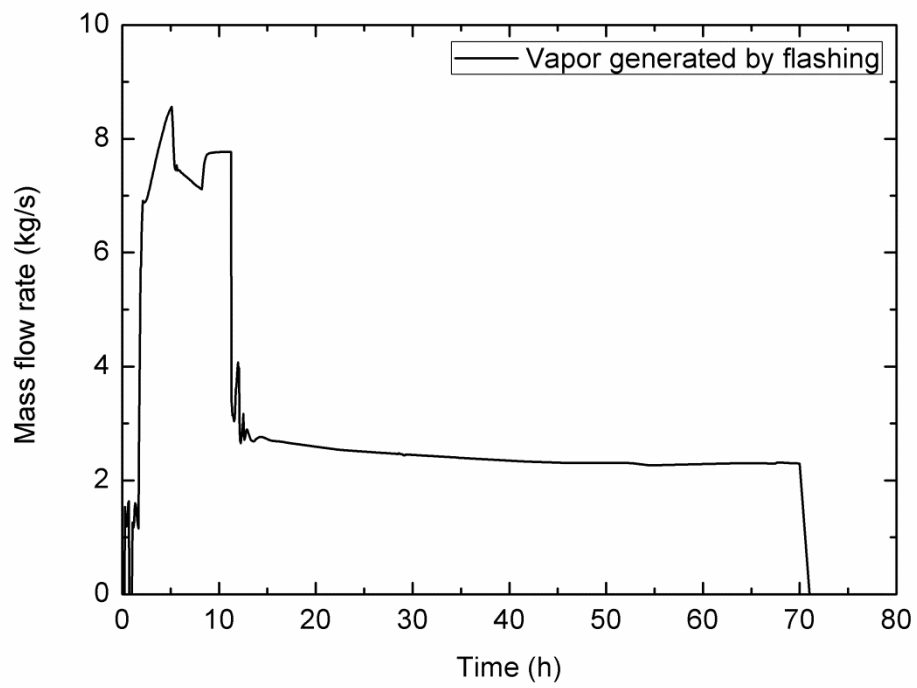


Figure 5-25 Steam generated by flashing

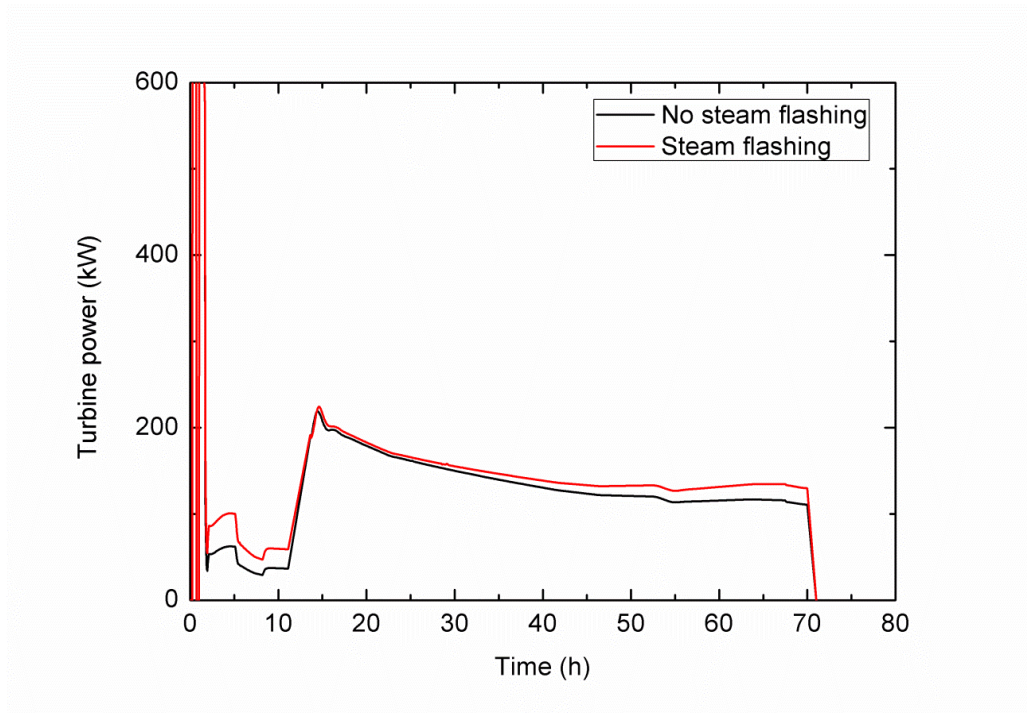


Figure 5-26 Steam flashing effect on turbine power

The increment of the turbine power allows the pump to inject more water into the RPV. The RPV water level comparison described in **Figure 5-27** shows that, due to this increment in the amount injected, the water level is stabilized in a higher height, above the MSL centerline height.

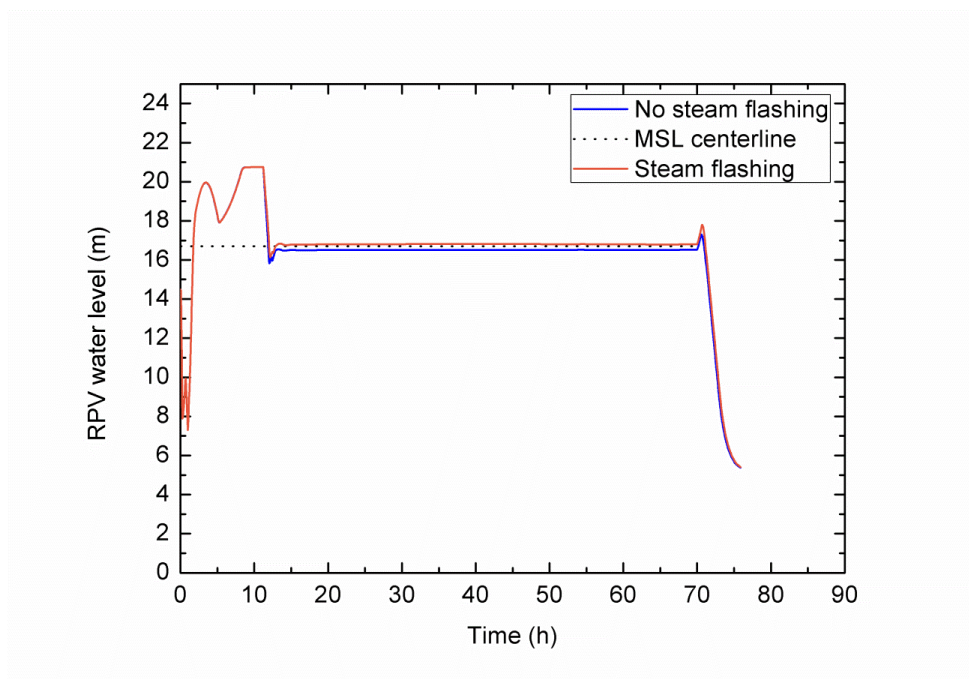


Figure 5-27 Steam flashing effect on RPV water level

It is remarkable the absence of difference in the computed water level during the first hours. It can be caused by the remaining steam mass in the upper plenum of the RPV which can only escape through the SRV once the RPV pressure exceeds the trigger pressure. This steam region would not be further compressed due to the water level increment and consequently would force the water level to be constant once reached some maximum height around 21m.

Finally, **Figure 5-28** shows and compares the RPV pressure behavior with and without considering the steam flashing in the RCIC turbine. Both pressures show a similar behavior but with an overall lower values in case of the steam flashing consideration.

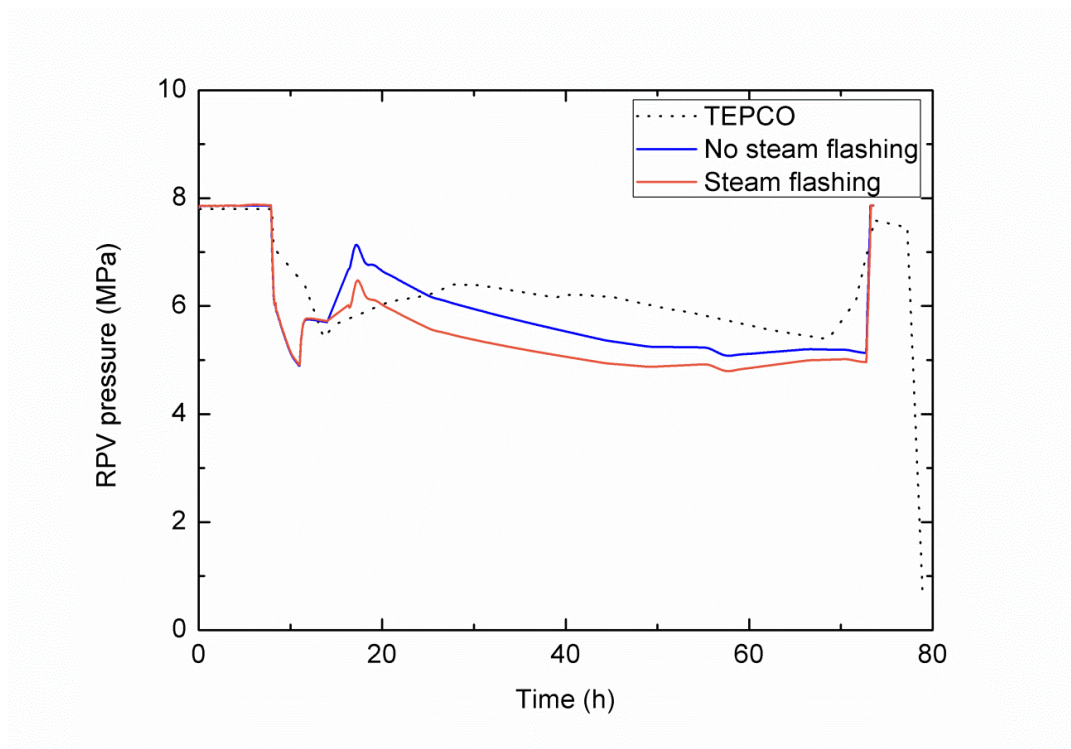


Figure 5-28 Steam flashing effect on RPV pressure

5.3- Comparison of F1D2 accident results obtained by different codes

As mentioned earlier in this dissertation, Fukushima accident has been widely analyzed by different laboratories, companies and research institutes. Despite huge part of the analysis results are still private data not available to the public, in this section the results obtained

in this dissertation by using RELAP are compared to the results obtained by the Institute of Applied Energy and TEPCO.

The IAE used SAMPSON code to perform their simulations of all the different reactors of Fukushima Daiichi. Regarding Unit 2 they also assumed degradation in the turbine due to the water flow and developed their own turbine degradation coefficient. The data used for the comparison corresponds to their findings which were presented on ICONE23. [42]

TEPCO used MAAP code (previously described in Chapter 1), In their assumptions they directly assumed a reduction of a 66% of the injected water from the RCIC [23]

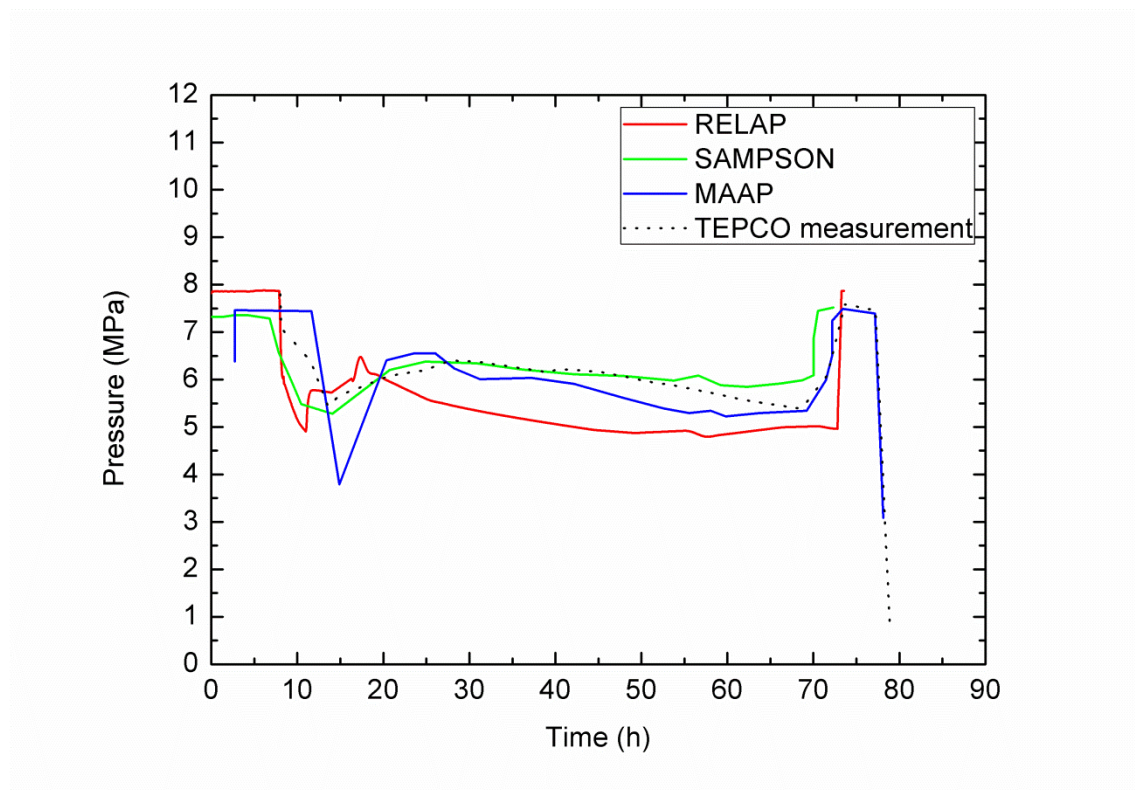


Figure 5-29 RELAP-SAMPSON-MAAP RPV pressure comparison

Figure 5-29 shows the RPV pressure computed by RELAP, MAAP and SAMPSON. Despite all three of them show the same pressure behavior; initial fast reduction followed by a pressure increment and a second reduction, the IAE computed pressure describes a better agreement with the measured values probably due to the iteration process used to develop their degradation coefficient.

The pressure computed by TEPCO shows a lowest point of 4MPa far below the values computed by the other codes.

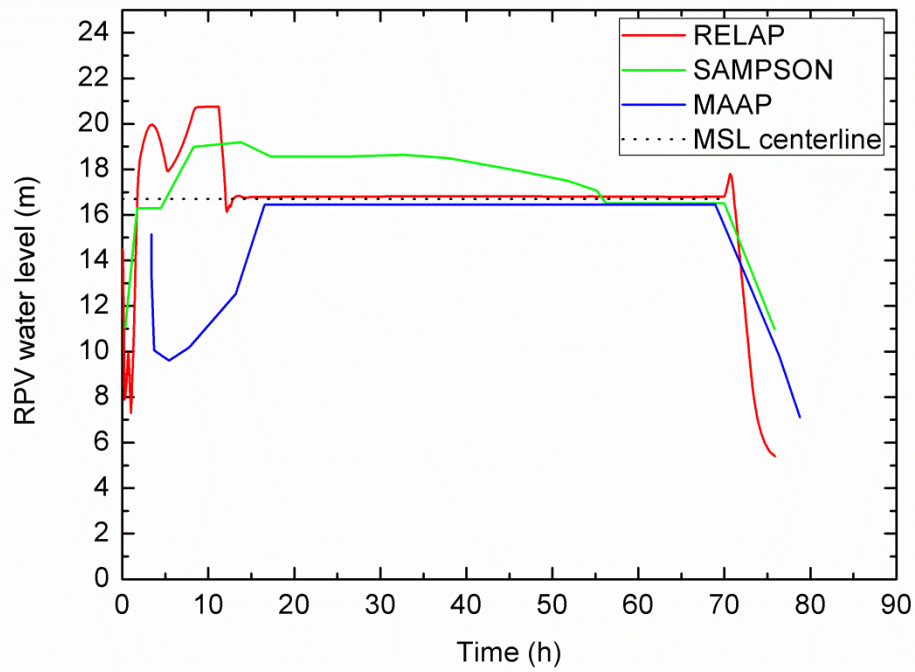


Figure 5-30 RELAP-SAMPSON-MAAP RPV water level comparison

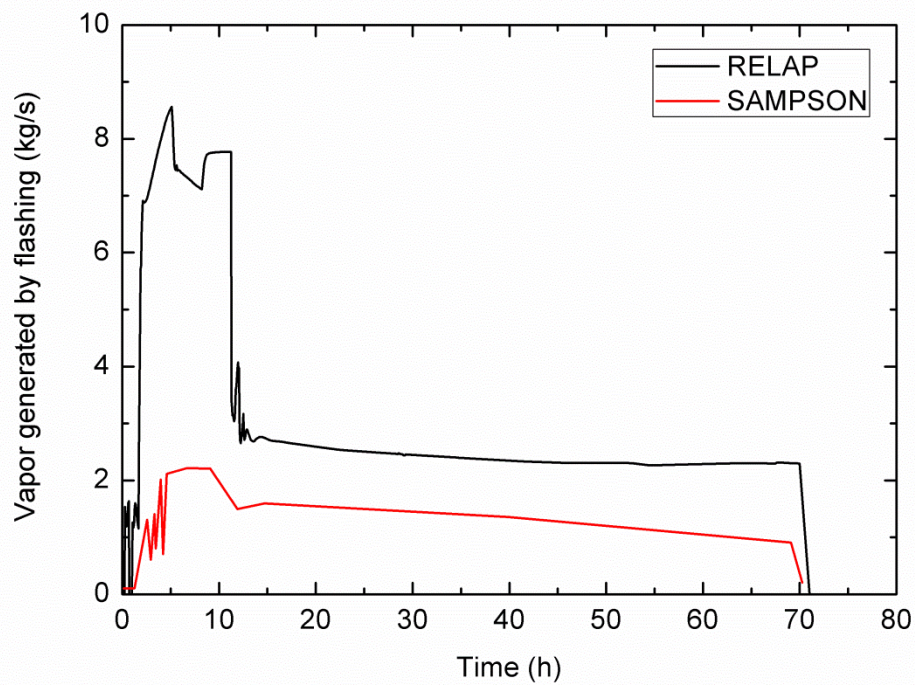


Figure 5-31 RELAP-SAMPSON steam generated by flashing

Figure 5-30 show the computed RPV water level. Regarding the water level, a huge discrepancy can be observed depending of which code has been used and which assumptions have been made.

Since TEPCO directly reduced the overall water injected to a 30% of its design value, the computed level based on their analysis show low values during the first hours while RELAP and SAMPSON analysis show higher values due to the high amount of injected water. Also, MAAP analysis does not consider the steam flashing

Regarding the SAMPSON analysis, it show a behavior more similar to the one obtained by RELAP. In both cases, the computed water level exceeds the MSL height during the first hours of RCIC operation. The main difference is that while in RELAP the water level quickly decays until it stabilizes at MSL height in case of SAMPSON that decay is slower lasting for almost 60h before reaching the MSL.

One important thing to mention is that, in fact, the RELAP analysis made in this dissertation is the only one to quantitatively explain its degradation coefficient based on known theories and principles; TEPCO directly reduced the injected water to a 30% but without any quantitative explanation about the reasons behind. In case of IAE, their degradation coefficient is an iteration-generated value that allow their computational results to match TEPCOs measurements and that is the reason why SAMPSON pressure results show the best agreement with the onsite measurements.

Figure 5-31 shows the steam generated by flashing on RELAP and SAMPSON analyses (MAAP does not consider such phenomenon). The computed values are higher in RELAP analysis especially during the first 10h and can be an explanation about the water level difference between both studies.

Despite the differences in the results, all three codes present good agreement with TEPCO measurements and provide a realistic explanation of the F1D2 accident progression. That discrepancy can be explained by the influence of several factors.

- The code used: each code has its own correlations and equations that make it unique as described in **Table 1-3**

- The information available: The data is important in order to be able to nodalize with accuracy complex component such as turbines. The lack of specification data has been one of the major issues when doing this study
- The nodalization: Severe accident codes provide plenty of freedom to create a nodalization; it can be more or less complex depending on the circumstances. Different nodalizations of the same system can lead to different results
- Initial assumptions: The assumptions made during the analysis also have a large impact on the final results; the application of steam flashing, the degradation coefficient...

5.4- Summary

This chapter shows and discusses the main results obtained by simulating the F1D2 accident conditions in RELAP.

The first set of simulations correspond to a turbine single phase flow scenario which main objective is to verify the RCIC nodalization, and specifically the RCIC pump homologous curves, with the data specified in the RCIC system specification sheet. The results for both, high and low pressure points, show good agreement with the design parameters proving the accuracy of the nodalization for complex simulations

The first two-phase flow simulations are done under the open-loop configuration. This configuration uses the measured RPV pressure and the flow quality obtained in the numerical analysis to compute the RCIC turbine, and the RCIC system, performance during the F1D2 accident. The simulation shows a reduction around 2 in the power generated by the turbine due to the water presence. That reduction allows the injected and extracted to be equal avoiding the computed mass unbalance which is not physically possible.

The results also described the temperature and pressure increment in the S/C during the RCIC operation time as well as the steam generated extracted to the drywell through the vacuum breakers.

The hypothetical torus room flooding might affect the turbine performance by changing the S/C (turbine downstream) conditions. A sensitive analysis is performed to evaluate the

pressure and temperature reduction as well as to compare the values with the S/C pressure measured by TEPCO. The computed flooding height that matches better with the measured values correspond to an 80% of the total room height. Despite the relative large difference in the S/C properties, it has been proved that its effect on the turbine performance can be neglected.

The last set of simulations is done under the close-loop configuration; a simplified version of the RVP is added to close the loop in order to analyze the RCIC performance avoiding the main disadvantages of the open-loop configuration. As can be observed, the RPV water level between both configurations only differ at the beginning precisely when the lack of RPV pressure data makes the open-loop less accurate. At last, the computed RPV pressure is compared with the measured one and, despite showing some discrepancies, both show the same behavior during the RCIC operation time. The discrepancies can be generated by the use of a simplified RPV nodalization.

The steam flashing is also considered and its effects are discussed; it increases the fluid quality in the turbine which eventually leads to a more power, higher RPV water level and lower RPV pressure. Despite the differences, no major behavior discrepancies are appreciated in the RPV water level or pressure behaviors.

The dissertation results have been compared with other parallel analyses carried on by IAE and TEPCO. Apart from the small differences in the computed results which can be easily explained by several differences in the analyses, the RELAP analysis made in this dissertation is the only one to quantitatively explain its degradation coefficient based on known theories and principles; TEPCO directly reduced the injected water to a 30% but without any quantitative explanation about the reasons behind. In case of IAE, their degradation coefficient is an iteration-generated value that allows their computational results to match TEPCOs measurements.

The use of principles and models such the critical flow models while developing the degradation coefficient provides a larger validation to the theories supporting the turbine degradation phenomenon.

Chapter 6 Conclusions

The objective of this paper was focused on Fukushima Unit 2 analysis uncertainties originated from the RCIC operation which directly related with the RCIC turbine behavior. The most important analysis was based on the assumption that the turbine is underperformance due to the presence of water in the flow. A new model was developed with the consideration of two phase flow degradation.

The first main conclusion extracted from this study is the successfully development of the turbine power degradation coefficient based on the Unit 2 RCIC turbine design parameters which were used to estimate several geometric parameters and the use of the Homogeneous Equilibrium Model (HEM) and Non-Homogeneous Equilibrium Model (NHEM) critical flow models.

For the verification, the degradation coefficient from both models were included in the RCIC system numerical analysis based on TEPCOs measurements and the corresponding results compared with the IAE data. The analysis proved that degradation in the turbine is needed for the numerical results to match the measured data. Due to the low average quality of the resulting flow, the NHEM model was selected due to its better accuracy at low qualities.

The degradation coefficient developed in this study, unlike the IAE coefficient which is just a generated value to force the matching between their computation analysis and TEPCOs data, provides a reason about why the turbine power is reduced based on the moisture energy loss due to water presence. It is also is easy to develop and can be adjust to other turbines with almost no complication if the design values are available.

In conjunction with the numerical analysis, a complete new brand RCIC nodalization was created to reproduce the RCIC system performance and evaluate the turbine behavior during the F1D2 accident including the degradation coefficient. To use the nodalization, the homologous curves for the RCIC pump were developed based on the pump performance curves and the data from the RCIC specification sheet.

The computational analysis also proved to be useful to perform auxiliary sensitivity analysis related to steam flashing and the torus room flood. The torus room flood greatly

affects the S/C conditions but despite the relative large effect on the suppression chamber, the overall effect in the turbine, and consequently in the RCIC system, can be neglected.

On the other hand, the steam flashing indeed caused an effect on the computed results in the turbine and eventually increasing the RPV water level and reducing the RPV pressure. Despite the differences, though, no major behavior discrepancies are appreciated in the RPV water level or pressure behaviors.

The second main conclusion is the quantitatively verification of the initial assumptions thank to the RELAP/ScdapSIM computational analysis, especially the RPV water level; TEPCOs data show a constant RPV water level throughout the 70h of RCIC system operation time but could not be true, in fact, what TEPCO measurements show is that the water level in the RPV was at least at the same height of the MSL.

The computational results from the close loop configuration show, not only similar values and behavior to the TEPCO data, but also that the initial assumption of constant RPV water level is, indeed, true almost all the time showing only a higher water level values at the beginning of the accident and just for a small amount of time due to the degradation suffered by the turbine.

The computational results have been verified by comparing them with the results from other analysis. The major achievement of this study is that, in fact, is the only to provide a quantitative explanation of the presence of the degradation phenomenon based on known models and equations.

The implications of that behavior of the RCIC; being capable to keep the water level constant at MSL height and the core covered for long periods of time are immense. The results prove that the RCIC system has, somehow, a feedback capability. In other words, the system by itself has the ability to cool down the reactor and successfully delay the core meltdown without any human interaction. This capability is interesting enough to be studied in detail and to be taken into consideration for future accident management not only for BWR but also for PWR.

References

- [1] Boiling Water Reactor. [Internet].
http://en.wikipedia.org/wiki/Boiling_water_reactor
- [2] *Boiling water reactor (BWR) systems*. NRC. <http://www.nrc.gov/>
- [3] Hellemans, M., "The Safety Relief Valve Handbook: Design and Use of Process Safety Valves to ASME and International Codes and Standards", Elsevier 2009)
- [4] Yamanaka, Y., et al., "*The Accident Analysis for Unit 1-3 at Fukushima Dai-ichi Nuclear Power Station*", International Meeting on Severe Accident Assessment and Management: Lessons Learned from Fukushima Dai-ichi, San Diego California, November 11-15, 2012, 2012.
- [5] HUMPHRIES, L., et al., "*MELCOR Best Practices - An Accident Sequence Walkthrough*", First meeting of the European MELCOR user group hosted by Paul Scherrer Institut, Villingen Switzerland, December 15-16, 2008.
- [6] Pellegrini M, Suzuki H, Mizouchi H, Naitoh M. *Early Phase Accident Progression Analysis of Fukushima Daiichi with the Sampson Code – Unit 3*. The Institute of Applied Energy, Minato-ku, Tokyo 2013
- [7] *Terry turbine maintenance guide, RCIC application*. EPRI. Final report. September 2012
- [8] *Standard Technical Specifications General Electric Plants, BWR/4*. NUREG-1433 Vol. 1, Rev.3. June 2004
- [9] *BWR/6 General Description of a Boiling Water Reactor*. GE Nuclear Energy. <http://www4.ncsu.edu/>
- [10] The National Diet of Japan "*The Official report of the Fukushima Nuclear Accident Independent Investigation Commission*" Executive summary (2012)
- [11] Information Portal for the Fukushima Daiichi Accident Analysis and Decommissioning Activities. [Internet]. Japan: TEPCO. Available from: <https://fdada.info/>

- [12] Sehgal, B.R., "*Nuclear safety in light water reactors: Severe accident phenomenology*", Academic Press, New York (2011)
- [13] Šadek, S., S. Špalj, and B. Glaser, "*Influence of modelling options in RELAP5/SCDAPSIM and MAAP4 computer codes on core melt progression and reactor pressure vessel integrity*", Science and Technology of Nuclear Installations, **2010**, 2009)
- [14] Nuclear Safety Analysis Division. *RELAP5/MOD3.3 CODE MANUAL VOLUME I: CODE STRUCTURE, SYSTEM MODELS, AND SOLUTION METHODS*, Inc.. Rockville, Maryland. Idaho Falls, Idaho. December 2001
- [15] Haste, T., et al., "*MELCOR/MACCS simulation of the TMI-2 severe accident and initial recovery phases, off-site fission product release and consequences*", Nuclear Engineering and design, **236**, 1099-1112 (2006)
- [16] Summers, R.M., et al., "*MELCOR computer code manuals*", Sandia National Labs., Albuquerque, NM (United States); Oak Ridge National Lab., TN (United States) (1995)
- [17] Maolong L. *STUDY ON CORE DEGRADATION AND MELT PROGRESSION IN BWR SEVERE ACCIDENT CONSIDERING THE DEPRESSURIZATION CAUSED BY SEVERE LOADINGS*. University of Tokyo. February 2014
- [18] "IAEA Safety Standards", Safety Guide No. NS-G-2.15, IAEA Severe Accident Management Programmes for Nuclear Power Plants (2009)
- [19] "REGDOC-2.3.2: Accident Management: Severe Accident Management Programs for Nuclear Reactors", Canadian Nuclear Safety Commission (2013)
- [20] E. F. Church. *Steam Turbines – Third edition*. McGraw-Hill Book Company. New York 1950
- [21] A. S. Leyzerovich. *Wet-Steam Turbines for Nuclear Power Plants*. PennWell corporation. Oklahoma 2005
- [22] Critical flow. [Internet]. <http://www.thermopedia.com/content/267/>

- [23] N. Masanori et. al. *State Of The Art SAMPSON Analysis and Its Future Improvements For Calculations Of The Fukushima Daiichi NPP Accident*. The 15th International Topical Meeting on Nuclear Reactor Thermal - Hydraulics, NURETH-15. NURETH15-601. Pisa, Italy, May 12-17, 2013
- [24] Takahashi A, Pellegrini M, Suzuki H, Mizouchi H, Naitoh M. *Accident Analysis of Fukushima Daiichi Nuclear Power Plant Unit 2 by the SAMPSON Severe Accident Code*. Proceeding of the 22th International Conference on Nuclear Engineering, ICONE22. ICONE22-30670. Pague, Czech Republic, July 7-11, 2014.
- [25] K.H. Ardron , R.A. Furness. *A STUDY OF THE CRITICAL FLOW MODELS USED IN REACTOR BLOWDOWN ANALYSIS*. Nuclear Engineering and Design 39 (1976) 257-266
- [26] G. B. Wallis, *Critical Two-Phase Flow*. Int. J. Multiphasc F/ow Vol. 6, pp. 97-112 Pergamon/Elsevier, 1980
- [27] E. Elias et. al. *Two-Phase Critical Flow*. Int. J. Multiphase Flow Vol. 20, Suppl., pp. 91-168, 1994. Elsevier Science Ltd. 14 February 1994
- [28] H. K. Fauske, *CONTRIBUTION TO THE THEORY OF TWO-PHASE, ONE-COMPONENT CRITICAL FLOW*. Argonne National Laboratory ANL-6633
- [29] S. W. Kieffer. *Sound Speed in Liquid-Gas Mixtures' Water-Air and Water-Steam*. Journal of Geophysical Research. VOL. 82, NO. 20. JULY 10, 1977
- [30] *The Euler Turbine Equation*. [Internet].
<http://web.mit.edu/16.unified/www/FALL/thermodynamics/notes/node91.html>
- [31] Hoshi H, Ogino M, Kawabe R, Fukasawa M. *MELCOR Analysis on Tepco's Fukushima Dai-Ichi NPS Accident*. The 15th International Topical Meeting on Nuclear Reactor Thermal - Hydraulics, NURETH-15. NURETH15-653. Pisa, Italy, May 12-17, 2013
- [32] Mizokami S, Yamanaka Y, Watanabe M, Honda T, Fujii T, Kojima Y, Paik C.H., Rahn F. *State Of The Art Maap Analysis and Future Improvements on TEPCO Fukushima-Daiichi NPP Accident*. The 15th International Topical Meeting on Nuclear Reactor Thermal - Hydraulics, NURETH-15. NURETH15-536. Pisa, Italy, May 12-17, 2013

- [33] N. Masanori et. al. *Analysis of Accident Progression of Fukushima Daiichi Nuclear Power Plant with SAMPSON Code – (2) Unit 2*. The 15th International Topical Meeting on Nuclear Reactor Thermal - Hydraulics, NURETH-15. NURETH15-075. Pisa, Italy, May 12-17, 2013
- [34] Nuclear Safety Analysis Division. RELAP5/MOD3.3 CODE MANUAL VOLUME II: USER'S GUIDE AND INPUT REQUIREMENTS. Information Systems Laboratories, Inc.. Rockville, Maryland. Idaho Falls, Idaho. December 2001
- [35] Nuclear Safety Analysis Division. RELAP5/MOD3.3 CODE MANUAL VOLUME IV: MODELS AND CORRELATIONS. Information Systems Laboratories, Inc.. Rockville, Maryland. Idaho Falls, Idaho. December 2001
- [36] Nuclear Safety Analysis Division. RELAP5/MOD3.3 CODE MANUAL VOLUME VIII: PROGRAMMERS MANUAL. Information Systems Laboratories, Inc.. Rockville, Maryland. Idaho Falls, Idaho. December 2001
- [37] Allison C. M., Hohorst J. K., Allison B. S., Konjarek D, Bajs T, Pericas R, Reventos F, Lopez R. Preliminary Assessment of the Possible BWR Core/Vessel Damage States for Fukushima Daiichi Station Blackout Scenarios Using RELAP/SCDAPSIM. Science and Technology of Nuclear Installations. Hindawi Publishing Corporation. Volume 2012. 6 March 2012
- [38] *Flash evaporation*. [Internet]. http://en.wikipedia.org/wiki/Flash_evaporation
- [39] *The Centrifugal Pump*. Grundfos Research and Technology. <http://grundfos.com/>.
- [40] *Chapter 24 Centrifugal pumps*. [Internet]. <http://www.ivorbittle.co.uk/Books/>
- [41] *Centrifugal pumps for general marine duties*. [Intenet]. <http://www.machineryspaces.com/centrifugal-pump.html>
- [42] Takahashi A, Pellegrini M, Suzuki H, Mizouchi H, Naitoh M. *Simulation analysis on accident at Fukushima Daiichi Nuclear Power Plant Unit 2 by SAMPSON code*. Proceeding of the 23th International Conference on Nuclear Engineering, ICONE23. ICONE23-1517. Chiba, Japan, May 17-21,2015.